R & M No.3828

PROCUREMENT EXECUTIVE, MINISTRY OF DEFENCE

Aeronautical Research Council
Reports and Memoranda

AN EXTENSION TO THE METHOD OF GARABEDIAN AND KORN FOR THE CALCULATION OF TRANSONIC FLOW PAST AN AEROFOIL TO INCLUDE THE EFFECTS OF A BOUNDARY LAYER AND WAKE

by

M.R. Collyer

Aerodynamics Department, RAE Farnborough, Hants

London: Her Majesty's Stationery Office
1978

PRICE £8 NET

AN EXTENSION TO THE METHOD OF GARABEDIAN AND KORN FOR THE CALCULATION OF TRANSONIC FLOW PAST AN AEROFOIL TO INCLUDE THE EFFECTS OF A BOUNDARY LAYER AND WAKE

by M. R. Collyer

Aerodynamics Department, RAE Farnborough, Hants

Reports and Memoranda No.3828*
July 1977

SUMMARY

A numerical method has been developed for calculating compressible (including transonic) flow past a single aerofoil with an allowance for viscous effects, providing that the boundary layer is fully attached over the aerofoil surface. This method has been developed by combining an iterative scheme for the inviscid flow, originally established by Garabedian and Korn, with an integral method (the lag entrainment method of Green *et al*) for the calculation of compressible turbulent boundary layers. The inviscid scheme has been modified to incorporate a boundary condition on the aerofoil surface, which is imposed on the velocity normal to the surface, with a corresponding boundary condition for the wake. Wake curvature effects are also included. An iterative procedure is established, which iterates between successive calculations of the pressure distribution and of the displacement thickness of the boundary layer and wake. Results are presented from a computer program (VGK) and comparisons are made with experimental measurements and other theoretical results.

* Replaces RAE Technical Report 77104 - ARC 37680

LIST OF CONTENTS

1 INTRODUCTION

In recent years various theoretical methods have been developed for predicting the pressure distribution, lift and drag for steady inviscid flow past two-dimensional lifting aerofoils[1-5,16]. These methods are based on schemes in which the inviscid equations are represented in finite difference form, and solutions sought by iterative techniques. It is, however, well known that viscous effects are important for the range of Mach numbers and Reynolds numbers at which a typical aerofoil is designed to operate, and hence, more recently, efforts have been made to develop theoretical models which incorporate the effects of viscosity[6-10]. The present work is concerned with an improved treatment of this topic and with the development of a computer program, named VGK, which is based on an inviscid scheme devised by Garabedian and Korn[2,3]. This Report gives a description of the mathematical model on which the program is based, together with results for various aerofoils, while a companion note describes the computer program and contains instructions on running it.

The project may be regarded as an extension of previous work at the RAE by Firmin[6] and Firmin and Jones[7,8]. In these Reports the viscous effects are included by an amalgamation of a scheme for inviscid flow calculations which determines a pressure distribution on the aerofoil surface and along the wake, with an integral method for predicting the development of the turbulent boundary layer and wake in a given pressure distribution providing the boundary layer is fully attached. In the first Report, an interim method was developed, based on a simple inviscid scheme devised by Lock *et al*, for calculating the pressure distribution. The boundary layer development is determined by an entrainment method due to Green[13] and includes a contribution from wake curvature. In the subsequent work[7,8] a more sophisticated inviscid scheme was adopted, which led to the development of the RAE Transonic Aerofoil Program. This is based on an iterative procedure for solving the transonic small perturbation (TSP) equations, originally devised by Murman and Cole[1], and modified subsequently at RAE by Albone *et al*[5]. The turbulent boundary layer method used is the 'lag-entrainment' method of Green *et al*[14], in which the boundary layer development is predicted by the forward integration of three simultaneous ordinary differential equations, namely the momentum integral equation, the entrainment equation and an equation for the rate of change of the entrainment coefficient derived from the turbulent energy equation. Starting from the stagnation point, a laminar boundary layer is first calculated by Thwaites' method, extended for compressible flows by the Stewartson-Illingworth transformation[15]. At a certain transition point a

turbulent boundary layer is assumed to develop, and the laminar boundary layer calculations form initial conditions.

In the present development of the problem of including viscous effects the boundary-layer method employed by Firmin and Jones[7,8] is retained, but the inviscid scheme is replaced by a more accurate one due to Garabedian and Korn[2,3] (referred to hereafter as G & K). This scheme consists of a conformal transformation of the aerofoil into the interior of the circle $|r| = 1$, which was developed initially by Sells[16,17], combined with an iterative solution of the exact irrotational, isentropic equations in a manner similar to that used by Murman and Cole[1]. An iterative procedure is employed to obtain consistent solutions for the inviscid flow and the boundary layer. Thus, after every few iterations of the inviscid scheme the current pressure, on the aerofoil surface and along the wake, is calculated, and this is used to determine the current boundary layer displacement and momentum thicknesses. Boundary conditions for the inviscid scheme, which are modified to take account of the viscous effects, are formed by the 'equivalent source' method of Lighthill[18], and in this manner the repetition of the mapping procedure after every boundary layer calculation is obviated. Under-relaxation is used in applying the boundary conditions. Allowance for curvature effects of the boundary layer on the aerofoil surface and of the wake are included in these boundary conditions. The application of the method is restricted to cases where the boundary layer remains attached everywhere.

Other attempts at creating a program for transonic flows with viscous effects, based on the inviscid G & K program, have been developed recently by Bauer and Garabedian[4,9] and Bavitz[10]. For the turbulent boundary layer analysis in the former case a relatively simple integral method due to Nash and MacDonald[19] is used, while in the latter a more sophisticated differential scheme developed by Bradshaw *et al*[20,21] is employed. For both of these methods the turbulent boundary layer is calculated over the aerofoil surface only, so that no wake effects are included. Each employs a similar numerical procedure, different from the one adopted here, by seeking a nearly converged inviscid solution before calculating a pressure distribution which is used to determine the boundary layer displacement thickness. This is then added to the aerofoil normal to produce an equivalent 'inviscid aerofoil', and the resulting shape is mapped conformally as though it was the original aerofoil.

In section 2 the inviscid method on which the G & K analysis is based is described briefly, as well as the modifications to it required to include

different boundary conditions due to viscous effects. A full description is given in section 3 of each of these changes to the boundary conditions on the aerofoil surface and along the wake. In section 4 a description of the interactive procedure between the inviscid analysis and the boundary layer calculations is presented, together with various smoothing and extrapolation procedures employed near to the trailing edge in order to aid convergence. The convergence of the interactive process is also discussed. In section 5 results are presented for the NACA 0012 aerofoil, the RAE 2822 aerofoil and an aerofoil designed by the hodograph method of Ref 3 (referred to as 'Korn No.1'). These have been used as test cases for the computer program. These results are compared with experiments and other theoretical methods.

2 FORMULATION OF THE COMPRESSIBLE FLOW EQUATIONS WITH VISCOUS EFFECTS

2.1 The basic inviscid method

A brief summary of the theory and numerical analysis associated with the inviscid method of G & K[2,3] is presented here. The basic theory consists of two parts. Firstly, the exterior of the aerofoil in the (x,y) plane is mapped conformally into the interior of the unit circle $|r| = 1$,

where
$$x + iy = F(re^{i\theta}) \tag{1}$$

denotes the mapping function, and the transform derivative is defined by

$$B = |F'(re^{i\theta})| \quad . \tag{2}$$

This is the Sells' transformation[16,17]. The second part consists of solving a second order partial differential equation, which can be derived in terms of the (r,θ) coordinate system as follows. The equation of motion for irrotational isentropic flow (obtained by combining the equation of continuity with the Euler equation) may be written as

$$a^2 \operatorname{div} \underline{u} = \underline{u}.\operatorname{grad} (\tfrac{1}{2}\underline{u}^2) \tag{3}$$

where $\underline{u} = \operatorname{grad} \phi$ is the velocity (non-dimensionalised by the free-stream velocity U_∞ ,

and a is the speed of sound (also non-dimensionalised) given by Bernoulli's equation

$$\tfrac{1}{2}\underline{u}^2 + \frac{a^2}{\gamma - 1} = \tfrac{1}{2} + \frac{M_\infty^{-2}}{\gamma - 1} \tag{4}$$

where $\gamma (= 1.4)$ is the ratio of specific heats,
and M_∞ is the free-stream Mach number.

Equation (3) may be written with r and θ as independent variables in the form

$$(a^2 - \bar{u}^2)\phi_{\theta\theta} - 2\bar{u}\bar{v}r\phi_{r\theta} + r^2(a^2 - \bar{v}^2)\phi_{rr} + a^2 r\phi_r + \bar{u}\bar{v}\phi_\theta + r(\bar{u}^2 + \bar{v}^2)(\bar{u}B_\theta + r\bar{v}B_r) = 0 , \tag{5}$$

where $\bar{u}$ and $\bar{v}$ are the non-dimensional components of velocity in the θ and r directions respectively, defined by

$$\bar{u} = \frac{1}{B_r}\phi_\theta \quad \text{and} \quad \bar{v} = \frac{1}{B}\phi_r . \tag{6}$$

In order to remove the singularity in ϕ at $r = 0$ (corresponding to the free stream in the physical plane), a modified potential Φ is introduced by setting

$$\phi = \Phi + \frac{\cos(\theta + \alpha)}{r} \tag{7}$$

with $\alpha = \bar{\alpha} - \alpha_0$,
where $\bar{\alpha}$ is the angle of incidence
and α_0 is the zero-lift angle for incompressible flow.
A modified mapping function ω is introduced by setting

$$\omega = r^2 B . \tag{8}$$

Both Φ and ω are now regular as $r \to 0$. A further restriction is imposed on ω by normalizing it so that $\omega \to 1$ as $r \to 0$. This implies that the chord of the aerofoil, S , is no longer arbitrary, but is instead determined by the mapping analysis. The final form of the partial differential equation for Φ is

$$(a^2 - \bar{u}^2)\Phi_{\theta\theta} - 2r\bar{u}\bar{v}\Phi_{r\theta} + r^2(a^2 - \bar{v}^2)\Phi_{rr} - 2\bar{u}\bar{v}\Phi_\theta + r(a^2 + \bar{u}^2 - 2\bar{v}^2)\Phi_r + r^{-1}(\bar{u}^2 + \bar{v}^2)(\bar{u}\omega_\theta + r\bar{v}\omega_r) = 0 \tag{9}$$

with

$$\left.\begin{aligned} \bar{u} &= \omega^{-1}[r\Phi_\theta - \sin(\theta + \alpha)] \\ \bar{v} &= \omega^{-1}[r^2\Phi_r - \cos(\theta + \alpha)] \end{aligned}\right\} \quad . \tag{10}$$

The boundary conditions to be satisfied concern the normal velocity on the aerofoil surface, and the flow at infinity. On $r = 1$, $\phi_r = 0$, *ie*

$$\Phi_r = \cos(\theta + \alpha) \qquad \text{on} \quad r = 1 \; . \tag{11}$$

At $r = 0$, Φ satisfies the boundary condition.

$$\Phi = \frac{\Gamma_0}{2\pi} \tan^{-1}\left[\left(1 - M_\infty^2\right)^{\frac{1}{2}} \tan(\theta + \alpha)\right] \tag{12}$$

where the circulation, Γ_0, is determined from the Kutta condition that $\phi_\theta = 0$, and hence

$$\Phi_\theta = \sin\alpha \tag{13}$$

at the trailing edge $(\theta = 0, r = 1)$.

In the numerical analysis the governing partial differential equations (4) and (9), are approximated by finite difference equations. A grid is set up in the computing (θ,r) plane (see Fig 1) such that the point $P_{i,j}$ is defined by

$$\theta = (i - 1)\frac{\pi}{m}, \qquad r = 1 - \frac{(j - 1)\pi}{n} \; .$$

For the derivatives in the r direction (which is normal to the direction of flow at the aerofoil surface and nearly normal to it close to the aerofoil) central differences are used throughout. For the derivatives in the θ direction, corresponding approximately to the direction of flow, central differences are used in subsonic (elliptic) regions of flow, while in the supersonic (hyperbolic) regions backward differences are used on the upper surface $(\pi \leqslant \theta \leqslant 2\pi)$ and forward differences on the lower surface $(0 \leqslant \theta \leqslant \pi)$; this allows for the correct physical domains of dependence. At each iteration the equations are solved successively along radial lines advancing from $\theta = \pi$ to $\theta = 2\pi$ and then from $\theta = \pi$ to $\theta = 0$ (see Fig 1). The equations are not solved along the radial line $i = 1$, corresponding to $\theta = 0$. Instead the

value of Φ is updated by adding a constant Γ_0 to the solution obtained along the radial line $i = mm$, corresponding to $\theta = 2\pi$, where Γ_0 is adjusted at the end of every cycle so that the jump in the value of Φ satisfies the Kutta condition that $\phi_\theta = 0$ at the trailing edge. A detailed explanation of how this condition is applied in the finite difference scheme is given in Appendix A.

2.2 Alterations to the flow field calculations to include viscous effects

The alterations to the basic inviscid scheme, described in the previous section, in order to include viscous effects, result in changes to the boundary conditions on the aerofoil surface and in the wake. These have been formulated by Lock[22].

The effect of the viscous layers (boundary layer and wake) on the flow about the aerofoil is represented by defining an 'equivalent inviscid flow'. This is identical to the real flow outside of these viscous layers, and is continued analytically inside of them onto the surface of the aerofoil and the centre line of the wake. The boundary condition for this inviscid flow on the aerofoil surface is equivalent to a distribution of sources, required to make up the mass deficit produced by the boundary layer. Assuming that the velocity component, u, parallel to the surface, may be regarded as (approximately) constant across the boundary layer, we have effectively, in the inviscid model the component of non-dimensional velocity v, normal to the surface given by

$$v = \frac{1}{\rho}\frac{\partial}{\partial s}(pq\delta^*) \tag{14}$$

where δ^* is the displacement thickness and the total velocity q and the density ρ are evaluated at the aerofoil surface, rather than at the edge of the boundary layer. The velocity components u,v are defined as

$$u = \frac{\partial\phi}{\partial s}, \quad v = \frac{\partial\phi}{\partial n} \tag{15}$$

where s is the distance measured along the surface from the leading edge and n is the distance normal to the surface, and ρ is defined by

$$\rho = \left\{1\Big/\left(1 + \frac{\gamma - 1}{2}M^2\right)\right\}^{\gamma-1} \tag{16}$$

which is the ratio of the density to its value at the stagnation point, and M is the local Mach number at the surface in the equivalent inviscid flow.

The boundary condition on the aerofoil surface has to be transformed into a condition in the computing plane on the circle $r = 1$. The relationship between the velocity components u,v in the physical plane to the velocity components $\bar{u},\bar{v}$ in the computing plane, on the aerofoil surface, is determined by the relationship

$$\frac{\partial}{\partial n} = -\frac{1}{B}\frac{\partial}{\partial r} , \quad \frac{\partial}{\partial s} = \pm\frac{1}{B}\frac{\partial}{\partial \theta} \tag{17}$$

where the upper sign refers to the upper surface of the aerofoil and the lower sign to the lower surface (see Fig 2). Thus, from (6)

$$u = \pm\bar{u} , \quad v = -\bar{v} . \tag{18}$$

When the boundary condition is transformed into the computing plane δ^* needs to be scaled by a factor S, because of the normalization of B as $r \to 0$ adopted in the basic analysis (*cf* section 2.1, p 5). Thus if we define $\bar{\delta}^* = \delta^*/S$ (the non-dimensional value with respect to the chord), then we have from (14), on the upper surface of the aerofoil, on $r = 1$

$$\frac{\partial\phi}{\partial r} = -\frac{S}{\rho}\frac{d}{d\theta}(\rho q\bar{\delta}^*) \equiv \tau^{(1)}(\theta) \qquad (\pi \leq \theta \leq 2\pi) \tag{19}$$

while on the lower surface of the aerofoil, on $r = 1$

$$\frac{\partial\phi}{\partial r} = \frac{S}{\rho}\frac{d}{d\theta}(\rho q\bar{\delta}^*) \equiv \tau^{(1)}(\theta) \qquad (0 \leq \theta \leq \pi) . \tag{20}$$

Thus by differentiating equation (7) the boundary condition to be applied on $r = 1$ is

$$\Phi_r = \tau^{(1)}(\theta) + \cos(\theta + \alpha) . \tag{21}$$

Similar considerations are applicable in the wake, where the variation in displacement thickness can be interpreted as a distribution of sinks along the rear dividing streamline. In this case, if δ^*_w represents the total displacement thickness of the wake, applying (14) leads to a jump in the normal velocity, v, across the wake, such that

$$\Delta(v) = \frac{1}{\rho}\frac{d}{ds}(\rho q \delta^*_w) \quad . \tag{22}$$

(The notation $\Delta(v)$ implies $v|_{\theta=2\pi} - v|_{\theta=0}$.) In order to apply this condition it is strictly necessary to know the position of the wake in the (r,θ) plane. This is not known in advance so that an approximation is introduced by applying the boundary condition along the radial line $\theta = 0$. From the basic analysis of Sells[16,17] the direction of the line $\theta = 0$ near to $r = 1$ is determined so as to bisect the trailing edge angle. If s is measured from the trailing edge along the line $\theta = 0$ (in the physical plane), then from (1), (2) and (8) we have

$$\left|\frac{ds}{dr}\right| = \frac{\omega(r,0)}{r^2} \quad . \tag{23}$$

Thus

$$s = \int_r^1 \frac{\omega(r,0)}{r^2}\, dr \, . \tag{24}$$

To transform the boundary condition (22) from the physical plane into the computing plane we introduce the coordinate transformation

$$\frac{\partial}{\partial n} = -\frac{1}{Br}\frac{\partial}{\partial \theta} \quad , \qquad \frac{\partial}{\partial s} = -\frac{1}{B}\frac{\partial}{\partial r} \tag{25}$$

where s is the distance measured along the wake and n is the distance normal to it (see Fig 3). Hence, the velocity components in the physical and computing plane are linked by the relationship

$$u = -\bar{v} \, , \qquad v = -\bar{u} \quad . \tag{26}$$

Thus, from (10), (22) and (25) we have along $\theta = 0$ the boundary condition that

$$\Delta(\Phi_\theta) = \frac{rS}{\rho}\frac{d}{dr}(\rho q \bar{\delta}^*_w) \equiv \sigma^{(1)}(r) \, . \tag{27}$$

A further effect to be included arises from the curvature of the wake. In order to match the pressure change across the wake in both the viscous and equivalent inviscid flows, it is necessary to introduce a boundary condition on the jump in the tangential velocity u across the wake (see Ref 22), such that

$$\Delta(u) = - q\kappa(\delta^*_w + \theta_w) \tag{28}$$

where θ_w is the momentum thickness and the curvature κ is given in Appendix E (equation (E-7))

$$\kappa = \frac{1}{q}\frac{\partial q}{\partial n} \quad . \tag{29}$$

In equation (28) q and κ are taken as the means of the values on each side of the wake. In the computing plane this condition is also applied along the line $\theta = 0$, and with the coordinate transformation (25), leads to a condition that

$$\Delta(\Phi_r) = BSq\kappa(\bar{\delta}^*_w + \bar{\theta}_w) \equiv \sigma^{(2)}(r) \tag{30}$$

along $\theta = 0$* . This is equivalent to

$$\frac{d}{dr}(\Delta\Phi) = \sigma^{(2)}(r) \tag{31}$$

so that

$$\Delta\Phi \equiv \Gamma(r) = \Gamma_0 - \int_r^1 \sigma^{(2)}(r)dr \quad . \tag{32}$$

A further change to the inviscid scheme, associated with the previous one, is introduced in order to allow for the effect of the curvature of the aerofoil and wake on the pressure change across the viscous layers. This change is greater in the equivalent inviscid flow than in the real viscous flow, and consequently the pressure on the surface of the aerofoil or the centre line of the wake (as calculated for the equivalent inviscid flow) needs to be adjusted before it is used to calculate the boundary layer. It is shown in Ref 22 that the required pressure increment is

$$\Delta p \doteq - \kappa\rho q^2(\theta + \delta^*) \tag{33}$$

and this is equivalent (approximately) to correcting the calculated velocity

* The appearance of the factor S in equations (30) and (34) is due to the fact that, as calculated in the present method, the curvature κ corresponds to that in the flow in the physical plane about an aerofoil of chord S (*cf* p.5), whereas $\bar{\delta}^*$ and $\bar{\theta}$ are non-dimensionalised with respect to the chord.

q to q' ,

where
$$q' = q[1 + S\kappa(\bar{\delta}^* + \bar{\theta})] \quad , \tag{34}$$

with a similar correction occurring for the velocity in the wake.

One other change in the basic inviscid scheme concerns the solution of the finite difference form of equation (9) at the trailing edge. For the inviscid case it is sufficient to set $\bar{u} = \bar{v} = 0$ in order to determine the coefficients in the equation. However, in the viscous case (*ie* for the equivalent inviscid flow) it is necessary to adopt a more sophisticated scheme in which the finite difference equations are developed from the governing partial differential equation before the transformation to the computing plane (see Appendix C) and $\bar{u}$ and $\bar{v}$ are not set to zero.

3 REPRESENTATION OF THE BOUNDARY CONDITIONS IN FINITE DIFFERENCE FORM

3.1 Boundary conditions on the aerofoil surface

The governing equation (9) is of the form

$$A\Phi_{\theta\theta} + B\Phi_{\theta r} + C\Phi_{rr} = D \tag{35}$$

where
$$\left.\begin{aligned} A &= (a^2 - \bar{u}^2) \quad , \quad B = -2\bar{u}\bar{v}r \quad , \quad C = (a^2 - \bar{v}^2)r^2 \\ D &= 2\bar{u}\bar{v}\Phi_\theta - \left((a^2 + \bar{u}^2) - 2\bar{v}^2\right)\Phi_r - (\bar{u}^2 + \bar{v}^2)(\bar{u}\omega_\theta + \bar{v}\omega_r)r^{-1} \end{aligned}\right\} \quad , \tag{36}$$

and applies to the flow outside the viscous layers. In order to determine a solution along a radial line the variables A, B, C and D are treated as known quantities (using values derived from the previous iteration), and (35) is represented in finite difference form by a tri-diagonal system of equations

$$a_{ij}\Phi_{i,j-1} + b_{ij}\Phi_{ij} + c_{ij}\Phi_{i,j+1} = d_{ij} \tag{37}$$

where, in turn, (37) is solved successively for each of the values of i from $m/2$ to mm and $m/2$ to 2 . The elements of the arrays a,b,c and d can be defined in terms of known values of A,B,C,D and Φ evaluated at the various mesh points. This is exactly the same method of solution as in the basic inviscid model, and the only difference occurs in determining values for the coefficients for $j = 1$, (*ie* at the aerofoil surface in the equivalent inviscid flow).

In order to represent Φ_{rr} in finite difference form on the circle $r = 1$, it is necessary to expand Φ in a Taylor series;

$$\Phi_{i2} = \Phi_{i1} - \delta r(\Phi_r)_{i1} + \tfrac{1}{2}(\delta r)^2(\Phi_{rr})_{i1} ,$$

which leads to

$$(\Phi_{rr})_{i1} = \frac{2}{(\delta r)^2}(\Phi_{i2} - \Phi_{i1}) + \frac{2}{\delta r}(\Phi_r)_{i1} . \tag{38}$$

The second term on the right-hand side of (38) can be evaluated by using the boundary condition (21). To determine $\Phi_{r\theta}$ on the circle $r = 1$, the expression

$$\Phi_{r\theta} = \tau^{(2)}(\theta) - \sin(\theta + \alpha) \tag{39}$$

is used,

where
$$\tau^{(2)} = \frac{d}{d\theta}\left(\tau^{(1)}(\theta)\right). \tag{40}$$

The remaining term, $\Phi_{\theta\theta}$, can be expressed in finite difference form in the normal manner. It is thus possible to represent (35) in finite difference form on the circle $r = 1$, and hence determine values for the coefficients a,b,c and d for $j = 1$ in terms of known values of A,B,C,D, Φ, $\tau^{(1)}$ and $\tau^{(2)}$ evaluated at various mesh points. The details of this are given in Appendix A2. The solution at the trailing edge point also differs from the inviscid solution, and this is described in Appendix C3.

On both surfaces of the aerofoil δ^* is usually an increasing function of s, whereas q and ρ are, by comparison, more slowly varying functions of s. Thus, from (17) to (20), we may expect $\tau^{(1)} < 0$ for all values of θ. By using (15) we have

$$v = -\frac{\tau^{(1)}}{\omega} \quad \text{on} \quad r = 1 \tag{41}$$

and thus $v > 0$, which corresponds to a distribution of sources on the aerofoil surface. The value of $|\tau^{(1)}|$ usually increases from the leading edge with the maximum value occurring either close to the trailing edge, or in the region of a strong shock, if one exists. Typical maximum values for $|\tau^{(1)}|$ are about 0.03. At the trailing edge point the slope of δ^* is discontinuous (unless the

aerofoil has a cusped trailing edge), but since

$$\tau^{(1)} = \pm \frac{B}{\rho} \frac{d}{ds} (\rho q \delta^*) \tag{42}$$

and $B \to 0$ as $\theta \to 0, 2\pi$, then $\tau^{(1)} \to 0$ at the trailing edge. However v is not specified at the trailing edge. This quantity tends to a non-zero constant, but its values can only be determined by examining the limit of (40) as $\theta \to 0, 2\pi$.

3.2 Boundary condition arising from the wake thickness effect

In order to solve the finite difference equations along the radial line $i = mm$, corresponding to $\theta = 2\pi$, it is necessary to calculate derivatives of Φ, with respect to θ, by central difference formulae. For this purpose the 'fictitious' value of Φ along the radial line $i = mp$ $(mm + 1)$ is introduced (see Fig 4). This may be defined as the analytic continuation of Φ beyond $\theta = 2\pi$, so that

$$\Phi_{mp,j} = \Phi_{mm,j} + (\delta\theta)(\Phi_\theta)_{mm,j} + \tfrac{1}{2}(\delta\theta)^2(\Phi_{\theta\theta})_{mm,j} + O(\delta\theta)^3 . \tag{43}$$

Now

$$\Phi_{2,j} = \Phi_{1j} + (\delta\theta)(\Phi_\theta)_{1,j} + \tfrac{1}{2}(\delta\theta)^2(\Phi_{\theta\theta})_{1,j} + O(\delta\theta)^3 . \tag{44}$$

Subtracting, we obtain

$$\Phi_{mp,j} = \Phi_{2,j} + \Gamma_j + \delta\theta\sigma_j^{(1)} + \tfrac{1}{2}(\delta\theta)^2\Delta(\Phi_{\theta\theta})_j + O(\delta\theta)^3 \tag{45}$$

where

$$\Gamma_j = \Phi_{mm,j} - \Phi_{1j} . \tag{46}$$

It is shown in Appendix D.4 that the effect of the $O(\delta\theta)^2$ term in (45) is small and can be ignored, so that (45) reduces to

$$\Phi_{mp,j} = \Phi_{2j} + \Gamma_j + \delta\theta\sigma_j^{(1)} . \tag{47}$$

For the inviscid case $\sigma_j^{(1)} = 0$ for all values of j, and Γ_j reduces to a constant, Γ_0. In the viscous case, if the wake curvature effect is ignored, the jump in Φ, given by Γ_j, remains as a constant. However, in the fully viscous case, when the wake curvature effect is included, Γ_j varies with j since there is a jump in Φ_r across $\theta = 0, 2\pi$. It is necessary to

apply the Kutta condition (13) at the trailing edge, as in the inviscid scheme. This condition ensures that in the computing plane $\bar{u}$ approaches a finite limit as $\theta \to 0,2\pi$; otherwise, without this restriction, u would be infinite at the trailing edge in the physical plane. In this manner it is possible to determine Γ_j at $j = 1$. If the wake curvature effect is neglected, this condition determines the constant Γ_0 , and hence $\Phi_{mp,j}$ is determined. When the wake curvature effect is included, Γ_j , for $j \neq 1$, can be determined from equation (46), where details of the method of obtaining Φ_{ij} are given in the following section.

Along the wake we can expect δ^* to be a decreasing function of s . Thus we may expect $\sigma^{(1)}$ to be positive while from (22) and (27) we have

$$\Delta v = - \frac{r\sigma^{(1)}}{\omega} \quad ; \tag{48}$$

and hence $\Delta(v) < 0$ for all r . This corresponds to a distribution of sinks along the line $\theta = 0$. The function $\sigma^{(1)}$ is well defined and it can easily be represented in finite difference form by central differences. The function has no singularities either as $r \to 0$ or as $r \to 1$; in both cases $\sigma^{(1)} \to 0$. Thus Δv at the trailing edge can be determined by examining the limit of (48), as $r \to 1$. In the examples considered this value has been found to be non-zero and finite. For a typical aerofoil $\sigma^{(1)}$ attains its maximum value, of about 0.03, at about 5% of the chord behind the trailing edge.

3.3 Boundary condition arising from the wake curvature effect

The effect of this boundary condition is to alter, from the basic inviscid scheme, the manner in which the value of Φ along the radial line $i = 1$ (corresponding to $\theta = 0$), is derived from the value of Φ along the radial line $i = mm$ (corresponding to $\theta = 2\pi$). For the inviscid case, Φ_{ij} is obtained by adding a constant Γ_0 to $\Phi_{mm,j}$. When the wake curvature effect is included a similar situation exists, except that we must treat Γ as a function of r , as shown by equation (32). By applying (30) in finite difference form (using central differences) we obtain

$$(\Phi_{mm,j-1} - \Phi_{mm,j+1}) - (\Phi_{1,j-1} - \Phi_{1,j+1}) = 2(\delta r)\sigma_j^{(2)} \quad . \tag{49}$$

(Note that j decreases as r increases.) In order to reduce the determination of Φ_{ij} to an iterative procedure we require a further equation.

By considering the jump in Φ_{rr} we obtain

$$(\Phi_{mm,j-1} - 2\Phi_{mm,j} + \Phi_{mm,j+1}) - (\Phi_{1,j-1} - 2\Phi_{1j} + \Phi_{1,j+1}) = (\delta r)^2 \sigma_j^{(3)}, \quad (50)$$

where

$$\sigma^{(3)}(r) = \frac{d}{dr}\left(\sigma^{(2)}(r)\right) . \quad (51)$$

Combining (49) and (50) gives

$$\Phi_{1j} = \Phi_{mm,j} - \Gamma_{j-1} + (\delta r)\sigma_j^{(2)} + \tfrac{1}{2}(\delta r)^2 \sigma_j^{(3)} \quad (52)$$

since

$$\Gamma_{j-1} = \Phi_{mm,j-1} - \Phi_{1,j-1} . \quad (53)$$

Equations (52) and (53) can be used to develop an iterative procedure to determine Φ_{1j} for $j = 2...n$. As an initial condition the value of Φ_{11} is required. This is given by

$$\Phi_{11} = \Phi_{mm,1} - \Gamma_1 \quad (54)$$

where Γ_1 is determined from the Kutta condition at the trailing edge, as described in the previous section.

The function $\sigma^{(2)}$ is given by equation (30). In Appendix E a rigorous definition of the flow curvature, κ , in a general orthogonal curvilinear coordinate system (x_1,x_2) is obtained, and a suitable approximation for the present problem is given by equation (E-9). To obtain the flow curvature in the wake we set

$$x_1 = -r , \quad x_2 = -\theta , \quad h_1 = B , \quad h_2 = Br \quad (55)$$

and obtain

$$\kappa \equiv \kappa_0 + \kappa_1 = -\frac{1}{r}\frac{\partial}{\partial\theta}\left(\frac{1}{B}\right) - \frac{1}{B}\frac{\partial}{\partial r}\left(\frac{\bar{u}}{\bar{v}}\right) . \quad (56)$$

The first term represents the curvature of the line $\theta = 0$, and the second term arises from the curvature of the displacement surface relative to the line $\theta = 0$. This latter term takes slightly different values on either side of the line $\theta = 0$, when the wake thickness and curvature effects are included; hence a mean value is used to define $\sigma^{(2)}$.

The form that the expression $\sigma^{(2)}$ takes, both as $r \to 0$ and as $r \to 1$, needs careful consideration. The limits of $\sigma^{(2)}$ are determined by the magnitude of $B\kappa$. Now as $r \to 0$, B has a singularity of $0(r^{-2})$. However, in this region the effect of the two terms in (55) cancel, and when $\sigma^{(2)}$ is evaluated in finite difference form the resulting curve tends smoothly to zero as $r \to 0$.

There is greater difficulty in evaluating $\sigma^{(2)}$ in finite difference form near the trailing edge. This is largely due to the singular behaviour of the flow in this region in the present mathematical formulation of the problem. The situation is as follows: for a purely inviscid flow (or for the 'equivalent inviscid flow' if the wake curvature effect is *not* taken into account), it can be shown that in general the curvature of the dividing streamline approaches infinity at the trailing edge, like $s^{-\frac{1}{2}}$ (where s is the distance from the trailing edge); and this implies that $B\kappa$ approaches a finite, but non-zero, limit (since $B \sim s^{+\frac{1}{2}}$). However, when the effect of the wake curvature (equation (28)) is included, the interaction with the flow causes the curvature of the wake to be reduced to a finite value at the trailing edge (just as in the somewhat analogous case of the 'jet-flap' problem[32]); so that now $B\kappa \to 0$ and hence $\sigma^{(2)} \to 0$. This is of course essential in order to keep the pressure jump across the wake in the inviscid flow model finite at the trailing edge, since from (6), (26) and (30) we observe that

$$\Delta u = -\frac{\sigma^{(2)}}{B} . \tag{57}$$

In view of the facts stated above, it is not surprising that numerical difficulties occur in the evaluation of κ (and hence $\sigma^{(2)}$) near the trailing edge, particularly at the early stages of the iteration process. Referring to equation (56), we see that part of the trouble is due to the fact that the first term, κ_0 (the curvature of the line $\theta = 0$) does in general (for a cambered aerofoil) have a singularity (of order $\sigma^{-\frac{1}{2}}$) at the trailing edge, so that the finite value of κ which should eventually emerge from the calculations can only be achieved as a result of cancellation by an equal and opposite singularity in the second term, κ_1. Thus, although we do not actually need to know the value of κ at the trailing edge itself, we are in a situation where the values calculated at neighbouring points are inevitably subject to

some degree of arbitrariness. For example, the first term κ_0 can be evaluated by central difference analogous of either of the two (mathematically equivalent) equations

$$B\kappa_0 = \frac{1}{Br}\frac{\partial B}{\partial \theta} \tag{58}$$

or

$$B\kappa_0 = -\frac{B}{r}\frac{\partial}{\partial \theta}\left(\frac{1}{B}\right) . \tag{59}$$

Now the first of these equations would give an infinite value for $B\kappa_0$ at $r = 1$, $\theta = 0$, while the second would give the value zero; so clearly the values at the first few points behind the trailing edge will differ appreciably according to which formula is chosen. [In fact, the second formula (59) is used.] Furthermore, if the second term, $\kappa_1 = -\frac{1}{B}\frac{\partial}{\partial r}\left(\frac{\bar{u}}{\bar{v}}\right)$, were to be evaluated by a standard central difference expression, then it would not be possible to obtain a value at the first point behind the trailing edge, because the value of $\bar{u}$ is indeterminate at the trailing edge; so some extrapolation would be needed at this point.

As a result of these considerations, and after a good deal of numerical experimentation, the following procedure has been adopted. At a typical point P_j on the line $\theta = 0,2\pi$ (defined by $r = 1 - (j - 1)\delta r$), the value of $q\kappa$ is taken to be that calculated at the point P_{j+1} using the central difference form of equation (56). This is analagous to using a backward difference scheme (with respect to r)*. Finally, the values of $\sigma^{(2)}$ (equation (30)) are smoothed using the formulae (78) and (79) of section 4.3. Over the range of aerofoils that have been tested this procedure leads to a finite difference scheme which is numerically stable. In a typical situation it is found that $\sigma^{(2)}$ rises smoothly from zero at the trailing edge and reaches a maximum value at about 2-3% of the chord downstream of the trailing edge, and then decays to zero. Further justification for the use of this procedure is given in section 5.2.

3.4 Effect of surface and wake curvature

As we have already mentioned (see p 11), the calculated pressures on the aerofoil surface and along the wake need to be adjusted to take account of the flow curvature. The following adjustment to the calculated velocity q is required in order to give the velocity q' on the aerofoil surface used in

---

* The procedure described here is used with the 'coarse' (80 × 15) mesh. When the 'fine' (160 × 30) mesh is used, the value at P_j is taken to be that calculated at P_{j+2}.

determining the pressure distribution:

$$q' = q[1 + S\kappa(\bar{\delta}^* + \bar{\theta})] \tag{60}$$

where κ is the curvature of the displacement surface over the aerofoil. If the curvature is defined in a similar manner to the curvature of the wake, then setting

$$x_1 = \pm\,\theta,\ x_2 = r,\ h_1 = Br,\ h_2 = B \tag{61}$$

in equation (E-9) we obtain

$$\kappa \equiv \kappa_0 + \kappa_1 = \frac{1}{B^2}\,\frac{\partial}{\partial r}\,(Br) - \frac{1}{B}\,\frac{\partial}{\partial \theta}\left(\frac{\bar{u}}{\bar{v}}\right) . \tag{62}$$

The first term defines the curvature of the aerofoil surface and the second one determines the additional curvature arising from the displacement effect.

However, the curvature, as expressed by equation (62) is not satisfactory for determining a finite difference form for the expression, since the first term must be obtained by a first order (one-sided) approximation from a Taylor series expansion, and this was found to lead to inaccurate values for κ_0. Near to the trailing edge the expression for κ has two relatively large terms of opposite signs, so that an accurate evaluation of each is required. An alternative approximation to the curvature κ is given by

$$\kappa = \frac{d^2}{ds^2}\,(y + \delta^*) \tag{63}$$

(see equation (E-10) in Appendix E).

With the aid of (17) a simple finite difference approximation to (63) may be obtained from

$$\kappa = \frac{S}{\omega}\,\frac{d}{d\theta}\left\{\frac{1}{\omega}\,\frac{d}{d\theta}\,(\bar{y} + \bar{\delta}^*)\right\} , \tag{64}$$

where $\bar{y}$, like $\bar{\delta}^*$, is non-dimensionalised with respect to the chord S. This is evaluated by a standard central difference expression over an interval $2\delta\theta$, rather than $\delta\theta$, to enable the known values of ω at mesh points to be used. There are difficulties especially on the fine grid, of ensuring values of δ^* sufficiently smooth to obtain smooth second derivatives of the function. This occurs particularly near to the trailing edge where large variations in

δ^* occur. Hence it is necessary to use the coarse grid values of κ even for the fine grid, with linear interpolation and smoothing employed to determine values at intermediate grid points.

Over most of the aerofoil the curvature of the aerofoil surface is negative (convex), while that of the displacement surface is positive; only near to the trailing edge does the second effect usually predominate. The curvature effects, given by (64), are most important in this region, because of the relatively large values of δ^* . They may also become important in the region of a strong shock. For a lifting aerofoil typical maximum values of κ of about 0.4 occur close to the trailing edge on the upper surface, leading to values of $(q' - q) \sim 0.025$. In the process of an iterative scheme, with an interaction between the pressure distribution and the boundary layer development, it may be expected that in a converged solution the difference between q and q' will be substantially reduced.

In the wake the calculated velocity $q_\pm$ needs to be modified to give

$$q'_\pm = q_\pm\left[1 \pm S\kappa_\pm(\bar{\delta}^*_w + \bar{\theta}_w)_\pm\right] \tag{65}$$

where the upper and lower signs refer to the upper and lower surfaces of the wake respectively. The finite difference form of the expression for κ has already been described in the previous section. Without this effect included it is seen from (28) and (30) that

$$\Delta(u) = -\frac{\sigma^{(2)}}{B} \quad . \tag{66}$$

When the curvature correction is included we have, from (65)

$$\Delta(q') \doteq \Delta(u) + S\left[(q\kappa)_+(\bar{\delta}^*_w + \bar{\theta})_+ + (q\kappa)_-(\bar{\delta}^*_w + \bar{\theta}_w)_-\right] \tag{67}$$

and on substituting for $\Delta(u)$ and using the definition of $\sigma^{(2)}$ we have

$$\Delta(q') \doteq 0 \; . \tag{68}$$

Thus the velocities used to calculate the pressure distribution on the upper and lower sides of the wake are effectively the same.

4 FORMULATION OF THE INVISCID-VISCOUS INTERACTION SCHEME

4.1 The basic scheme

A basic feature of the interactive scheme is that the mapping analysis is performed once only, for a particular aerofoil. (In the VGK package the mapping analysis can be performed by either one of two alternative methods; *ie* either from a program based on the original G & K[2,3] mapping analysis or from the original Sells'[16,17] analysis. For further details see Ref 11.) A solution is then sought for a particular free-stream Mach number, angle of incidence, Reynolds number and position of the transition points. It is usual to increase the Mach number, increase incidence, or alter the viscous parameters in steps as with the basic inviscid program in order to calculate a solution. This is necessary in order to avoid problems of convergence. Thus, for an initial solution, after the mapping analysis, $\tau^{(i)}$ and $\sigma^{(i)}$, $i = 1,2$, are initialized to zero and the Φ-field is initialized according to the basic G & K analysis. At the start of the next calculation all parameters take the final values of the previous solution. For any solution a calculation can be performed either on a coarse (normally 80 × 15) or a fine (160 × 30) grid. It is usual to use the coarse grid solution as a basis for the fine grid solution. On proceeding from a coarse to a fine grid, linear interpolation is employed to determine initial values of the solution at the additional grid points.

At the start of a particular solution, a prescribed number, k_1, of inviscid flow field iterations is performed (with the current boundary conditions) before a new boundary layer is calculated. (The parameter k_1 is termed INVISC(1) in the FLOW program in the VGK package[11].) This allows the iterative procedure for the flow field calculations to respond to the changes in the basic parameters and so to avoid calculating boundary layers for unrealistic pressure distributions. This procedure is most important for the initial solution after the mapping and for fine grid solutions with strong shocks. Usually it is sufficient to set k_1 equal to 10 for these situations.

Before calculating the boundary layer, the velocity is calculated on the aerofoil surface, $r = 1$, and along the line $\theta = 0$, representing the wake. On the aerofoil surface the velocity q is given by

$$q^2 = \bar{u}^2 + (\tau^{(1)}/\omega)^2 \qquad (69)$$

where $\bar{u}$ is determined from (10) by using the latest values of Φ. On the upper surface of the wake

$$q_+^2 = \bar{u}_+^2 + \bar{v}_+^2 \tag{70}$$

where $\bar{u}_+$ and $\bar{v}_+$ are calculated from (10) similarly. On the lower surface of the wake the jump conditions on u and v can be used to determine

$$\bar{u}_- = \bar{u}_+ - \frac{r}{\omega}\sigma^{(1)} \tag{71}$$

$$\bar{v}_- = \bar{v}_+ - \frac{r^2}{\omega}\sigma^{(2)} \tag{72}$$

from which q_-^2 may be calculated. The velocities q, q_+ and q_- are then corrected to allow for curvature, according to equations (60) and (65), in order to determine q'. The pressure coefficient, C_p, may be derived from the equation

$$C_p = \frac{2}{\gamma M_\infty^2}\left\{\left[1 + \frac{\gamma - 1}{2} M_\infty^2(1 - q'^2)\right]^{\gamma/(\gamma-1)} - 1\right\} \tag{73}$$

and in turn the pressure p/H, which is the ratio of static pressure to total pressure, may be obtained from the equation

$$p/H = \left(\frac{\gamma}{2} M_\infty^2 C_p + 1\right) \Big/ \left(1 + \frac{\gamma - 1}{2} M_\infty^2\right)^{\gamma/(\gamma-1)} . \tag{74}$$

This pressure distribution is used to calculate the current boundary layer.

The boundary layer on each surface is calculated separately. In order to determine the wake development, the computation over each surface of the aerofoil is extended beyond the trailing edge to obtain separately the part of the wake on either side of the dividing streamline originating at the trailing edge[14]. The pressure distribution is specified at mesh points around the circle $r = 1$ and along the line $\theta = 0$, but is specified for the boundary layer analysis as values at the corresponding x and z coordinate points, starting at the stagnation point rather than the leading edge and proceeding downstream towards infinity on each surface.

The boundary layer calculations produce values for the (non-dimensional) displacement thickness, $\bar{\delta}^*$, and the momentum thickness, $\bar{\theta}$, at the various mesh points. In the wake the separate values for $\bar{\delta}^*$ and $\bar{\theta}$, obtained on either side of the dividing streamline, are added together to form the total displacement thickness, $\bar{\delta}^*_w$, and the total momentum thickness, $\bar{\theta}_w$. Equations (19), (20), (27), (30), (40) and (51) are used to calculate τ and σ, and hence to determine the boundary conditions to be applied for the flow field calculations. Current values of Φ are used to form the values for q and ρ which are needed in order to evaluate τ and σ. Values of the curvature κ are determined from equations (56) and (62) in a similar manner.

Under-relaxation is employed in order to determine the actual values of $\tau^{(i)}$ and $\sigma^{(i)}$ used in the boundary conditions for the flow field calculations. Thus, at the previous boundary layer calculation a value of $\tau^{(i)}$ existed, say $\tau^{(i)}_{old}$, and a new value, $\tau^{(i)}_{new}$ say, has just been calculated. The actual value of τ used for the flow field calculations is given by

$$\tau^{(i)} = \tau^{(i)}_{old} + \varepsilon \left(\tau^{(i)}_{new} - \tau^{(i)}_{old} \right) \qquad (75)$$

where ε is an under-relaxation parameter, (termed ABCMAX in the VGK program[11]). A number of flow field iterations are performed with the new boundary conditions, the number being determined by a parameter k, (termed NVISCR in the VGK program[11]). Values for τ, σ and κ are not recalculated until after the next boundary layer calculation, (although it would be possible to update these values after every flow field calculation since new values of Φ are available).

After k flow field iterations have been performed the whole cycle is repeated. Thus, the current velocity on the aerofoil surface and along the wake is recalculated, and then the current pressure distribution is used to calculate the boundary layer. Hence, new values for $\tau^{(i)}$, $\sigma^{(i)}$ and κ are obtained and further flow field calculations are performed with the new boundary conditions. This process continues until either certain convergence criteria are satisfied or until a specified number of iterations are completed.

At the completion of the iterative procedure the lift and drag coefficients on the aerofoil are calculated. Firstly, the pressure distribution around the aerofoil is integrated and then separated into component form in order to obtain the lift coefficient, C_L, and the pressure-drag coefficient, C_{DP}. Similarly, the skin-friction drag coefficient, C_{DF}, is obtained through integrating the

shear-stress over the aerofoil surface. Also calculated is the viscous drag coefficient, C_{DV}, which is obtained from the momentum decrement far downstream and neglects any wave drag. The total drag coefficient, C_{DT}, is obtained from $C_{DP} + C_{DF}$; for subcritical flow C_{DT} should (approximately) equal C_{DV} (see section 5.3).

4.2 Convergence of the interactive scheme

The two parameters k and ε affect the convergence of the iterative scheme, and their effects are related. As the value of k increases, so relatively fewer boundary-layer calculations are performed, and it is therefore necessary to increase the under-relaxation parameter, ε, in order to produce the full effect of the boundary conditions in the flow field calculations. Ideally, to make sure the calculation has been fully corrected for viscous effects, ε should be set as high as possible and k as small as possible, but upper and lower bounds respectively need to be set otherwise the iterative process becomes divergent. These bounds are dependent on the particular solution being calculated and the starting conditions that prevail. On the basis of some numerical experiments a reasonable choice is to set $\varepsilon = 0.15$ and $k = 5$. For some subcritical solutions it is possible to increase ε slightly, while for cases especially on the fine grid, and with high Mach number or incidence, it is necessary to reduce ε significantly in order to achieve convergence.

The convergence test in the inviscid situation is based on examining changes from the previous iteration, both in Φ and the jump in Φ at the trailing edge. When the maximum value of any change, called the error level μ, is less than the convergence parameter set, then the solution is said to have converged. For a viscous solution it is necessary to include in this test, in some manner, the viscous parameters involved in the solution.

Originally a convergence test similar to that used in the small perturbation RAE Transonic Aerofoil Program was employed[7,8]. In this test the inviscid convergence test is unaltered, and when a specified convergence parameter is reached the calculation is completed by setting the under-relaxation factor ε equal to 1 in calculating $\tau^{(i)}$ and $\sigma^{(i)}$, so that the boundary conditions appropriate to the full current boundary-layer solution are used in the next flow field calculation. Further iterations are performed in the normal manner until the convergence limit is reached once more. This is considered as the converged solution. In a normal situation the solution is stable to this

disturbance and convergence is reached again within a few iterations. If the convergence is not achieved within a specified number of iterations then the process is repeated, when convergence is reached, by once more setting ε equal to 1. This procedure is repeated until convergence is attained within the specified number of iterations.

It was found with this scheme that for some cases, especially on a fine grid at a high Mach number or incidence, a solution which had converged according to the original (inviscid) criteria would not converge again when the full boundary-layer correction was applied (*ie* by setting $\varepsilon = 1$). It appears that this method can give too large a disturbance to the iterative procedure of the flow field calculation, even though it was otherwise converging satisfactorily. It therefore seems preferable to allow the solution to proceed without disturbing it in this way, and to include a further convergence test, based on examining the boundary-layer parameters. Hence, the viscous convergence test now adopted is to examine changes in the calculated values of τ from the previous iteration, and to determine a viscous error level, μ_v, as the maximum change, *ie*

$$\mu_v = \max \left(\tau^{(1)} - \tau^{(1)}_{old} \right) . \tag{76}$$

Both this test and the usual test on the values of Φ must be successful before convergence is said to be achieved.

Various schemes were tried to see if the rate of convergence could be increased. The underlying idea behind each of the proposals is that, since convergence problems usually occur in the initial stages of the iterative procedure for a new solution, then it would be possible to vary the under-relaxation parameter so that it is kept low initially and increased as a converged state is approached. Firstly, a simple procedure was introduced whereby the boundary-layer calculation is not performed when it would normally be due; if at this stage the inviscid error level, μ, is above a certain level then the iteration is ignored as far as counting iterations between boundary-layer calculations is concerned. Secondly ε is allowed to vary so that

$$\varepsilon = \min (\varepsilon_0, \varepsilon'(x,\mu)) \tag{77}$$

where ε_0 is a specified value of ε, and ε' varies with both x and μ. This variation in ε' is arranged so that when μ falls below a certain level

then $\varepsilon = \varepsilon_0$, and for larger values of μ the value of ε' decreases as μ increases. In this manner ε is kept low while the error level is high. The variation of ε' with x enables lower values of ε to be specified over the rear of the aerofoil where the maximum values of $\tau^{(i)}$ and $\sigma^{(i)}$ occur. This scheme also operates only while μ is relatively high. Although these various schemes were very successful for certain examples and increased the rate of convergence, universal parameters could not be found so that the schemes could be guaranteed to work for the general case. The difficulty seems to arise because the boundary layer can be very sensitive to small changes in pressure gradient and μ is not a good measure of this. A more rational approach tried was to relate ε to the boundary layer iteration count. Thus for the first few boundary-layer calculations the value of ε would be increased gradually to its full value ε_0. This scheme was also successful for particular solutions which otherwise would have diverged, but for other cases it did take more iterations for τ and σ to converge. Again it was felt that for general ease of use in the computer program, fixed values of ε and k should be specified ($k = 5$ and $\varepsilon = 0.15$ on the coarse grid and 0.075 with the fine grid). The option is available of altering these values if convergence problems appear. It is worthwhile to note that, for comparison with the RAE small-perturbation Transonic Aerofoil Program (VISTRAN), typical values used there are $\kappa = 10$ and $\varepsilon = 0.1$. The difference is consistent with arranging for the full effect of the boundary layer to be included in the calculation before convergence of the basic inviscid method would occur. The G & K method tends to converge, under normal circumstances, in a smaller number of iterations than the TSP method.

4.3 Smoothing and extrapolation near to the trailing edge

The trailing-edge point is a mesh point and since the transformation is singular at this point it is not possible to obtain directly values for $\bar{u}$ and $\bar{v}$ at the trailing edge. Furthermore, although the value of Φ at the trailing edge point is known it has been found to be unreliable when used to obtain $\bar{u}$ and $\bar{v}$ at the neighbouring points. Thus an extrapolation procedure is used to obtain values of q' at the trailing edge point and also close to it. Because of the usual density of mesh points near to the trailing edge, this implies, for both the coarse and fine grids, that the last mesh point on the aerofoil surface at which the velocity is calculated from Φ is at about 99% of the chord. Similarly, the first mesh point in the wake used is less than 1% of the chord downstream of the trailing edge.

The reason for the difficulty in the region of the trailing edge would seem to be that an iterative method is used in the inviscid-viscous interactive procedure, so that the current pressure distribution, rather than a smoother one resulting from a converged solution, is used to calculate the boundary layer, and similarly the modified boundary conditions are formed by using the velocity determined from current values of Φ which might not be smooth. The particular numerical scheme employed in the basic inviscid flow-field calculations sometimes gives, in the initial stages of the iterative procedure, an inconsistency in the extrapolated values of the velocity q' at the trailing edge, depending on whether the point is approached along one of the aerofoil surfaces or along the wake. It has been found that if the values of q' on either side of the trailing edge are not obtained by the extrapolation mentioned, then an oscillation may develop during the iterative procedure, in the values of τ and σ near to the trailing edge, which causes failures in the calculation.

The following scheme is incorporated in order to avoid these problems. For a coarse grid, on both upper and lower surfaces, the velocity q', on the aerofoil surface at one mesh point before the trailing edge is obtained by a linear extrapolation in x from the two values upstream of this point. A further linear extrapolation is employed to obtain values of q' at the trailing edge. A similar treatment takes place in the wake. The values of q' at the trailing edge are averaged to produce a trailing-edge velocity. A similar procedure takes place with the fine grid calculation, but to produce compatibility with the coarse grid solution the extrapolation procedure assigns values to q' at the trailing edge and at the three mesh points on either side.

A smoothing routine is employed to determine the actual values of q' which are used to determine the pressure. This routine is employed for all values of q' in the wake and for all values of q' over the last 10% of the chord, being progressively relaxed for the portion between 90% and 80% of the chord of the aerofoil. (This is achieved by a linear interpolation between the smoothed and unsmoothed values.) For the coarse grid, three iterations of smoothing are used, where the smoothed value, $\hat{q}'$, is given at the ith mesh point by

$$\hat{q}'_i = \tfrac{1}{4}(q'_{i-1} + 2q'_i + q'_{i+1}) \ . \qquad (78)$$

The value of q' at the trailing edge is fixed and remains unaltered. For the fine grid, the smoothing is obtained by ten iterations of a second order scheme

where

$$\hat{q}'_i = \frac{1}{16}(-q'_{i-2} + 4q'_{i-1} + 10q'_i + 4q'_{i+1} - q'_{i+2}) \quad . \tag{79}$$

At one mesh point before the trailing edge the first order smoothing given by (78) is used.

The smoothed values, $\hat{q}'$, rather than q' are not only used in equation (73) to determine the pressure, but also in determining values for τ and σ. The values of δ^* and θ resulting from the boundary-layer calculations are not smoothed. An option exists in the FLOW program[11] to enable the current values of τ and $\sigma^{(1)}$ to be smoothed near to the trailing edge, although this is not usually required. The smoothing routine is always used to obtain values for $\sigma^{(2)}$.

5 RESULTS FROM THE VGK PROGRAM

5.1 Basic test examples and features of the inviscid program

During the development of the program three aerofoils, with significantly different characteristics, were used as test cases. Subsequently the program has been used to obtain results for a variety of other aerofoils. The three aerofoils chosen were the NACA 0012, RAE 2822 and Korn Aerofoil No.1. The first, NACA 0012 is a conventional symmetrical aerofoil. The second aerofoil, RAE 2822 has a design pressure distribution of 'roof-top' type with moderate camber and some 'rear loading'. The third, Korn Aerofoil No.1, was designed by the inviscid hodograph method of Garabedian and Korn[3] to have a shock-free pressure distribution at the design condition, with the intention that the shock waves that form at off-design conditions should remain weak over a wide range of conditions. Experimental results are available for each aerofoil for comparison with the theoretical results from the program. An assessment of the measure of agreement between theory and experiment is handicapped by some uncertainty in the magnitude of wind-tunnel corrections necessary to reconcile measured data and free-air results. Other theoretical results are also available for comparison, although those presented here only include results for the Korn No.1 aerofoil.

As described earlier there exist two alternative programs in the VGK package for performing the mapping analysis. One is based on the G & K mapping routine[3], and the other on the original Sells' mapping program[17]. Blockley[23] has investigated the performance of the two alternative programs and suggested

that the latter program is preferable, mainly because it has been found that the Sells' routine would give a well-converged result for some aerofoils, while the G & K routine would not. This occurs primarily on thin aerofoils and particularly those with a small leading edge radius. In this work we did not investigate the mapping procedure directly, but we did construct a test which involves the results of the mapping analysis.

For each of the three aerofoils a mapping was performed using both the Sells' and the G & K programs with their respective default values chosen but without smoothing the original ordinates. An inviscid solution was then sought, for subcritical conditions, based on the two alternative mapping results. A highly converged solution was obtained, by allowing 100 iterations on the coarse grid and then a further 100 iterations on the fine grid. At this stage all the solutions seem to have converged fully in that no significant changes take place in the value of C_L from one iteration to the next. Results for the three aerofoils are shown in Table 1. For the NACA 0012 aerofoil a flow at zero incidence was chosen. The values of C_L obtained from both solutions were not precisely zero, although the accuracy was significantly better with the

Table 1

Comparison of solutions for different mapping procedures

Aerofoil	M_∞	α	Max local M	Sells		G & K	
				C_L	C_{DP}	C_L	C_{DP}
NACA 0012	0.72	0.0	0.98	0.00001	0.00012	0.00015	-0.00033
RAE 2822	0.676	1.06	0.97	0.5681	0.00012	0.5689	0.00042
Korn No.1	0.65	1.0	1.09 (Sells)	0.6205	0.00030		
			1.05 (G & K,400)			0.6109	0.00413
			1.07 (G & K,800)			0.6111	0.00113

solution based on the Sells mapping. Similarly, the value of C_{DP} predicted for the two aerofoils at inviscid subcritical conditions (which should be zero) also demonstrates that more accurate solutions are obtained by using the Sells mapping. For the Korn Aerofoil No.1, a slightly supercritical flow was obtained on the upper surface of the aerofoil but no sign of a shock wave exists in the pressure distribution. For this case significantly different estimates of C_{DP} are predicted, while the value of C_L also differs by nearly 2%. Because the G & K mapping does not seem to have converged very well with the recommended values it was performed again for 800 iterations, instead of 400. Subsequently the results from the inviscid flow calculation show a better agreement with the

results originating from the Sells mapping; but the comparatively large change in the value of C_{DP} between the calculations using 400 and 800 iterations suggest that even the latter may not be fully converged. This exercise demonstrates the differences that can occur by using different mapping procedures, and the importance of obtaining a well converged result from the mapping program. It also seems to indicate the superiority of the Sells' mapping program, and accordingly this mapping program was used for all the results shown subsequently in this Report.

In the inviscid G & K program there exist various parameters which can be varied by the user. The effect of altering these parameters has already been investigated by, for example, Blockley[23] and O'Mahoney *et al*[24]. Therefore, the corresponding parameters in the FLOW program of the VGK package are not altered as their effects have already been studied. In particular, the relaxation factors XS, XM and XPHI, which control the inviscid iterative procedure, and the artificial viscosity parameter, EP , are all allowed to take their default values. Similarly, consideration is not given to the effect either of altering grid size (although the effect of changing from one grid to another is considered), or of varying convergence levels. A converged solution is said to be attained when the inviscid error level falls below 0.0001 on the coarse grid or 0.00005 on the fine grid, together with a successful test on the viscous convergence parameter, which should fall below 0.0025 on the coarse grid and 0.001 on the fine grid. To determine that the values of C_D obtained are accurate, it is really necessary to examine the variation of C_D with iteration.

5.2 Interim steps in the final viscous solution

The separate effects of the boundary conditions on the aerofoil surface and along the wake have been studied. Thus different solutions can be obtained from the FLOW program of the VGK package by altering the parameter IVP, and these consist of:-

(a) - IVP = 0 - an inviscid solution;

(b) - IVP = 1 - displacement thickness effect is included in the aerofoil surface only;

(c) - IVP = 2 - in addition, the wake thickness effect is included;

(d) - IVP = 4 - in addition, the wake curvature effects and the curvature corrections to pressure on the aerofoil and wake are included.

A sequence of solutions was obtained, using the RAE 2822 aerofoil, to examine the various types of solution. Thus solutions were obtained for the following cases for each of the conditions (a)-(d):-

	M_∞	α	Reynolds No. (based on chord)	Transition location (in chords)
(i)	0.676	1.06°	5.76×10^6	0.11
(ii)	0.676	2.03°		
(iii)	0.7	2.3°	6.5×10^6	0.03
(iv)	0.725	2.3°		
(v)	0.725	2.62°		
(vi)	0.725	2.93°		

These range from a subcritical case through to a supercritical one with a strong shock. Example (i) has been used previously for other theoretical results, and experimental results from the RAE 8ft × 6ft tunnel are available for comparison with cases (ii), (iv) to (vi) (see section 5.4.2). Fine grid solutions were obtained for each of these cases, and (iii) was used as an interim step in the solution. The under-relaxation parameter ε was set at 0.15, until a fine grid solution was sought for case (v) when the parameter was reduced to 0.075.

A major problem experienced in the analysis was to obtain a converged solution with the wake curvature effects included. It has been explained in section 3.3 how this was achieved. For the first solution at $M_\infty = 0.676$, $\alpha = 1.06$ the values of the curvature terms in the wake, κ_0 and κ_1, defined by equation (56), and expressed in finite difference form, are shown in Fig 7. These were evaluated on the coarse grid from a solution in which the curvature effects were not included (IVP = 2). This leads to values of $\sigma^{(2)}$ which increase very steeply as the trailing-edge is approached, and these are shown in Fig 8 by the dotted line. Initially, a scheme was proposed whereby the values of $\sigma^{(2)}$ that were calculated (and setting $\sigma^{(2)} = 0$ at $r = 1$), were smoothed by using the smoothing formulae of section 4.3. The values of $\sigma^{(2)}$ resulting from this model are shown in Fig 8 by the dashed line, for a converged solution with wake curvature effects included (IVP = 4). However, this scheme provided a model which is numerically stable for this example, but the solutions diverged for the more severe cases (iv) to (vi). The scheme described in section 3.3, which was adopted, led to values of $\sigma^{(2)}$ which are also shown in Fig 8 by the full line for a converged solution with wake curvature effects included (IVP = 4). The value of C_L has been altered for a fine grid solution from 0.420 to 0.430 by this change in the model. It is perhaps disappointing that this change in lift occurs between the two solutions, since it suggests that the effects of wake curvature are slightly underestimated by the new scheme. The advantage of the new scheme, however, is that it provides solutions which have converged for all the test cases (i) to (vi) in roughly the same number of iterations whether or not the curvature effects are included. (A fully viscous solution for $M_\infty = 0.676$, $\alpha = 1.06$ is shown in Fig 15.)

An interesting test of the physical plausibility of the mathematical model used in the present method is to examine the smoothness of the effective displacement surface in the neighbourhood of the trailing edge. We can calculate an approximation to the slope of this surface in the following way. Over the aerofoil surface, we simply take the value of $\frac{dy}{dx} + \frac{v}{u}$. For convenience, the sign of v on the lower surface of the aerofoil is reversed, for this exercise only. In the wake, it is necessary to calculate first the slope of the line $\theta = 0$, by integrating κ_0 with respect to x from the trailing edge (using as starting condition the mean value of the slopes of the upper and lower surfaces of the aerofoil at the trailing edge) and then to add to this the appropriate value of $\frac{v}{u}$. An example is shown in Fig 9, using converged solutions (with the coarse grid) for the aerofoil RAE 2822, at $M_\infty = 0.676$, $\alpha = 1.06^\circ$. Values at the trailing edge and at grid points either side of the trailing edge are omitted since they are determined only by linear extrapolation. Results are given both for the full method and for the version in which curvature effects are not included. These results show that there exists a small discontinuity in the slope of the effective displacement surface at the trailing edge when curvature effects are not included, but that this discontinuity virtually disappears when they are included.

Comparisons of the important features of the fine grid results for the four types of solution, with IVP = 0, 1, 2 and 4, are shown in Table 2 for an example with fully subsonic flow and for an example with supercritical flow termination by a shock wave. It is seen that the trailing edge pressure does not vary greatly, for a particular value of IVP, as changes occur in the free-stream Mach number and incidence; but it does increase significantly in going successively from an inviscid calculation (IVP = 0), where $C_{p_{t.e.}}$ is predicted to be about 0.35 (but should of course strictly take its stagnation point value) to a viscous calculation without any wake effects (IVP = 1), giving $C_{p_{t.e.}} \doteq 0.26$, to either of the viscous calculations incorporating wake thickness effects, which give $C_{p_{t.e.}} \doteq 0.22$.

The reduction in lift coefficient from its inviscid value is also not very sensitive to the free stream conditions. It is interesting to note that the greatest reduction (26-28%) is predicted by the first viscous model (IVP = 1); that the introduction of wake thickness effects then increases C_L by 5-9%; and that the final introduction of wake curvature effects leads to

a further reduction of 2-3%. All these changes are in qualitative agreement with similar results obtained in earlier work on this subject[6,8]. The

Table 2

A comparison of inviscid and viscous solutions

	Inviscid	δ* on aerofoil surface only	δ* on aerofoil and wake	Full curvature effects included
C_p at t.e.	0.336	0.267	0.225	0.226
C_L	0.568	0.421	0.441	0.430 (0.420)*
Changes in C_L from previous solution	-	-26%	+5%	-2½% (-5%)*

(a) $M_\infty = 0.676$, $\alpha = 1.06^\circ$

C_p at t.e.	0.364	0.261	0.211	0.219
C_L	0.922	0.663	0.721	0.699
Change in C_L from previous solution	-	-28%	+9%	-3%

(a) $M_\infty = 0.725$, $\alpha = 2.3^\circ$

differences that occur in the pressure distribution are shown for the solution $M_\infty = 0.725$, $\alpha = 2.3^\circ$ in Fig 10. This demonstrates that altering the features of the mathematical model in the wake produces a significantly different pressure distribution over most of the aerofoil surface.

Finally, the difference is considered between a converged solution on the coarse and fine grids. For $M_\infty = 0.676$, $\alpha = 1.06^\circ$ C_L changes from 0.435 to 0.430 on changing from a converged solution on the coarse grid to one on the fine grid. For $M_\infty = 0.725$, $\alpha = 2.3^\circ$, C_L changes from 0.701 to 0.699; and for this example Fig 11 shows how the changes in grid size affect the solution on the upper surface where the maximum changes to C_p occur.

5.3 Calculation of drag

With the present method, there are in principle two possible ways of estimating the overall drag of the aerofoil, which may be termed the 'near field' and 'far field' approaches. In the former, one calculates separately the skin friction drag (C_{D_F}) by the boundary-layer method and the pressure drag (C_{D_P}) by

* Values using basic formula for wake curvature effects (see Fig 8).

integrating the streamwise component of the surface pressure, and then the total drag is given by adding the two components: $C_D = C_{D_T} = C_{D_F} + C_{D_P}$. In the latter, the drag is obtained in subcritical (or shock-free) flows from the momentum thickness of the wake far downstream of the aerofoil, again calculated by the boundary layer/wake method: $C_D = \frac{2\theta_\infty}{c} = C_{D_V}$ say. A straight test of the self-consistency of the present method is provided by comparing the values of C_D obtained in these two different ways, for purely subcritical flows. Some examples are given below:

NACA 0012 (Re = 3.5×10^6)	C_{D_F}	C_{D_P}	C_{D_T}	C_{D_V}	$\frac{C_{D_V} - C_{D_T}}{C_{D_V}}$
$M_\infty = 0.7$, $\alpha = 0$	0.00700	0.00229	0.00928	0.00976	0.049
$M_\infty = 0.72$, $\alpha = 0$	0.00694	0.00244	0.00938	0.00984	0.047
$M_\infty = 0.65$, $\alpha = 2^o$	0.00703	0.00230	0.00932	0.00984	0.053
RAE 2822 (Re = 6×10^6)					
$M_\infty = 0.676$, $\alpha = 1.06^o$	0.00610	0.00199	0.00809	0.00833	0.029

From this table it will be seen that the values of C_D predicted by the first method (C_{D_T}) are slightly smaller than those predicted by the second method (C_{D_V}), but that the discrepancy does not exceed about 5%. Since the estimates of C_{D_F} and C_{D_V} are considered more reliable than that of C_{D_P} , it is probable that the fault lies with the calculation of C_{D_P} . To put the matter in perspective, an error in C_{D_P} of 0.0005 for NACA 0012 could be due to a mean error in C_p of 0.015 over the last 10% of the chord (equivalent to an error in C_p of 0.03 at the trailing edge diminishing linearly to zero at $x/c = 0.9$). Now this neighbourhood is one in which the mathematical model used in the present method (based as it is on the assumptions that the conventional boundary-layer approximations are valid) is likely to be least reliable and the implication of the above discrepancy is that the interaction in this region is not represented sufficiently accurately. In fact, as will be seen in section 5.4 the method does appear to overestimate C_p at and near the trailing edge by an amount of this order (judged by comparison with experimental measurements). It should however be emphasised that these discrepancies in drag are quite small, and that in few (if any) of the other methods for this problem is it possible to make such a check at all - either because the accuracy of the pressure calculation near the leading edge is poor (as in Refs 6 to 8), or because no calculation of the wake development is made (Refs 9 to 10).

When the flow is supercritical, and shock waves are present, the problem of drag estimation becomes more complicated - and controversial. It is still

possible to use the first ('near field') approach, and calculations of C_{D_T} certainly show the expected increase in drag (at least qualitatively), as we shall see later. To apply the second ('far field') approach, it is necessary to add to the 'viscous' drag, C_{D_V}, an estimate of the wave drag (C_{D_W}, say). A method for doing this has been suggested by Murman and Cole[38], which requires a knowledge of the Mach number distribution upstream of the whole length of any shock waves that may be present. Although it would in principle be straightforward to apply this technique to the present method, this has not yet been implemented*. But it must be emphasised that the total drag arrived at in this way ($C_{D_V} + C_{D_W}$) would *not* in general agree with the alternative estimate C_{D_T}, mainly because of the 'non-conservative' difference scheme used in the present method. It remains uncertain which of these two estimates would show the better agreement with experiment; or whether it might be better still to use a 'conservative' difference scheme[4] for the inviscid part of the calculations (*cf* Ref 39).

5.4 Comparison with experiments

5.4.1 NACA 0012

For this aerofoil a range of fully viscous solutions (IVP = 4), for a fine grid, was obtained from the VGK program (using the Sells' mapping) at five different angles of incidence. The principal features of the results for $\alpha = 0^\circ$, 2° and 4° are summarized in Table 3. A series of experiments on the NACA 0012 aerofoil was performed in the 36in × 14in transonic wind tunnel at NPL, Teddington during 1967-1968 [25]. These have been used to make comparisons with the present theory. The Reynolds number in the experiment varied between 3×10^6 (at $M_\infty = 0.6$) and 3.7×10^6 (at $M_\infty = 0.8$). For the theoretical results a fixed value of $Re(= 3.5 \times 10^6)$ was taken and transition was also fixed, at 0.05 chord on both surfaces. O'Mahoney *et al* have also used these experimental data to compare with results from the inviscid G & K program.

In Fig 12 the variation of the lift coefficient, C_L, with M_∞ is shown for both theory (inviscid and viscous) and experiment. It is seen that there is a reduction in lift for the viscous solutions, compared to the inviscid solutions, which varies between 11% and 17% over the range of solutions considered. The values of C_L predicted by the viscous theory are still

* A version of this technique *has* been used with the RAE 'viscous' TSP method[8,29] and has been found to yield sensible results.

Table 3

Viscous solutions for NACA 0012

$\alpha = 0^{o}$

M_{∞}	C_L	C_{DT}	Local $(M)_{max}$
0.7	0.0004	0.00928	0.935
0.72	0.0004	0.00938	0.979
0.74	0.0004	0.00951	1.031
0.76	0.0003	0.01009	1.010
0.78	0.0003	0.01263	1.163
0.80	0.0005	0.01799	1.217
0.81	0.0005	0.02183	1.238
0.82	0.0004	0.02640	1.258

$\alpha = 2^{o}$

0.65	0.302	0.00932	1.009
0.67	0.311	0.00950	1.069
0.69	0.324	0.00995	1.136
0.71	0.338	0.01154	1.199
0.73	0.354	0.01467	1.252
0.75	0.369	0.01936	1.296
0.76	0.375	0.02228	1.315
0.77	0.380	0.02546	1.332

$\alpha = 4^{o}$

0.57	0.548	0.00962	1.089
0.59	0.560	0.00988	1.162
0.61	0.574	0.01046	1.218
0.63	0.591	0.01199	1.254
0.65	0.608	0.01485	1.295
0.67	0.628	0.01909	1.335
0.68	0.637	0.02231	1.353
0.69	0.647	0.02553	1.371

considerably higher than the uncorrected experimental results. However, the statement made in Ref 25 that "the tunnel conditions are close to those giving blockage-free and lift-interference-free conditions" is now believed to be incorrect; according to 'classical' wind tunnel interference theory[36] it is in fact impossible that both parts of this statement can be simultaneously true. By assuming that the conditions are indeed blockage-free (for which there is substantial experimental confirmation), Blockley and Hodges[37] have deduced values

for the standard lift-interference parameters, δ_0 and δ_1 (-0.088 and +0.068) and in this way corrections to the experimental values of α and C_L may be readily obtained. The effect of these corrections to the experimental values of C_L is shown in Fig 12 by the vertical arrows, and it is seen that reasonably good agreement between theory and experiment is now achieved. The theoretical values of C_L are still slightly greater than the experimental values, but the discrepancy does not exceed about 5%, which is probably within the limits of accuracy of the experiment (bearing in mind the uncertainty of the interference corrections), as well as those of the present theory.

The variation of the total drag coefficient, C_{DT} (of section 5.3), with M_∞ is shown in Fig 13. At zero incidence reasonable agreement is obtained between theory and experiment over the whole Mach number range 0.7 to 0.8, including both subcritical and supercritical conditions. The small discrepancy when the flow is subcritical would be reduced if C_{D_T} were replaced by the viscous drag coefficient, C_V (shown by the dotted line in Fig 13). Experimental results are also shown for nominal values of α of 2° and 4°, together with theoretical results, both for these same values of α and also at $\alpha = 1.75^\circ$ and 3.5°, which give values for the lift coefficient close to the corresponding (uncorrected) experimental values. Comparing the calculated values of C_{D_T} at $\alpha = 1.75^\circ$ and 3.5° with those measured at $\alpha = 2^\circ$ and 4° respectively we note that for subcritical conditions the theory appears to underestimate the drag by an amount that increases with α. At least part of this discrepancy can be explained by two possible defects in the experimental technique, namely

(a) for subcritical conditions the roughness band used to fix transition (at $x/c = 0.05$) at zero incidence may lead to 'over-fixing' at higher values of α, and hence cause a spurious increase in measured drag.

(b) it has been suggested by Thompson[40] that the general tendency that has been noted for experimental measurements of drag, made by the wake traverse technique under nominally two-dimensional conditions, to increase more rapidly with C_L (or α) than is predicted by any of the accepted theories, may be partly due to a three-dimensional lateral convergence of the streamlines at the edge of the boundary layer on the upper surface of the model caused by the growth of the boundary layer on the side walls of the wind tunnel, particularly if the aspect ratio of the model (1.4 in this case) is low.

At supercritical conditions the general agreement between theoretical and experimental values of C_D appears to be more satisfactory. However, it must be pointed out that if the theoretical drag level for subcritical conditions were adjusted to agree with experiment (or vice versa), then the increase in drag with Mach number when shock waves appear would definitely be overestimated by the theory (even at $\alpha = 0$). This phenomenon has been observed on a number of other aerofoils, and must therefore be considered a weakness of the present method, at least in its current form. (See the remarks at the end of section 5.3.)

A final point of interest is the influence of the boundary layer on the position of the shock wave occurring on the upper surface for supercritical flow. A comparison is shown in Fig 14, for $M_\infty = 0.82$ and zero angle of incidence, of the pressure distributions calculated with and without boundary layers and from an experiment. (Solutions for the fully viscous method (IVP = 4) have been obtained from the VGK program only up to a value of M_∞ of 0.82, although, judging by the level of the shape factor for the boundary-layer profile, separation has not occurred at this Mach number, and further solutions at higher Mach numbers could easily be obtained.) Note that the effect of the rapid growth of the boundary layer (shown inset in Fig 14) due to the pressure rise through the shock is to cause a marked rounding in the Mach number (or pressure) distribution, both upstream and downstream of the shock. Because of this, it is difficult to define the position of the shock wave as precisely as for the inviscid solution. However, it would seem that the shock position is further forward by about 2% of the chord for the viscous solution. A similar result occurs for solutions at other Mach numbers.

5.4.2 RAE 2822

The theoretical solutions obtained from the VGK program for the RAE 2822 aerofoil have already been listed in section 5.2. The principal features of the results are summarized in Table 4. Experimental results are available for a model of 610mm (2ft) chord spanning the 8ft × 6ft transonic wind tunnel at RAE[26]. A number of experimental results were obtained covering a range of Mach number and angle of incidence at Reynolds number up to 6.5×10^6. Boundary-layer transition was fixed by bands of ballotini, of 1.2 mm (0.0002c) diameter at $M_\infty = 0.676$ and of 2.5 mm (0.0004c) diameter at $M_\infty = 0.725$. The angle of incidence in the experiments has been adjusted to allow for tunnel interference effects (and called the effective angle of incidence) and no blockage correction

was considered necessary. For the following examples comparisons were made at a given effective angle of incidence rather than at a given lift coefficient.

The main features of the experimental results are included in Table 4.

Table 4

Viscous solutions from VGK program for RAE 2822 aerofoil and experimental values

M_∞	α	VGK theory			Experiment		
		C_L	C_{D_T}	Local $(M)_{max}$	C_L	C_D	Transition position (x/c)
0.676	1.06°	0.431	0.0081	0.921	-	-	-
0.676	2.03°	0.590	0.0083	1.077	0.566	0.0085	0.11
0.725	2.3°	0.699	0.0119	1.181	0.658	0.0107	0.03
0.725	2.62°	0.759	0.0143	1.212	0.743	0.0127	0.03
0.725	2.93°	0.815	0.0177	1.249	0.802	0.0175	0.03

Comparisons of theoretical and experimental distributions of C_p are shown in Figs 16-19. For the two solutions at $M_\infty = 0.676$ the boundary layer transition position was taken to be at 11% of the chord, and there is a noticeable disturbance to the theoretical pressure distribution in this region (Fig 15)*, due to the discontinuity in δ^* assumed at transition. This disturbance is intensified for the solution at $\alpha = 2.03^\circ$ (Fig 16), since the flow is slightly supersonic in the region of boundary-layer transition and evidence of a weak shock exists in the theoretical pressure distribution. For the three solutions at $M_\infty = 0.725$ (shown in Figs 17a, 18 and 19) the shape of the C_p curves obtained from the theoretical results varies smoothly with incidence. In general, the main differences that occur between the experimental measurements and the theoretical results are (i) a slightly more positive value of C_p on the lower surface for the theoretical values, (ii) a different slope of the pressure distribution along the forward part of the upper surface ahead of the shock (this may be partly influenced by different disturbances at transition), (iii) the shock position is further back for the experimental values, by about 10% of the chord, (iv) a greater slope of $-C_p$ for the experimental values along the rear half of the upper surface, and (v) the trailing edge pressure is slightly overestimated by the theory in all cases.

* No experimental measurements are available at this particular condition.

It is interesting to note that the change in wind tunnel blockage which would be required to improve the agreement between the measurements and results from the VGK program, for lower surface values of the pressure, is about 0.008 in free-stream Mach number. It would not be unreasonable to suggest that such a blockage correction could be undetected in experimental work. The solution for $M_\infty = 0.725$, $\alpha = 2.3^\circ$, shown in Fig 17a, is therefore reconsidered, and a solution from the VGK program sought for $M_\infty = 0.733$, $\alpha = 2.3^\circ$, and this is shown in Fig 17b. The predicted value of C_L is 0.709, and $C_D = 0.0141$. There is now very good agreement over the lower surface between theory and experiment. Two features which have also been improved in a comparison of the upper surface values is (i) the slope of the pressure distribution before the shock, and (ii) the position of the shock, which now agrees well with the experiment. However, there is a greater discrepancy between the actual levels of pressure on the upper surface forward of the shock. This feature could be improved if the angle of incidence in the theory were decreased slightly. A further consideration to take into account is the effects of transition fixing in the experiment, by allowing for an increment in momentum thickness at transition in the theory. A solution from the VGK program was therefore obtained for $M_\infty = 0.733$, $\alpha = 2.3^\circ$, with an increase of 0.0002 in momentum thickness at transition on both the upper and lower surfaces. The value of C_L is 0.689 and $C_D = 0.0144$. The major change in the pressure distribution, apart from near to transition, occurred on the forward part of the upper surface, with the shock position moving back by about 3%.

It may well be possible to obtain a very good agreement between theory and experiment for pressure distribution and C_L by allowing small changes in the free-stream Mach number and incidence from those quoted as the experimental values. This exercise is not proceeded with further, since the current version of the VGK program does not contain the effects of a 'quasi-conservative'[4] finite difference scheme for the treatment of shocks. This additional feature would need to be included in the theory for a proper evaluation exercise to be undertaken.

5.4.3 Korn No.1

This aerofoil was designed by the inviscid hodograph method of Garabedian and Korn[3] to achieve a shock-free flow at $M_\infty = 0.75$, $\alpha = 0^\circ$ with $C_L = 0.67$. A large number of new* experimental results for this aerofoil have been obtained

* Earlier experimental results, at higher Reynolds numbers, were obtained at NAE, Ottawa: see Ref 35.

Table 5

Viscous solutions from VGK program for Korn No.1 aerofoil

M_∞	α	C_L	C_{D_T}	Local M_{max}
0.76	0.0^o	0.444	0.0101	1.145
0.76	0.25^o	0.498	0.0105	1.168
0.76	0.5^o	0.554	0.0115	1.190
0.76	0.75^o	0.607	0.0135	1.208
0.76	1.0^o	0.657	0.0163	1.225
0.76	1.25^o	0.702	0.0195	1.242
0.76	1.5^o	0.744	0.0232	1.258

recently by ARA[27], in their 18in × 8in transonic wind tunnel. These tests were carried out over a range of Mach numbers from 0.5 to 0.8, usually at a Reynolds number of 6×10^6 with transition fixed at 7% of the chord. A correction to the incidence has been made to allow for tunnel interference effects, and no blockage correction was considered necessary. For the purposes of comparison with experiment a series of solutions has been obtained from the VGK program at a Mach number, $M_\infty = 0.76$ (slightly above the design value) over a range of incidence, from $\alpha = 0^o$ to 1.5^o, at the same Reynolds number and transition position as in the experiments. The lift and drag coefficients and the maximum local Mach number are given in Table 5.

Experimental results are available at $M_\infty = 0.76$ (approximately) over a range of incidence. At $\alpha = 0.62^o$ (Fig 22) the experimental results have the distinctive feature of a marked double shock system on the upper surface. At higher incidences (Figs 20 and 21) this shock structure disappears and is replaced by an approximately constant value of C_p on the forward half of the upper surface followed by a strong shock. At lower incidences the double shock system is present in a modified form with a similar distribution of C_p (Fig 23). These features are present in the experiments, at similar incidences, over a range of Mach numbers from 0.75 to 0.77. Experimental results are available at $M_\infty = 0.76$ for $\alpha = 1.66^o$, 1.17^o and 0.71^o with $C_L = 0.708$, 0.603 and 0.496 respectively. These seem to be directly comparable with solutions from the VGK program at $\alpha = 1.5^o$, 1.0^o and 0.5^o respectively, since in each case the lower surface values of C_p are in excellent agreement, even though the values of C_L are slightly different. The comparisons are shown in Figs 20 to 22.

For the solution at the highest incidence (Fig 20) there is reasonable agreement over the upper surface, and the shock position is also similar.

However, the slopes of C_p over the rear part of the upper surface show a similar difference between theory and experiment as for the RAE 2822 aerofoil, as does the trailing edge pressure. As the incidence is decreased so the solution obtained from the VGK program varies in a smooth manner, and no double shock system appears for $\alpha = 0.5^o$ (Fig 22). A discussion on the effects of tunnel interference is given in the following section (5.5). At lower incidences better agreement in values of C_p on the upper surface is again apparent. In Fig 23 the theoretical results from the VGK program for $M_\infty = 0.76$, $\alpha = 0$ are compared to the experimental results obtained at $\alpha = 0.23^o$ with $C_L = 0.408$. On this occasion there is a larger difference in incidence between theory and experiment, so that the pressure distributions are not matched so well on the lower surface. However, better agreement is obtained on the upper surface than in Fig 22, and results show that a further slight decrease in incidence, in the theory, would provide better agreement, although of course there would then be a bigger difference on the lower surface.

5.5 Comparison with other viscous theoretical results

In this section the results from the small perturbation RAE Transonic Aerofoil Program (VISTRAN)[7,8] are compared to results from the VGK program. There is little doubt that, in principle, the present method should produce the more accurate solution: the mathematical models used to allow for viscous effects are essentially the same in both methods, but the inviscid part of the VGK method is nominally exact, while several approximations are involved in the TSP method. The Korn No.1 aerofoil is used as a test aerofoil. In section 5.5.1 some free air results are considered. First, solutions are compared for a low value of the free-stream Mach number (0.5); and then comparisons are made for two angles of incidence at a higher (supercritical) Mach number, 0.76.

The VISTRAN program has an option for computing flow past an aerofoil in a solid, porous or slotted wind-tunnel,[28,29] and in section 5.5.2 this facility is used to examine the differences between theory and experiment noted in the previous section.

5.5.1 Free-air results

Experimental results for the Korn No.1 aerofoil exist at $M_\infty = 0.5$ over a range of incidence, all for $Re = 4 \times 10^6$. As a typical example an experimental result at $\alpha = 2.74^o$ was considered, for which $C_L = 0.621$. A solution from the VGK program at $\alpha = 2.74^o$ provides very good agreement with the experiment for the lower surface values of C_p, but produces a higher peak value

of $-C_p$ on the upper surface (see Fig 24). The predicted value of C_L is 0.674. As was noted with an earlier example, if the theoretical value of the incidence is decreased then this would produce a better agreement in C_p values on the upper surface but a poorer agreement on the lower surface. However, as the main purpose is to compare results with the VISTRAN program a solution from this program was obtained at $M_\infty = 0.5$, $\alpha = 2.74^\circ$, and this is also shown in Fig 24. The predicted value of C_L is 0.643. Over the lower surface there is almost exact agreement in the C_p values between both theories and the experiment. However, on the upper surface there is better agreement between the viscous TSP theory and experiment, which is perhaps fortuitous in view of the approximation in the theory.

Further examples on the comparison between solutions from the VISTRAN and the VGK programs are considered for the situation in which there is supercritical flow. Thus a solution from the VISTRAN program was obtained for $M_\infty = 0.76$, $\alpha = 1.5^\circ$, for which $C_L = 0.769$. This is included in Fig 20. The solution at a lower incidence, $\alpha = 0.5^\circ$, is also included in Fig 22 (for which $C_L = 0.551$). It is seen that reasonable agreement occurs between the two theories. This agreement is to be expected as the inviscid TSP method depends upon assigning certain values to various parameters, and these have been determined mainly through comparison with inviscid results from the original G & K program over a range of conditions, for a number of aerofoils. These aerofoils have included the Korn No.1 aerofoil*.

The G & K method seems to be more sensitive to local changes in aerofoil ordinates and the local effects of boundary layer transition. For example, in the low Mach number solution, shown in Fig 24, it is seen that the disturbance to the peak value of $-C_p$ on the upper surface, for results from the VGK program, is due to the occurrence of boundary layer transition at 7% of the chord.

5.5.2 Results with allowance for tunnel interference

The inviscid TSP program developed by Albone *et al*[5] for calculating flow flow past an aerofoil in unconfined flow, has been modified by Catherall[28]

---

* It should be noted that comparison between the inviscid form of the two theories (TSP and G & K) for the same aerofoil are given in Ref 23, Part II, section 4.8. These show a similar degree of agreement. For example Fig 20 of the present Report should be compared with Fig 48 of Ref 23, (for $M_\infty = 0.75$, $C_L = 0.63$).

to take account of boundaries above and below the aerofoil. In this manner the effect of the wind tunnel walls on the flow can be modelled. The tunnel walls can be either solid, porous or slotted. (This problem has also been investigated by Murman[39]). Test aerofoils used by Catherall included the Korn No.1 aerofoil and the NACA 0012 aerofoil. The results demonstrate that for NACA 0012 at $M_\infty = 0.75$, $\alpha = 3.07^\circ$ a strong shock occurs for free-air conditions (see Fig 6 of Ref 28); and this flow structure is only slightly modified by the presence of the tunnel walls (slotted tunnel walls were considered). However, for the Korn aerofoil at a lower angle of incidence, $\alpha = 0.5^\circ$, with $M_\infty = 0.75$, the effect is much greater and the shock structure is substantially modified from free-air conditions, with a double shock occurring when the presence of the tunnel walls is allowed for (see Fig 7 of Ref 28).

There exists a version of the VISTRAN program[29] in which the effect of tunnel walls is included in a similar manner to the inviscid version of the TSP program. By using this program it is possible to compare results directly with uncorrected experimental data, and hence to ascertain the differences between theory and experiment. The input parameters to the tunnel interference program necessary to specify the wind tunnel parameters are H , F and P where H is the tunnel half height in chords, F is a slot parameter and P is a porosity factor. This last parameter needs to be determined empirically, and the precise value is often difficult to establish. For the purposes of comparison with the ARA experiments[27], values of 1.8, 0.1155 and 0.4 were taken for H , F and P respectively; the definition of the first two is unambiguous but the choice of P (corresponding to $\beta/P = 1.6$) is somewhat arbitrary.

The tunnel interference version of the VISTRAN program should strictly be used at the geometric incidence, which for the case shown in Fig 25 (corrected $\alpha = 0.71^\circ$) is 0.86°. However, in the previous work an attempt has been made to match the solutions from the VGK program and experiment by matching lower surface values of the pressure rather than using the effective incidence of the experiments. It has been seen that it is necessary to reduce the effective incidence by about 0.2° in order to achieve this match. Initially, a solution from the tunnel interference VISTRAN program was obtained at $\alpha = 0.75^\circ$. This solution produced a nearly constant value of C_p on the forward part of the upper surface followed by a single shock. But as the maximum value of $-C_p$ on the lower surface was less than the experimental value it would seem necessary to reduce the incidence slightly in order to make a reasonable comparison. Accordingly, a solution at $\alpha = 0.6^\circ$ was obtained, and this is shown in Fig 25. (The predicted value of C_L is 0.487.)

In order to compare with a free-air result from the VISTRAN program a solution is obtained from that program for $\alpha = 0.2^{o}$, which leads to good agreement in pressure on the lower surface between the free-air and the tunnel interference results (see Fig 25). However, the upper surface pressure distribution also matches quite well, and thus it appears that the additional effects* of tunnel interference are small. (A solution from the VGK program at $\alpha = 0.25^{o}$ shows similar features to the free-air result from VISTRAN.) For this one example, the results from VISTRAN show that, effectively tunnel corrections are equivalent to a reduction in α of about 0.4^{o}, in order to achieve agreement with C_p on the lower surface when comparing results in a wind tunnel to those in free-air. This is consistent with the reduction of 0.36^{o}, considered in Fig 22, in order to obtain agreement between the experiment and the VGK theory. It has already been mentioned that there is some uncertainty about assigning a value to the porosity factor P, and if it were decreased then the tunnel interference effects would be larger. This exercise has demonstrated that differences between the VGK theory and experimental results for this aerofoil probably cannot be accounted for by tunnel interference effects. It is a possibility that including a conservative finite difference scheme in the VGK theory would produce a better agreement with experiments.

It might be possible to modify the VGK program to calculate flow past an aerofoil in a tunnel as well as in free-air. Indeed this problem has been considered recently for the inviscid situation by Kacprzynski[31]. However, because of the difficulty of representing the effect of tunnel walls in the computing plane of the present model, it is possible that the Sells' transformation is not ideal and that a better approach would be to use a rectangular mesh where the potential equations are solved with interpolated boundary conditions. For the present an estimate of the tunnel interference effects can only by obtained by first comparing the free-air version of the VISTRAN program to the VGK results, and then using the VISTRAN program to estimate the tunnel interference effects.

6 CONCLUSIONS

The aim of this work has been to develop a computer program (VGK) based on modifications to the inviscid Garabedian and Kron computer package for calculating steady two-dimensional viscous flow past a lifting aerofoil at transonic speeds, which will supersede the small perturbation RAE Transonic Aerofoil Program as

---

* *ie* the curvature of the flow induced by the walls is small compared with the change in effective angle of incidence.

far as free-air calculations are concerned. The inviscid method adopted was based on the most accurate numerical model available at the inception of the work. (Subsequently Bauer *et al*[4] have produced a sequel to the original Garabedian and Korn program which incorporates various alternative schemes for the treatment of shocks. These have not been included in the initial version of the VGK program). In order to calculate the turbulent boundary layer an integral method was preferred to a differential one, mainly because of the iterative approach adopted in the inviscid-viscous interactive scheme, which requires a computationally efficient method for the boundary layer calculations. However, the lag-entrainment method has shown an accuracy in comparison with a wide range of experiments which is at least as good as most finite-difference methods.

A user's guide to the VGK program for its operation on an ICL 1906S computer is available[11]. The running time for a particular calculation to converge depends largely on the starting conditions prescribed. However, a typical coarse grid calculation might take the order of 100 iterations to achieve the standard level of convergence, with a boundary-layer calculation performed every five iterations and an under-relaxation factor of 0.15. Further refinement on a fine grid to a higher level of accuracy might require a further 100 iterations. The time required for the former calculation is about two minutes and for the latter about five minutes.

The mathematical model, as represented by the VGK program, should describe the viscous flow past a lifting aerofoil as well as can be obtained from any theoretical model which is based essentially on representing the viscous effects as a disturbance to the inviscid flow, rather than solving the full Navier-Stokes equations in some manner. The features which are not described adequately by the present approach relate to conditions of high free-stream Mach number or large angles of incidence. Under these conditions flow separation can occur near to the trailing edge or at a shock, which is not allowed for in the turbulent boundary layer model. Also the treatment of shocks and of the interaction of the shock wave and boundary layer for an unseparated flow is not properly represented in the VGK model; nor is the flow in the immediate neighbourhood of the trailing edge. Both these problems have been discussed recently by Melnik *et al*[33,34], who show how 'triple deck' solutions in these regions can be obtained. Any further major refinements to the present model would seem to lie in incorporating a better treatment of these features.

These are minor ways in which the present VGK model could be enhanced. The smoothing routine in the region of the trailing edge and the smoothing of the

curvature effect in the wake could be improved, although these are not likely to alter the present results greatly, but undoubtedly some very local smoothing routine is required near to the trailing edge region because of the inviscid viscous-interactive scheme that is adopted. Possible ways of increasing the rate of convergence of the iterative procedure in the inviscid-viscous interactive scheme have been shown to be of use for specific examples. Although it has not been possible to produce a scheme which is completely satisfactory for the general situation, more work on this topic could produce a saving in computing time. Finally, it is intended to alter the present model to allow for the treatment of flow past aerofoils with a blunt trailing edge, and to include alternative schemes for the treatment of shock waves.

Acknowledgments

The author would like to acknowledge the many profitable discussions of the problem he has had with Dr R.C. Lock, Mr A.F. Jones and Mr M.C.P. Firmin. In particular Dr Lock formulated the analysis of Appendix E, Mr Jones helped with the initial development of the VGK program, and Mr Firmin provided advice on the use of the VISTRAN program.

Appendix A

APPLICATION OF THE KUTTA CONDITION IN THE INVISCID SCHEME

At the end of every flow field sweep a new value for $\Phi_{mp,j}$ is defined, where $mp = mm + 1$, which is used to determine a solution along the radial line $i = mm$ (see Fig 1). Thus at the end of the $(k-1)$th flow field calculation

$$\Phi_{mp,1}^{(k-1)} = \Phi_{2,1}^{(k-1)} + \Gamma_0^{(k-1)} \quad . \tag{A-1}$$

At the end of the subsequent flow field sweep

$$\Phi_{mp,1}^{(k)} = \Phi_{2,1}^{(k)} + \Gamma_0^{(k)} \quad . \tag{A-2}$$

The Kutta condition gives $\phi_\theta = 0$ at the trailing edge, and from (13) we have

$$\Phi_\theta = \sin \alpha \ . \tag{A-3}$$

By applying this condition in finite difference form, we obtain

$$\frac{1}{2\delta\theta}\left(\Phi_{mp,1}^{(k)} - \Phi_{m,1}^{(k)}\right) - \sin \alpha = 0 \ . \tag{A-4}$$

From (A-2) we have

$$\Gamma_0^{(k)} = \Phi_{m,1}^{(k)} - \Phi_{2,1}^{(k)} + 2\delta\theta \sin \alpha \ . \tag{A-5}$$

The current value of $\Phi_{2,1}$ can be determined from its previous value. Hence from (A-1)

$$\Gamma_0^{(k)} = \Gamma_0^{(k-1)} + \Phi_{m,1}^{(k)} - \Phi_{mp,1}^{(k-1)} + 2\delta\theta \sin \alpha \ . \tag{A-6}$$

A relaxation factor ε_Γ is introduced so that the actual equation used in the iterative procedure to update Γ_0 is given by

$$\Gamma_0^{(k)} = \Gamma_0^{(k-1)} + \varepsilon_\Gamma \left\{\frac{1}{2\delta\theta}\left(\Phi_{m,1}^{(k)} - \Phi_{mp,1}^{(k-1)}\right) + \sin \alpha\right\} \ . \tag{A-7}$$

It is usual to set $\varepsilon_\Gamma = 1$, which in fact is equivalent to using an over-relaxation factor of $\frac{1}{2\delta\theta}$. [This looks like an accidental error in the program of Ref 3, but apparently causes no trouble.]

Appendix B

FORMULAE FOR THE COEFFICIENTS IN THE FINITE DIFFERENCE EQUATION ON THE CIRCLE $r = 1$

The region in which $\pi \leqslant \theta \leqslant 2\pi$ is considered first. If the governing equation is elliptic, *ie* $(\bar{u}^2 - a^2) < 0$, then $\Phi_{\theta\theta}$ can be represented by central differences;

$$(\delta\theta)^2 \Phi_{\theta\theta} = \Phi_{i+1,1} - 2\Phi_{i,1} + \Phi_{i-1,1} \qquad \text{(B-1)}$$

and the coefficients $a_{i,1}$, $b_{i,1}$, $c_{i,1}$ and $d_{i,1}$ of equation (37) are determined in terms of A, B, C and D (equation (36)) by the relationship

$$\left.\begin{aligned} a_{i,1} &= 0 \\ b_{i,1} &= -2A - 2C\frac{(\delta\theta)^2}{(\delta r)^2} \\ c_{i,1} &= 2C\frac{(\delta\theta)^2}{(\delta r)^2} \\ d_{i,1} &= (\delta\theta)^2 D - A(\Phi_{i+1,j} + \Phi_{i-1,1}) - 2C\frac{(\delta\theta)^2}{\delta r}\cos(\theta + \alpha) \\ &\quad - B(\delta\theta)^2[\tau^{(2)} - \sin(\theta + \alpha)] - 2C\frac{(\delta\theta)^2}{\delta r}\tau^{(1)} \end{aligned}\right\} \qquad \text{(B-2)}$$

where the variables A, B, C, D, $\tau^{(1)}$ and $\tau^{(2)}$ can be evaluated at mesh points around the circle $r = 1$. If the governing equation is hyperbolic, *ie* $(\bar{u}^2 - a^2) > 0$, then $\Phi_{\theta\theta}$ is represented by backward differences:

$$(\delta\theta)^2 \Phi_{\theta\theta} = (\Phi_{i,1} - 2\Phi_{i-1,1} + \Phi_{i-2,1}) + \varepsilon(\Phi_{i,1} - 3\Phi_{i-1,1} + 3\Phi_{i-2,1} - \Phi_{i-3,1}) \qquad \text{... (B-3)}$$

with a similar expression for $\Phi_{\theta r}$,

where $$0 < \varepsilon = (1 - \lambda\delta\theta) < 1 . \qquad \text{(B-4)}$$

The coefficients $a_{i,1}$, $b_{i,1}$, $c_{i,1}$ and $d_{i,1}$ are given by

$$
\left.
\begin{aligned}
a_{i,1} &= 0 \\
b_{i,1} &= (2 - \lambda\delta\theta)A - 2C\frac{(\delta\theta)^2}{(\delta r)^2} \\
c_{i,1} &= 2C\frac{(\delta\theta)^2}{(\delta r)^2} \\
d_{i,1} &= (\delta\theta)^2 D + A\left\{(5 - 3\lambda\delta\theta)\Phi_{i-1,1} - (4 - 3\lambda\delta\theta)\Phi_{i-2,1} + (1 - \lambda\delta\theta)\Phi_{i-3,1}\right\} \\
&\quad - 2C\frac{(\delta\theta)^2}{\delta r}\cos(\theta + \alpha) - (\delta\theta)^2 B[\tau^{(2)} - \sin(\theta + \alpha)] \\
&\quad - 2C\frac{(\delta\theta)^2}{\delta r}\tau^{(1)} \ .
\end{aligned}
\right\} \quad \text{(B-5)}
$$

Similar equations apply if $0 \leq \theta \leq \pi$. If the equation is elliptic then the suffix $i - 1$ is replaced by $i + 1$ etc. If the equation is hyperbolic then as well as replacing the suffix $i - 1$ by $i + 1$, we also replace $\delta\theta$ by $-\delta\theta$ and λ by $-\lambda$.

Appendix C

SOLUTION AT THE TRAILING EDGE

At the trailing edge point $B \to 0$, and from equation (8) $\omega \to 0$, and thus $\bar{u}$ and $\bar{v}$, defined by (10), both tend to infinity unless the terms in square brackets tend to zero. In inviscid flow $\bar{v} = 0$ everywhere on the aerofoil surface, and hence $\bar{v} = 0$ at the trailing edge, while application of the Kutta condition (13) ensures that

$$\Phi_\theta \to \sin \alpha \qquad \text{for} \quad r = 1 \,, \quad \text{as} \quad \theta \to 0, 2\pi \tag{C-1}$$

so that $\bar{u}$ may be finite at the trailing edge. Unless the aerofoil has a cusped trailing edge, $\bar{u}$ does in fact tend to zero, so there is no difficulty in determining the coefficients in the governing partial differential equation when expressed in finite difference form at the trailing edge (*ie* $\bar{u} = \bar{v} = 0$). In the viscous flow, although $\bar{v}$ is non-zero over the aerofoil surface, we have the condition (41) that $\tau^{(1)} \to 0$, and that $\bar{v}$ numerically approaches a finite limit at the trailing edge. Also $\bar{u}$ does not tend to zero, although the Kutta condition ensures that (C-1) holds. Therefore the previous numerical scheme is not applicable for the viscous flow. However, this difficulty can be overcome by a different procedure. Normally the co-ordinate transformation is introduced before the governing partial differential equation is expressed in finite difference form, but for the viscous flow this process is reversed. This is because in the physical plane the finite difference equation is properly defined at the trailing edge point, and is given to a sufficient approximation by

$$(a^2 - u^2)\Phi_{xx} + \phi_{yy} = 0 \,, \tag{C-2}$$

(assuming that $v \ll u$). A diagram of the situation in this region, both in the physical plane and in the computing plane is shown in Fig 6.

It now remains to demonstrate how this new scheme can be included in the original computing scheme. In the sweeping system adopted it is necessary to obtain a solution of (C-2) in finite difference form only at the mesh point B ($i = mm$, $j = 1$). To a first approximation we may suppose that the trailing edge angle of the aerofoil is small, and thus $S_B \doteq S_C$, so that a possible approximation of ϕ_{xx} is

$$\phi_{xx} = \frac{2}{(S_A + S_B)S_A}\phi_{A+} - \frac{2}{S_A S_B}\phi_{P_+} + \frac{2}{(S_A + S_B)S_B}\phi_B \qquad (C\text{-}3)$$

and ϕ_{yy} is defined by

$$\phi_{yy} = \frac{1}{S^2}\phi_Q - \frac{2}{S^2}\phi_{P_+} + \frac{1}{S^2}\phi_R^* \qquad (C\text{-}4)$$

with $\phi_R^* = \phi_R + \Gamma_1$ defined to allow for the jump in ϕ at the trailing edge. The positions of Q and R are arbitrary, although we have already defined PQ = PR (=S), and for further convenience they are specified such that $S^2 = S_A S_B$, and thus in the computing plane $PQ = \sqrt{\delta r \delta\theta}$. Finally, the value of ϕ at Q can be specified by interpolation in terms of its values at B, A_+ and E, which are neighbouring points in the computing plane. (A similar interpolation is required for ϕ_R.) Linear interpolation both in the r and θ directions gives

$$\left.\begin{aligned} \phi_Q &= \mu_1\phi_E + \mu_2\phi_{A_+} + \mu_3\phi_B \\ \phi_R &= \mu_1\phi_D + \mu_2\phi_{A_-} + \mu_3\phi_C \end{aligned}\right\} \qquad (C\text{-}5)$$

where

$$\left.\begin{aligned} \mu_1 &= (-1 + \sqrt{\lambda/2} + \sqrt{1/2\lambda}) \\ \mu_2 &= (1 - \sqrt{1/2\lambda}) \\ \mu_3 &= (1 - \sqrt{\lambda/2}) \end{aligned}\right\} \qquad (C\text{-}6)$$

and λ is defined by

$$\lambda = \frac{\delta\theta}{\delta r} = \frac{n}{m}\pi \ . \qquad (C\text{-}7)$$

Thus equation (C-2) can now be expressed in finite difference form using the values of Φ at eight mesh points for j = 1 and j = 2 in the r-direction and i = 1,2,m and mm in the θ-direction. If the original numerical scheme had been employed at the trailing edge, then values of Φ at j = 2 for i = 2 and i = m (*ie* at D and E) would not be used. In the physical plane this means that information would be used only at points in the x-direction, and thus the basic equation would not be represented properly in finite difference form in the computing plane.

Appendix D

SECOND-ORDER TERMS IN THE WAKE-THICKNESS BOUNDARY CONDITION

In order to determine $\Phi_{mp,j}$ to $O(\delta\theta)^2$ we need to know the jump in $\Phi_{\theta\theta}$ across $\theta = 0, 2\pi$. (See equation (45).) A sufficient approximation to this may be found by considering the small-disturbance approximation to the basic equation for ϕ, given by equation (5). Along $\theta = 0$, the velocity component $\bar{u}$, and all derivatives with respect to θ are neglected, and equation (5) becomes, with the aid of (6),

$$a^2\left(\phi_{\theta\theta} + r\phi_r + r^2\phi_{rr}\right) = \bar{v}^2 r^2\left(\phi_{rr} - \frac{\phi_r B_r}{B}\right). \tag{C-1}$$

Hence

$$\phi_{\theta\theta} = -(1 - M^2)r^2\phi_{rr} - \left(1 + \frac{rM^2B_r}{B}\right)r\phi_r \tag{C-2}$$

where $M^2 = v^2/a^2$ is the approximate local Mach number, and

$$\Delta(\Phi_{\theta\theta}) = -(1 - M^2)r^2\sigma^{(3)} - \left(1 + \frac{rM^2B_r}{B}\right)r\sigma^{(2)} \tag{C-3}$$

with $\sigma^{(2)}$ and $\sigma^{(3)}$ defined by (30) and (50) respectively.

An evaluation of the right-hand side of (C-3) in a typical example showed that its value did not exceed 0.04, and since, for the fine grid, $\frac{1}{2}(\delta\theta)^2 \doteq 8 \times 10^{-4}$, the value of the last term in (45) does not usually exceed 3×10^{-5}. This suggests that the term may be safely neglected, and a full calculation by a version of the program with this term included confirmed that the effect on the pressure distribution was negligible.

Appendix E

CALCULATION OF THE FLOW CURVATURE

We start by deriving general expressions for the curvature of a streamline in orthogonal curvilinear coordinates, and then go on to obtain approximations suitable for use in the present application.

E.1 Streamline curvature in general orthogonal coordinates

We consider an orthogonal coordinate system (x_1,x_2), with metric components (h_1,h_2), in which the velocity components are (μ_1,μ_2).

Referring to Fig 5, we see that the curvature, κ, of the streamline PQ, is given by

$$\kappa = \frac{d}{ds}(\varepsilon + \psi) \ . \qquad \text{(E-1)}$$

Here $\varepsilon = \tan^{-1}\left(\frac{\mu_2}{\mu_1}\right)$ is the inclination of the streamline to the x_1 direction,

s is the distance along the streamline,

and ψ is the inclination of the x_1 coordinate line to a fixed reference direction.

Now, to first order, we see that

$$\frac{RQ}{PR} = \frac{\mu_2}{\mu_1}$$

so that

$$RQ = \frac{\mu_2}{\mu_1} h_1 dx_1$$

and

$$\frac{RQ}{RS} = \frac{\mu_2}{\mu_1}\frac{h_1}{h_2}\frac{dx_1}{dx_2} \ .$$

Thus the point Q has coordinates $\left(x_1 + dx_1, x_2 + \frac{\mu_2}{\mu_1}\frac{h_1}{h_2} dx_1\right)$.

Hence the change in ε from P to Q is

$$\delta\varepsilon = dx_1\left(\frac{\partial\varepsilon}{\partial x_1} + \frac{\mu_2 h_1}{\mu_1 h_2}\frac{\partial\varepsilon}{\partial x_2}\right) . \qquad \text{(E-2)}$$

Now the change in ψ from P to Q is

$$\delta\psi = \kappa_1 PR + \kappa_2 RQ$$

$$= \kappa_1 h_1 dx_1 + \kappa_2 \frac{\mu_2}{\mu_1} h_1 dx_1 \quad , \tag{E-3}$$

where κ_1 and κ_2 are the curvatures of the coordinate lines (positive if the line is concave to the left in the positive direction) and are given by

$$\kappa_1 = -\frac{1}{h_1 h_2}\frac{\partial h_1}{\partial x_2} , \quad \kappa_2 = \frac{1}{h_1 h_2}\frac{\partial h_2}{\partial x_1} \quad . \tag{E-4}$$

Combining (E-1), (E-2) and (E-3), and noting that

$$ds = h_1 dx_1 \sec \varepsilon ,$$

we obtain the equation

$$\kappa = \frac{1}{q}\left(\frac{\mu_1}{h_1}\frac{\partial \varepsilon}{\partial x_1} + \frac{\mu_2}{h_2}\frac{\partial \varepsilon}{\partial x_2} + \mu_1\kappa_1 + \mu_2\kappa_2\right) \tag{E-5}$$

where $q = \sqrt{\mu_1^2 + \mu_2^2}$ is the total velocity.

As a digression, we note that for an irrotational flow, the relationship

$$\frac{\partial}{\partial x_1}(h_2\mu_2) = \frac{\partial}{\partial x_2}(h_1,\mu_1)$$

is equivalent to

$$\mu_1\kappa_1 + \mu_2\kappa_2 = \frac{1}{h_2}\frac{\partial \mu_1}{\partial x_2} - \frac{1}{h_1}\frac{\partial \mu_2}{\partial x_1} \quad ,$$

and this may be used to eliminate the coordinate line curvatures from equation (E-5) leading eventually to the alternative expression

$$\kappa = \frac{1}{q^2}\left(-\frac{\mu_2}{h_1}\frac{\partial q}{\partial x_1} + \frac{\mu_1}{h_2}\frac{\partial q}{\partial x_2}\right). \tag{E-6}$$

It may be easily shown that this is equivalent to the familiar expression for the streamline curvature in irrotational flow:

$$\kappa = \frac{1}{q}\frac{\partial q}{\partial n} \qquad \text{(E-7)}$$

in streamline coordinates, n being the direction normal to the streamline. However, for present purposes equation (E-5) is the more convenient.

E.2 Approximation for small perturbations from a coordinate line

In both the cases where we need to calculate the flow curvature in the present problem - for the equivalent inviscid flow on the surface of the aerofoil and in the wake - we can assume that the angle between the local velocity vector and a coordinate line (either $r = 1$, for the aerofoil surface, or $\theta = 0$, for the wake) is small. Taking this coordinate line to be a line x_2 = constant (*ie* PR in Fig 5), this implies that

$$\varepsilon \triangleq \frac{\mu_2}{\mu_1}$$

is small. We require to calculate κ correct to order (ε), so that we can neglect terms of order (ε^2).

Thus, $q = \mu_1 + O(\varepsilon^2)$, and equation (E-5) becomes

$$\kappa = \kappa_1 + \frac{1}{h_1}\frac{\partial}{\partial x_1}\left(\frac{\mu_2}{\mu_1}\right) + \frac{\varepsilon}{h_2}\frac{\partial \varepsilon}{\partial x_2} + \varepsilon\kappa_2 + O(\varepsilon^2) .$$

The last two terms can be further approximated by making use of the equation of continuity, div $(\rho\underline{\mu}) = 0$; this gives

$$\frac{\partial}{\partial x_1}(h_2\rho\mu_1) + \frac{\partial}{\partial x_2}(h_1\rho\mu_2) = 0 ,$$

so that

$$\kappa_2 + \frac{1}{h_2}\frac{\partial \varepsilon}{\partial x_2} = -\frac{1}{h_1}\frac{1}{\rho\mu_1}\frac{\partial}{\partial x_1}(\rho\mu_1) + O(\varepsilon) .$$

Hence

$$\kappa = \kappa_1 + \frac{1}{h_1}\frac{\partial}{\partial x_1}\left(\frac{\mu_2}{\mu_1}\right) - \frac{1}{h_1}\frac{\mu_2}{\mu_1}\frac{1}{\rho\mu_1}\frac{\partial}{\partial x_1}(\rho\mu_1) + O(\varepsilon^2) . \qquad \text{(E-8)}$$

Now the last tern in this expression, though not strictly of order (ε^2), will usually be numerically much smaller than the second term (because the quantity multiplying ε is $\frac{\partial}{\partial x_1}(\log \rho\mu_1)$), and may therefore be neglected. We therefore use finally the expression

$$\kappa \doteq \kappa_1 + \frac{1}{h_1}\frac{\partial}{\partial x_1}\left(\frac{\mu_2}{\mu_1}\right) \qquad \text{(E-9)}$$

where $\kappa_1 = -\frac{1}{h_1 h_2}\frac{\partial h_1}{\partial x_2}$ is the curvature of the x_1 line, and the second term is $\frac{d\varepsilon}{ds}$, s being the distance along the x_1 line and ε the angle between it and the direction of flow. This formula may appear 'obvious', but the argument given above (in the sentence between (E-8) and (E-9)) shows that an additional assumption, other than that ε is 'small', is required to justify it.

It may also be shown that the expression (E-9) for the flow curvature at the aerofoil surface in the equivalent inviscid flow is in fact approximately equal to the curvature of the displacement surface. For the second term $\left(\frac{d\varepsilon}{ds}\right)$ may be written, using equation (14), as

$$\frac{d}{ds}\left\{\frac{1}{\rho q}\frac{d}{ds}(\rho q \delta^*)\right\} = \frac{d^2\delta^*}{ds^2} + \frac{d}{ds}\left[\delta^* \frac{1}{\rho q}\frac{d}{ds}(\rho q)\right] ,$$

and the term inside the square bracket is generally numerically small compared with $\frac{d\delta^*}{ds}$ (as has been verified in a typical example).

Hence

$$\frac{d\varepsilon}{ds} \doteq \frac{d^2\delta^*}{ds^2}$$

and so

$$\kappa \doteq \kappa_1 + \frac{d^2\delta^*}{ds^2} \doteq \frac{d^2}{ds^2}(y + \delta^*) \qquad \text{(E-10)}$$

LIST OF SYMBOLS

a	local speed of sound
a,b,c,d A,B,C,D	coefficients defined in section 3.1
B	mapping transform derivative
c	aerofoil chord
C_{D_F}	skin friction drag coefficient
C_{D_P}	form drag coefficient
C_{D_T}	total drag coefficient ($= C_{D_F} + C_{D_P}$)
C_{D_V}	viscous drag coefficient
C_L	lift coefficient
C_p	local pressure coefficient
C^*_p	critical pressure coefficient (local M = 1)
i	mesh point in tangential direction of computing plane
j	mesh point in radial direction of computing plane
k	relative frequency of boundary layer calculations
k_1	number of flow field calculations performed for a new case before re-calculating a new boundary layer
m	number of intervals in computing plane around aerofoil
mm	defined as $m + 1$
mp	defined as $mm + 1$
M	local Mach number
M_∞	free-stream Mach number
n	distance normal to aerofoil surface and wake
n	number of intervals in radial direction of the computing plane
nn	defined as $n + 1$
p	local pressure
p/H	ratio of static pressure to total pressure
q	local velocity
q'	local velocity corrected for curvature effects
$\hat{q}$	smoothed values of the velocity q'
q_+	local velocity on upper surface of wake
q_-	local velocity on lower surface of wake
r	coordinate in radial direction in circle plane
s	distance along the aerofoil surface and wake (measured from the leading edge)
S	scaling factor introduced by normalizing ω
S, S_A, S_B, S_C	distances defined in section 3.5

LIST OF SYMBOLS (continued)

$\underline{u}$	non-dimensional velocity in vector form
u	velocity component along aerofoil surface or wake
$\bar{u}$	velocity component in the θ direction in the computing plane
$\bar{u}_+$	$\bar{u}$ on upper surface of wake
$\bar{u}_-$	$\bar{u}$ on lower surface of wake
U_∞	free-stream velocity
v	velocity component normal to aerofoil surface or wake
$\bar{v}$	velocity component in the r direction in the computing plane
$\bar{v}_+$	$\bar{v}$ on upper surface of wake
$\bar{v}_-$	$\bar{v}$ on lower surface of wake
x	coordinate in the free-stream direction
x_T	transition position
y	coordinate normal to the free-stream direction
$\bar{\alpha}$	angle of incidence
α_0	zero lift angle for incompressible flow
α	defined as $\bar{\alpha} - \alpha_0$
β	$\sqrt{1 - M_\infty^2}$
γ	ratio of specific heats (= 1.4)
Γ_0	circulation
Γ	jump in Φ across wake
δ_0 δ_1	parameters used in wind tunnel interference calculations
δ^*	boundary layer displacement thickness on aerofoil surface
$\bar{\delta}^*$	non-dimensionalised with respect to chord (= δ^*/S)
δ^*_w	total displacement thickness of wake
$\bar{\delta}^*_w$	non-dimensionalised with respect to chord (= δ^*_w/S)
δr	distance between grid points in radial direction of computing plane
$\delta\theta$	distance between grid points in tangential direction of computing plane
ε	under-relaxation parameter of viscous-inviscid interaction scheme
$\varepsilon_0, \varepsilon'$	parameters controlling variation in ε, defined in section 4.2
θ	coordinate in tangential direction of computing plane
θ	boundary layer momentum thickness on aerofoil surface
$\bar{\theta}$	non-dimensionalised with respect to chord (= θ/S)
θ_w	total boundary layer momentum thickness of wake
$\bar{\theta}_w$	non-dimensionalised with respect to chord (= θ_w/S)
κ_0	curvature of aerofoil surface or wake

LIST OF SYMBOLS (concluded)

κ_1	curvature of displacement surfaces relative to the aerofoil surface or wake
κ	total curvature ($= \kappa_0 + \kappa_1$)
λ	defined as $\delta\theta/\delta r$
μ	current error level of iterative scheme for flow field calculations
μ_v	current error level of boundary conditions
μ_1, μ_2, μ_3	coefficients defined in section 3.5
ρ	local density
$\sigma^{(1)}(r)$	function which determines the wake thickness effect
$\sigma^{(2)}(r)$	function which determines the wake curvature effect (equation (30) or equation (31))
$\sigma^{(3)}(r)$	defined as $d/dr\ (\sigma^{(2)})$
$\tau^{(1)}(\theta)$	function which determines the boundary layer thickness effect on the aerofoil surface
$\tau^{(2)}(\theta)$	defined as $d/d\theta(\tau^{(1)})$
ϕ	velocity potential
Φ	modified velocity potential to remove singularity at infinity
ω	modified mapping transform derivative ($= r^2 B$)

REFERENCES

No.	Author	Title, etc
1	E.M. Murman J.D. Cole	Calculation of plane, steady transonic flows. AIAA Journal, Vol.9, No.1, pp 114-121 (1971)
2	P.R. Garabedian D.G. Korn	Analysis of transonic aerofoils. Comm. Pure and Appl. Maths, Vol XXIV, pp 841-851 (1971)
3	F. Bauer P.R. Garabedian D.G. Korn	Supercritical wing sections. Lecture notes in Economics and Mathematical Systems. Springer-Verlag (1972)
4	F. Bauer P.R. Garabedian D.G. Korn A. Jameson	Supercritical Wing Sections II. Lecture Notes in Economics and Mathematical Systems Springer-Verlag (1975)
5	C.M. Albone D. Catherall M.G. Hall Gaynor Joyce	An improved numerical method for solving the transonic small perturbation equations for flow past a lifting aerofoil. RAE Technical Report 74056 (1974)
6	M.C.P. Firmin	The calculation of pressure distribution, lift and drag on single aerofoils at subcritical speeds. Part I - Interim Method. RAE Technical Report 72235 (1973)
7	M.G. Hall M.C.P. Firmin	Recent developments in methods for calculating transonic flows over wings. ICAS Paper 74-18 (1974)
8	M.C.P. Firmin A.F. Jones	The calculation of pressure distribution, lift and drag on single aerofoils at supercritical speeds. RAE Technical Report (in preparation)
9	F. Bauer P.R. Garabedian	Computer simulation of Shock Wave Boundary Layer Interactions. Comm. Pure and Applied Mathematics, Vol XXVI, pp 659-665 (1973)
10	P.C. Bavitz	An analysis method for two-dimensional transonic viscous flow. NASA TN D-7718 (1975)

REFERENCES (continued)

No.	Author	Title, etc
11	M.R. Collyer	A user's guide to a program for computing viscous transonic flows past aerofoils (Garabedian and Korn method). RAE unpublished material (1976)
12	R.C. Lock P.G. Wilby P.J. Powell	The prediction of aerofoil pressure distribution for sub-critical viscous flows. The Aeronautical Quarterly, Vol XXI, Part 3 (1970)
13	J.E. Green	Application of Head's entrainment method to the prediction of turbulent boundary layers and wakes in compressible flow. ARC R & M No.3788 (1972)
14	J.E. Green D.G. Weeks J.W.F. Brooman	Prediction of turbulent boundary layers and wakes in compressible flows by a lag-entrainment method. ARC R & M No.3791 (1973)
15	N. Curle	The laminar boundary layer equations. Oxford Mathematical Monograph (1962)
16	C.C.L. Sells	Plane subcritical flow past a lifting aerofoil. Proc. Roy. Soc. (London) Vol 308(A), pp 377-401 (1968)
17	D. Catherall D.N. Foster C.C.L. Sells	Two-dimensional incompressible flow past a lifting aerofoil. RAE Technical Report 69118 (1969)
18	M.J. Lighthill	On displacement thickness. J. Fluid Mech, Vol 4, pp 383-392 (1958)
19	J.F. Nash A.G.J. MacDonald	The calculation of momentum thickness in a turbulent boundary layer at Mach numbers up to unity. Aeronautical Research Council CP No.93 London (1967)
20	P. Bradshaw D.H. Ferriss N.P. Atwell	Calculation of boundary-layer development using the turbulent energy equation. J. Fluid Mech. Vol 28, Pt 3, pp 593-616 (1967)
21	D.H. Ferriss P. Bradshaw	A computer program for the calculation of boundary layer development using the turbulent energy equation. NPL Aero Report 1269 (1968)

REFERENCES (continued)

No.	Author	Title, etc
22	R.C. Lock	Calculation of viscous effects on aerofoils in compressible flow. Fifth Australasian Conference on Hydraulics and Fluid Mech., Christchurch, NZ (1974)
23	R.H. Blockley	A comparison of various numerical methods for calculating inviscid isentropic flow over two-dimensional aerofoils. DRIC S & T Memo-4-75 (1975)
24	R. O'Mahoney R.C. Lock Gaynor Joyce	Notes on a computer program of Garabedian and Korn for computing steady, inviscid, two-dimensional transonic flows past an aerofoil. RAE unpublished material (1973)
25	N. Gregory P.G. Wilby	NPL 9615 and NACA 0012. A comparison of aerodynamic data. Aeronautical Research Council CP No.1261, London (1973)
26	P.H. Cook M.A. MacDonald M.C.P. Firmin	Aerofoil RAE 2822 - Pressure distributions and boundary layer and wake measurements. RAE unpublished material (1977)
27	-	Unpublished ARA data on Korn No.1 aerofoil.
28	D. Catherall	The computation of transonic flows past aerofoils in solid, porous or slotted wind tunnels. Agard Conference Proceedings, No.174, London (1975)
29	M.C.P. Firmin S. Billington	The calculation of pressure distribution lift and drag, at supercritical speeds on single aerofoils mounted in wind tunnels. RAE Technical Report (in preparation)
30	E.M. Murman	Computation of wall effects in ventilated transonic wind tunnels. AIAA Paper 72-1007 (1972)

REFERENCES (concluded)

No.	Author	Title, etc
31	J.J. Kacprzynski	Transonic flowfield past two-dimensional airfoils between porous wind-tunnel walls. AIAA Journal, Vol. 14, No.4, pp 533-535 (1976)
32	D.A. Spence	A treatment of the jet flap by thin-aerofoil theory. Proc. Roy. Soc. (A), 238 (1956) (see also 'Wake curvature and the Kutta condition', J. Fluid Mech, 44 (1970)
33	R.E. Melnik B. Grossman	Further developments in an analysis of the interaction of a weak normal shock wave with a turbulent boundary layer. Symposium Transonicum II, p 262, Springen Verlag, (1976)
34	R.E. Melnik R. Chow	Asymptotic theory of two-dimensional trailing-edge flows. NASA SP-347, p 177 (1975)
35	J.J. Kacprzynski	A second series of wind tunnel tests of the shockless lifting aerofoil No.1. NRC, NAE Wing Tunnel Project Rep.5X5/0062 (1972)
36	E.W.E. Rogers	Subsonic wind tunnel wall corrections. AGARDograph 109, Chaps.V and VI (1966)
37	R.H. Blockley M.D. Hodges	Comparisons between selected experimental data and first-order viscous theory for subcritical flow over two-dimensional aerofoils. ESDU Memorandum (to be issued) (1976)
38	E.M. Murman J.D. Cole	Inviscid drag at transonic speeds. AIAA Paper 74-540 (1974)
39	F. Bauer D. Korn	Computer simulation of transonic flow past aerofoils with boundary layer correction. Proc. AIAA 2nd Computational Fluid Dynamics Conference, p 184 (1975)
40	B.G.J. Thompson	RAE unpublished material (1972)

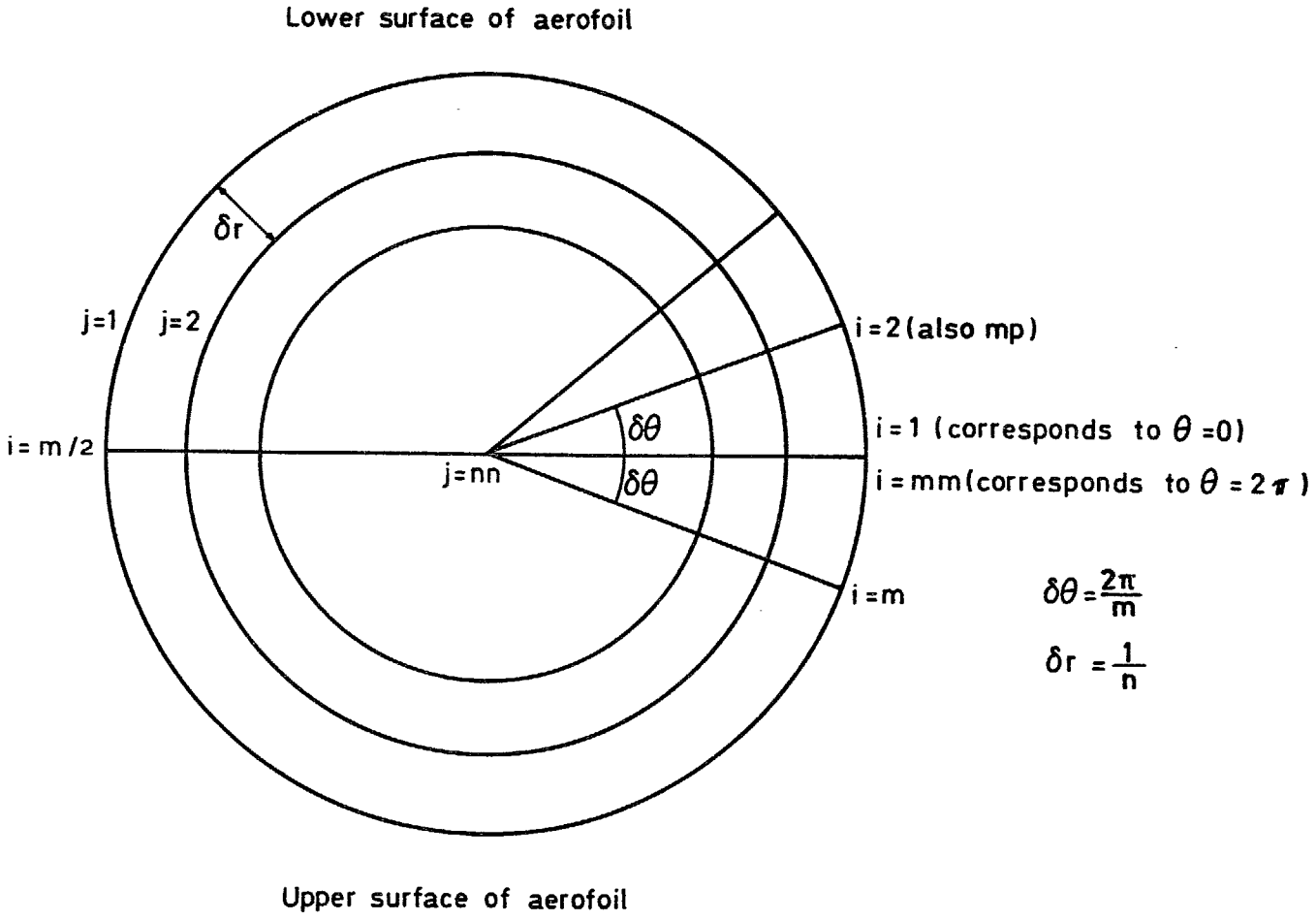

Fig 1 Numerical scheme in (r, θ) plane

Fig 2

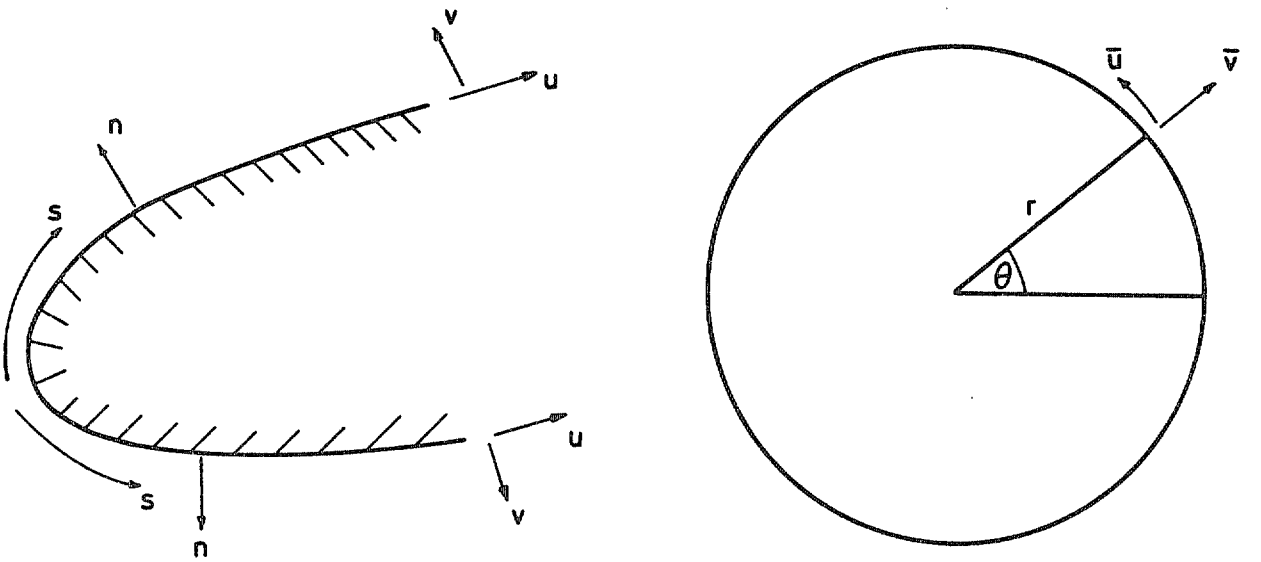

Fig 2 Relationship between parameters in the physical plane and the computing plane on the aerofoil surface

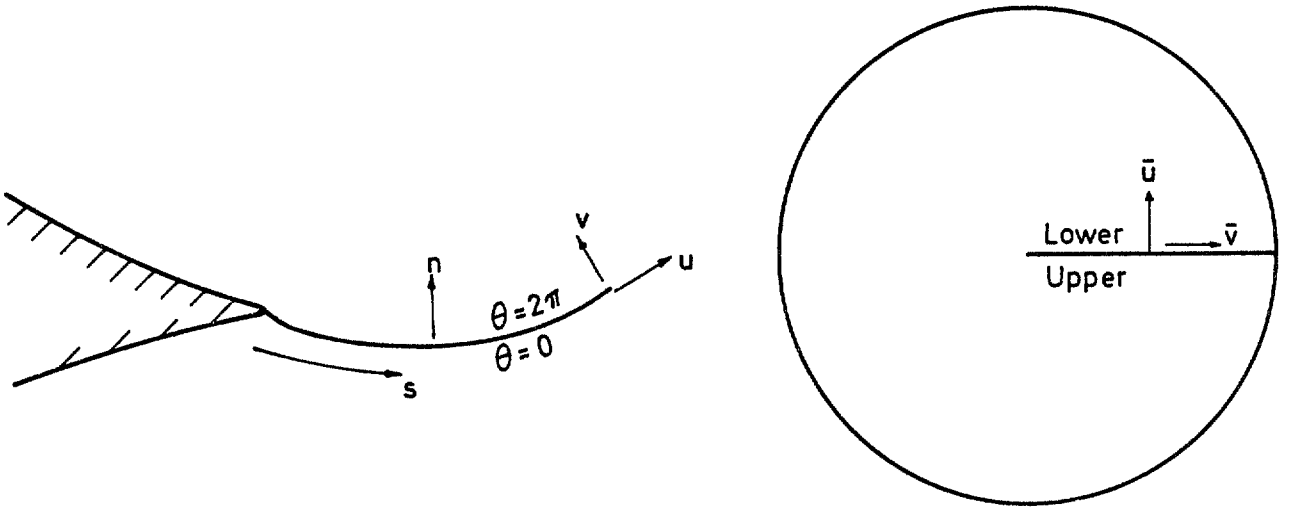

Fig 3 Relationship between parameters in the physical plane and the computing plane for the wake

Fig 4

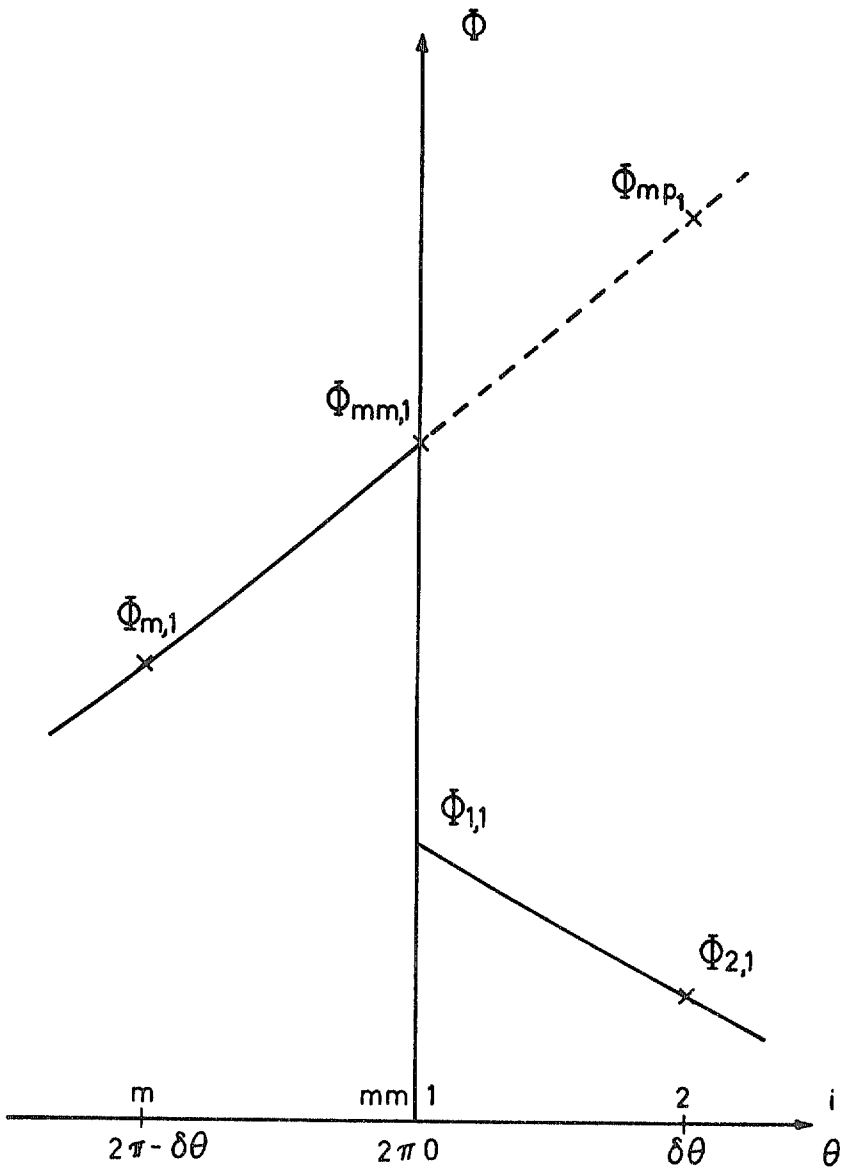

Fig 4 Sketch of Φ for r = 1 in region of $\theta = 0$

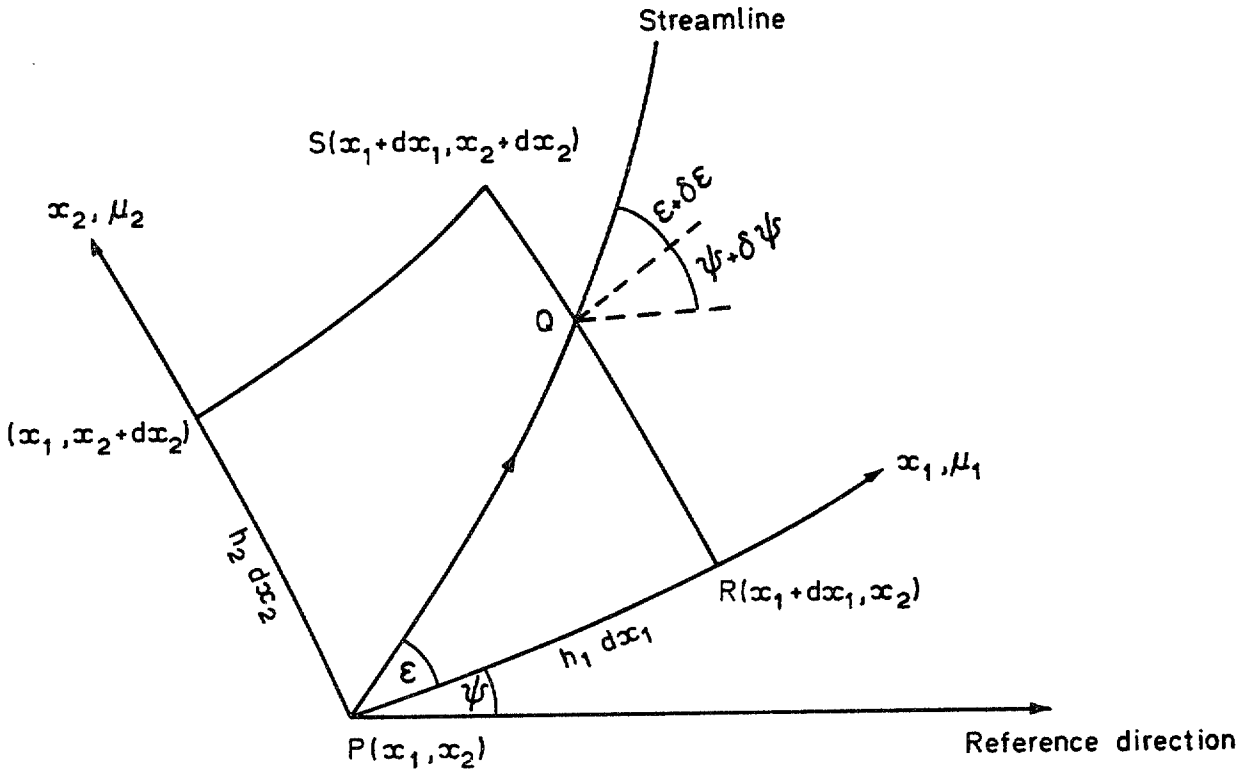

Fig 5 Definition of the general orthogonal coordinate system

Fig 6

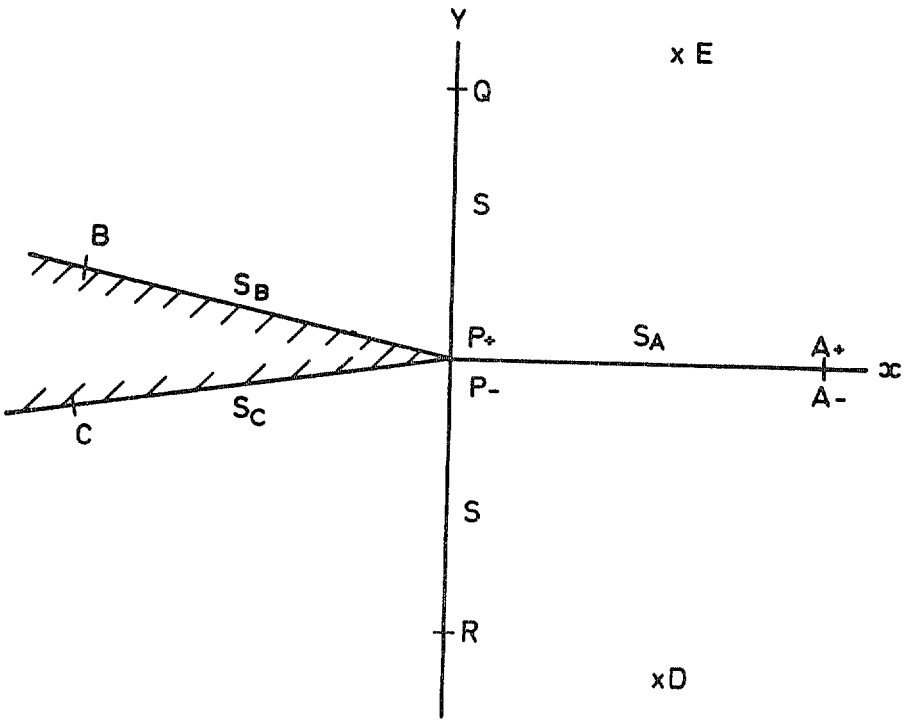

a Physical plane

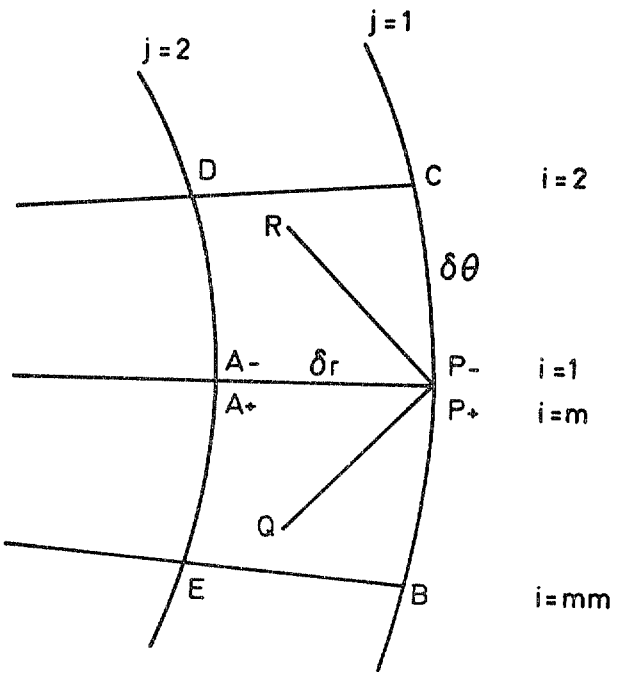

b Computing plane

Fig 6 Finite difference scheme employed at the trailing edge

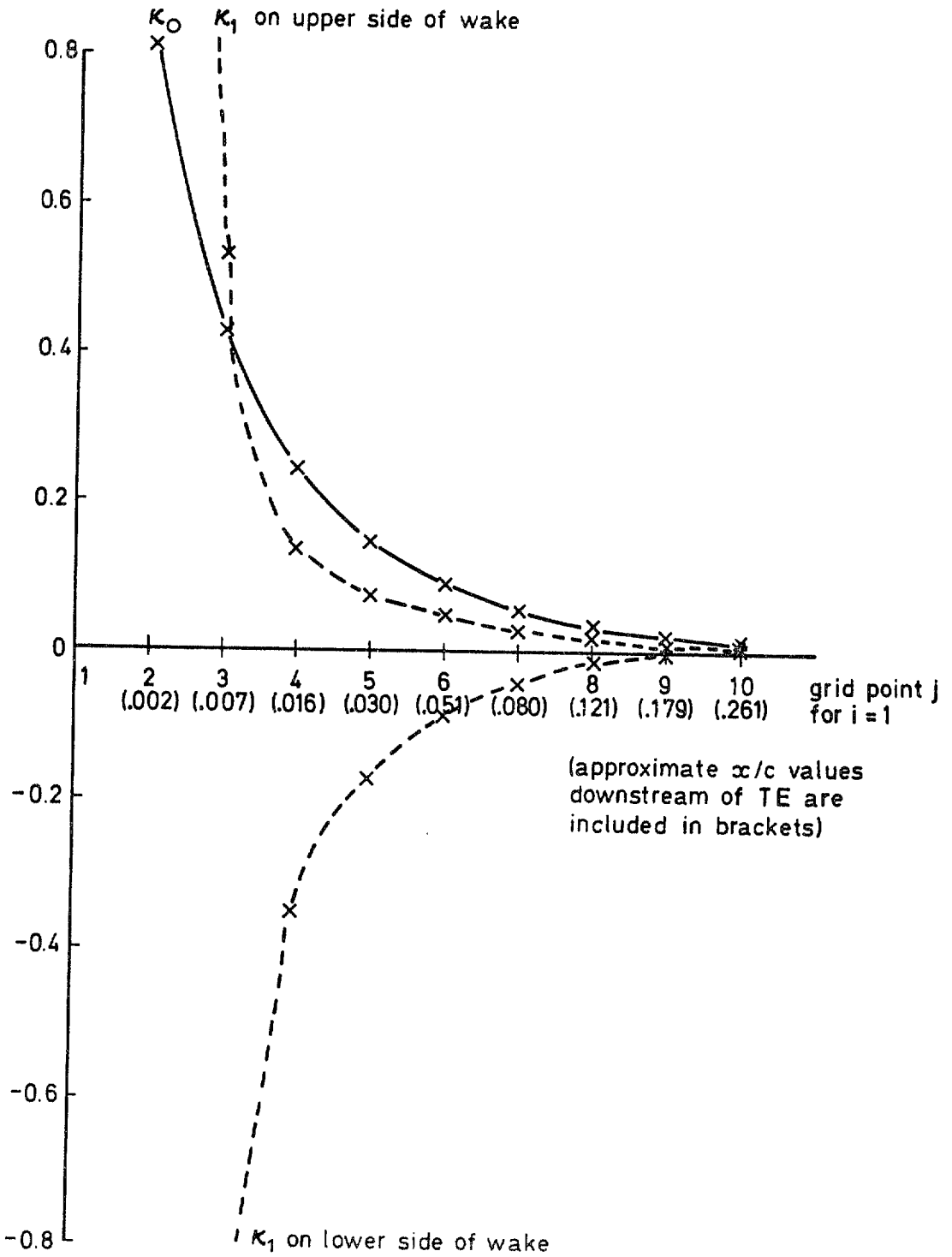

Fig 7 Values of κ_0 and κ_1 at mesh points along $\theta = 0$ on a coarse grid for the RAE 2822 aerofoil at $M_\infty = 0.676$ and $\alpha = 1.06°$

Fig 8

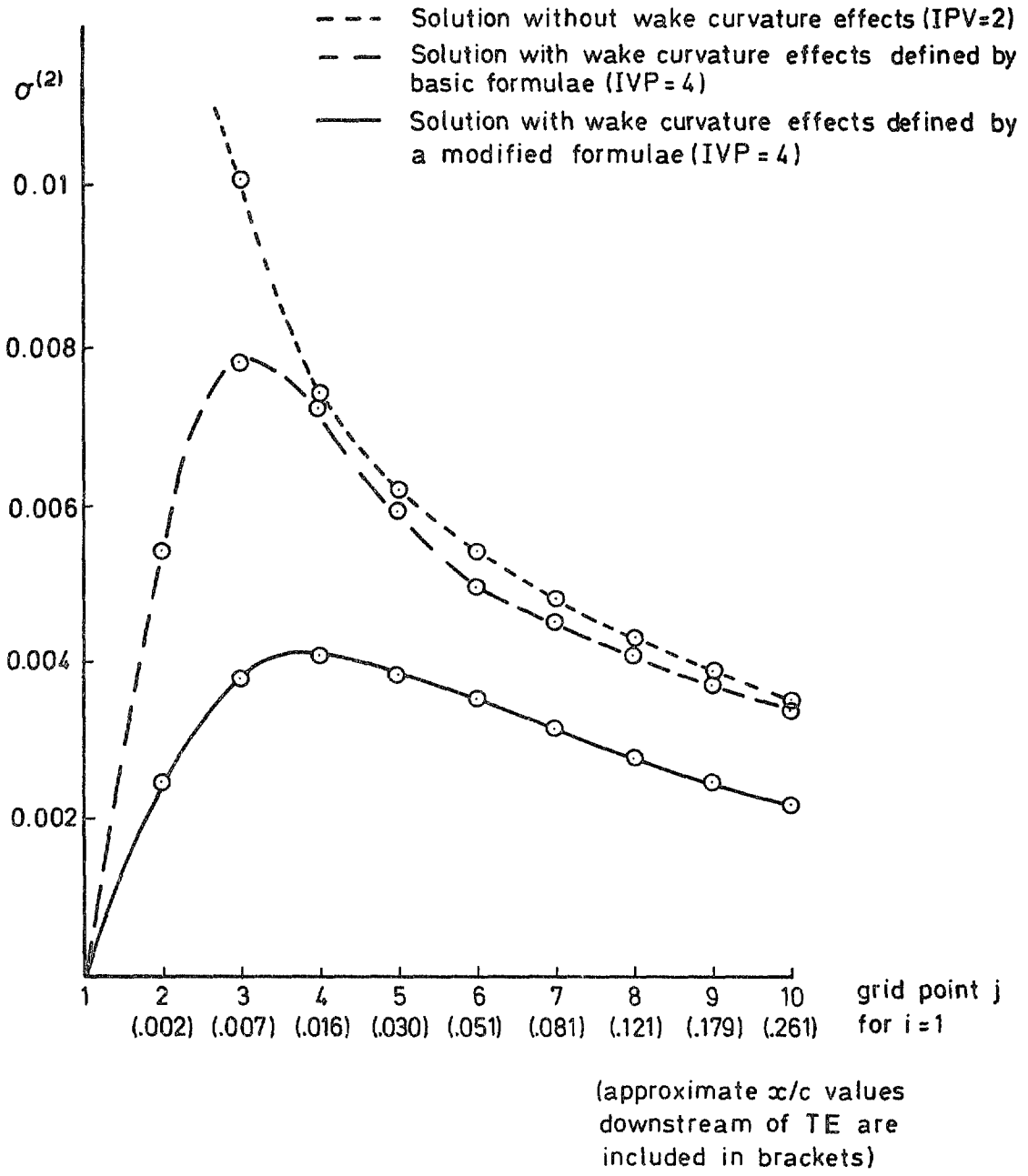

Fig 8 Comparison of values of $\sigma^{(2)}$ on a coarse grid for the RAE 2822 aerofoil at $M_\infty = 0.676$, $\alpha = 1.06°$

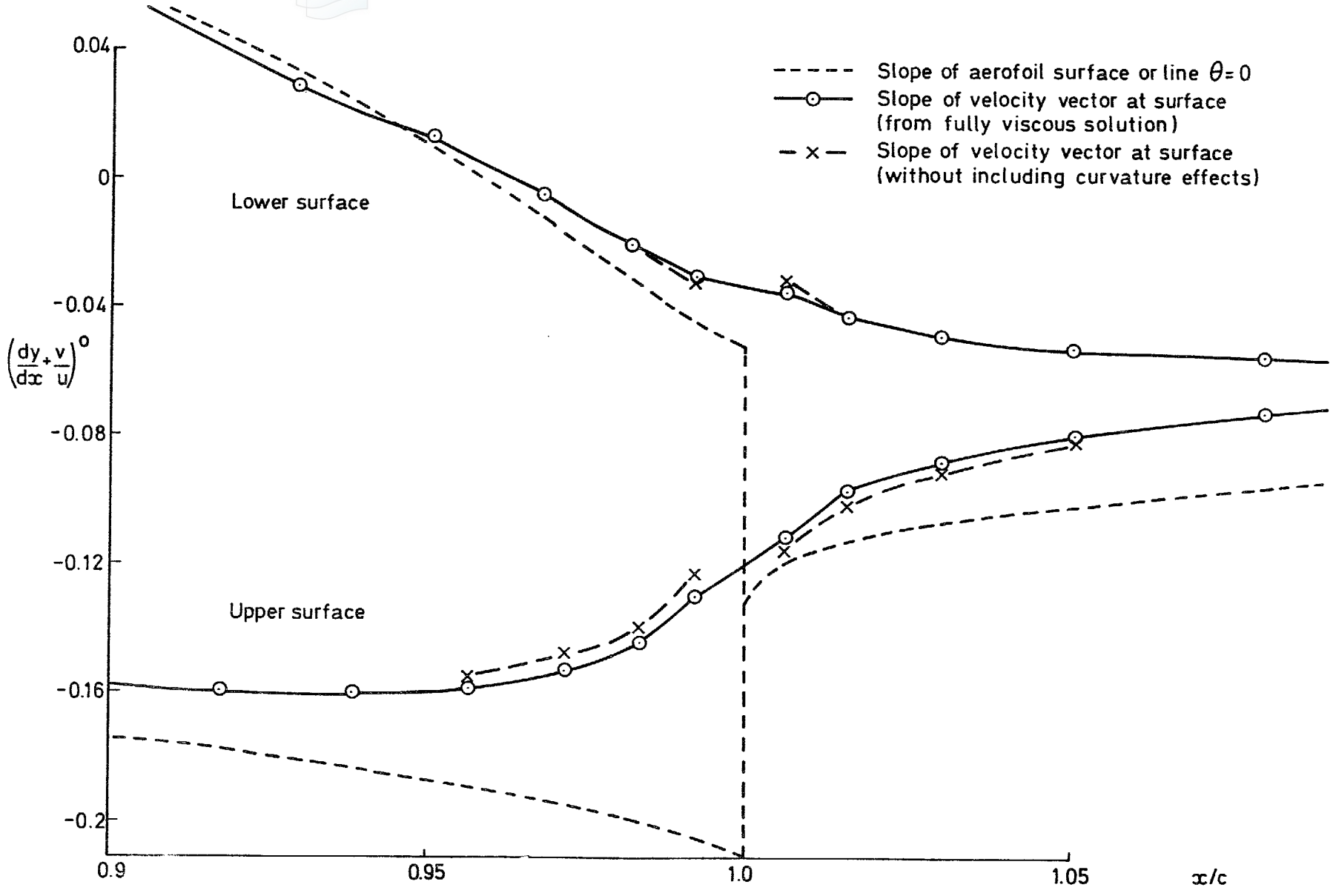

Fig 9 Slope of $\left(\frac{dy}{dx}+\frac{v}{u}\right)$ near trailing edge for RAE 2822 aerofoil at $M_\infty = 0.676$, $\alpha = 1.06°$

Fig 10

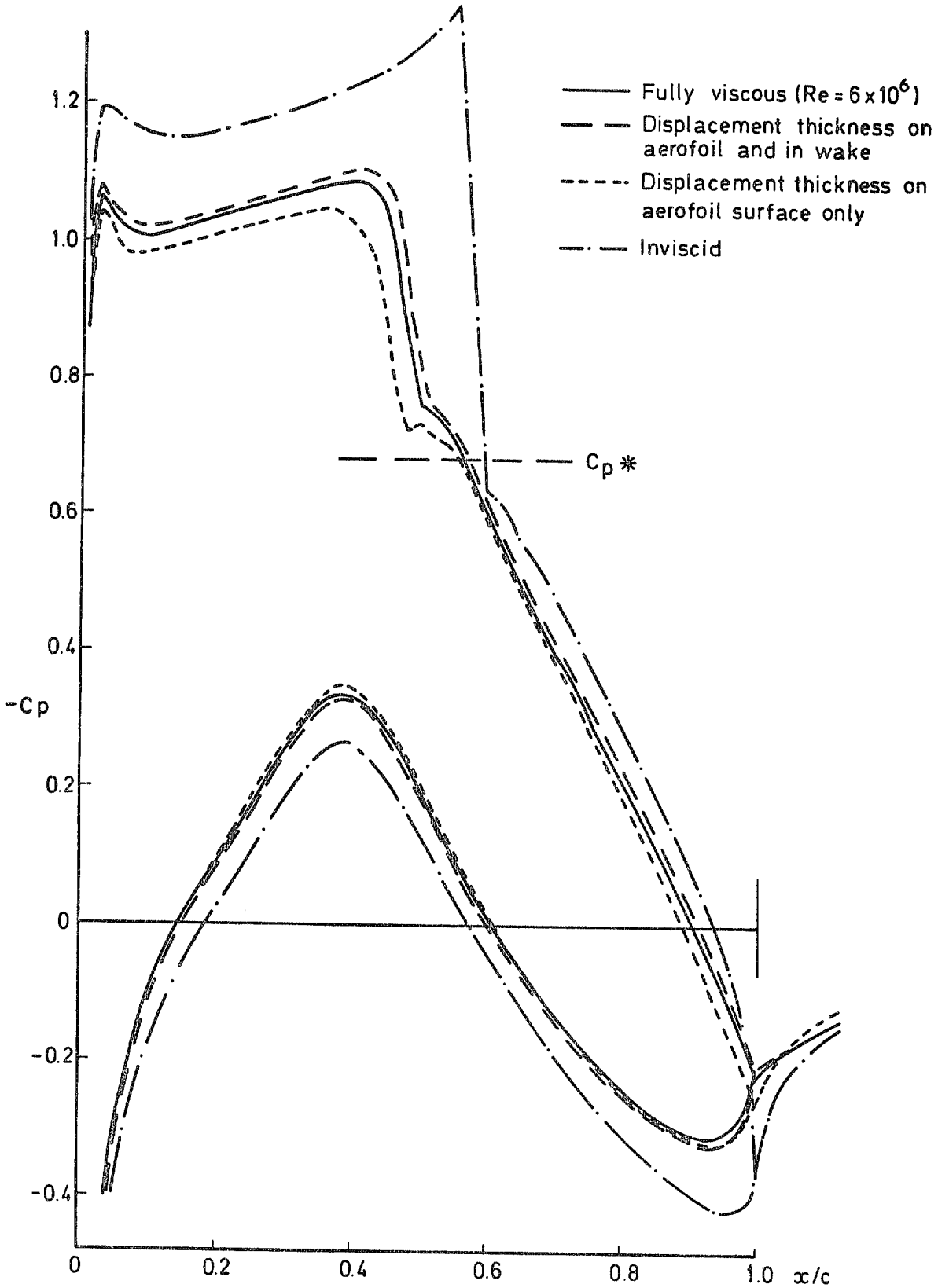

Fig 10 Various solutions for RAE 2822 aerofoil at $M_\infty = 0.725$, $\alpha = 2.3°$

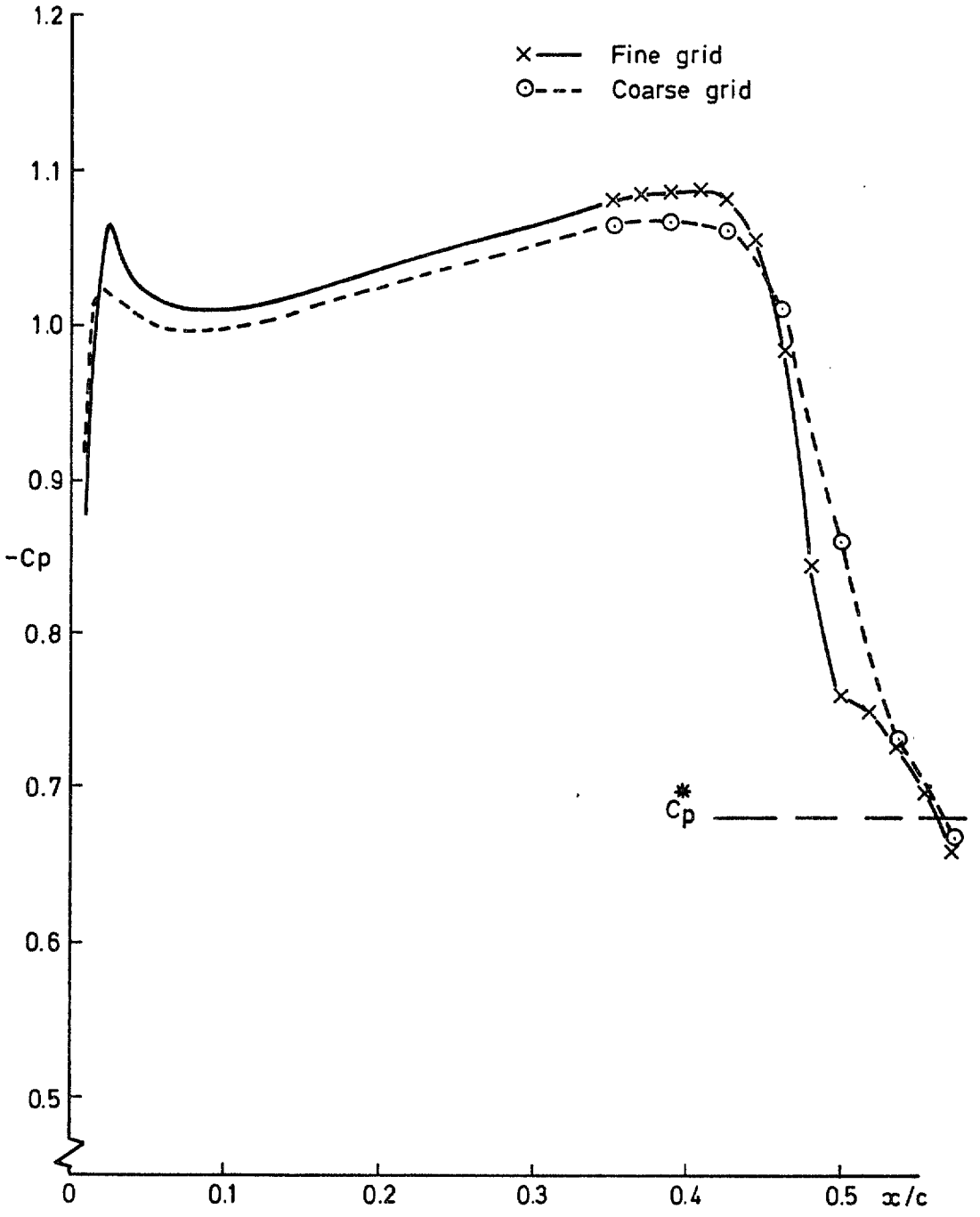

Fig 11 Comparison of coarse and fine grid solutions on the upper surface for RAE 2822 aerofoil at $M_\infty = 0.725$, $\alpha = 2.3°$

Fig 12

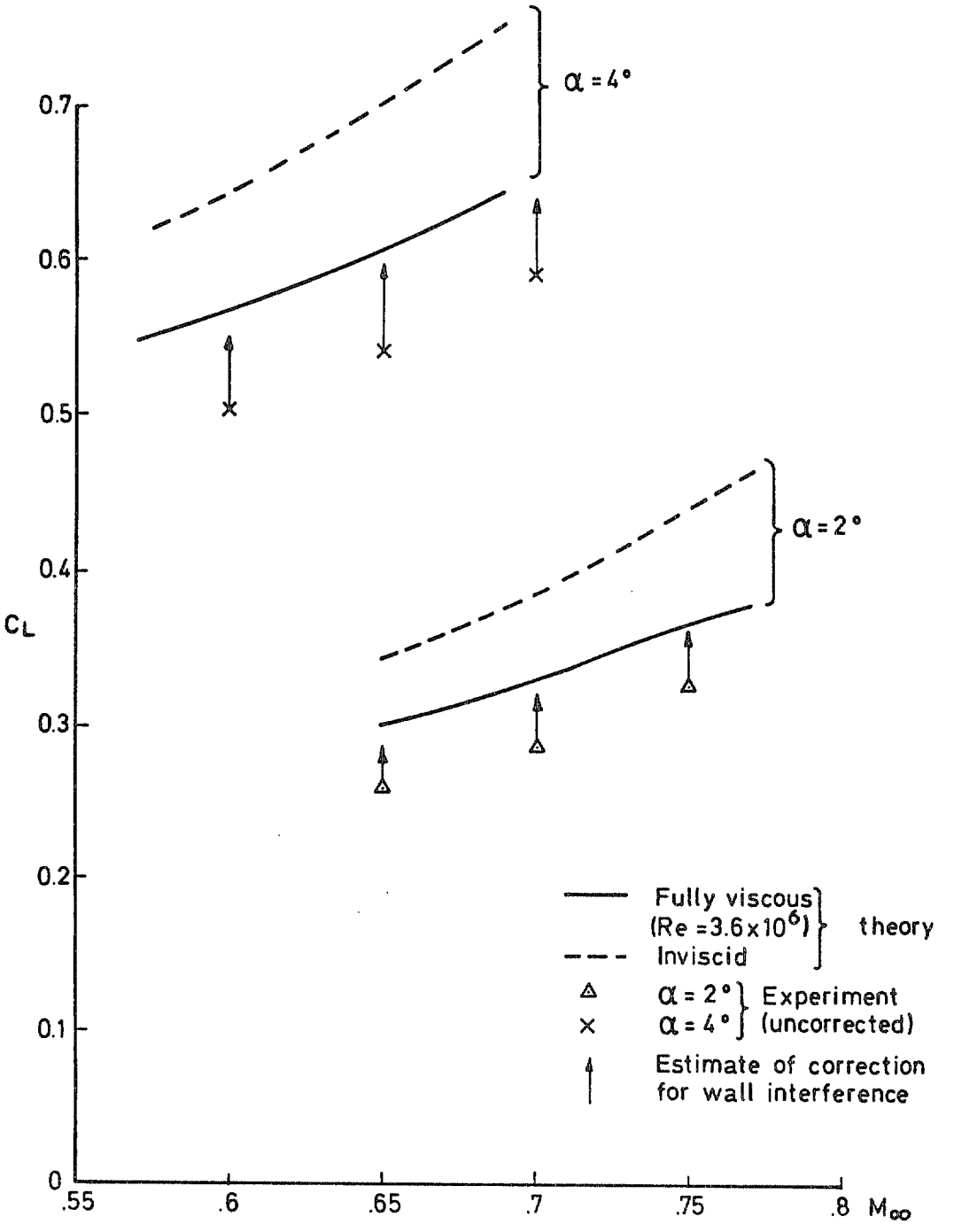

Fig 12 Variation of C_L with M_∞ for NACA 0012 aerofoil

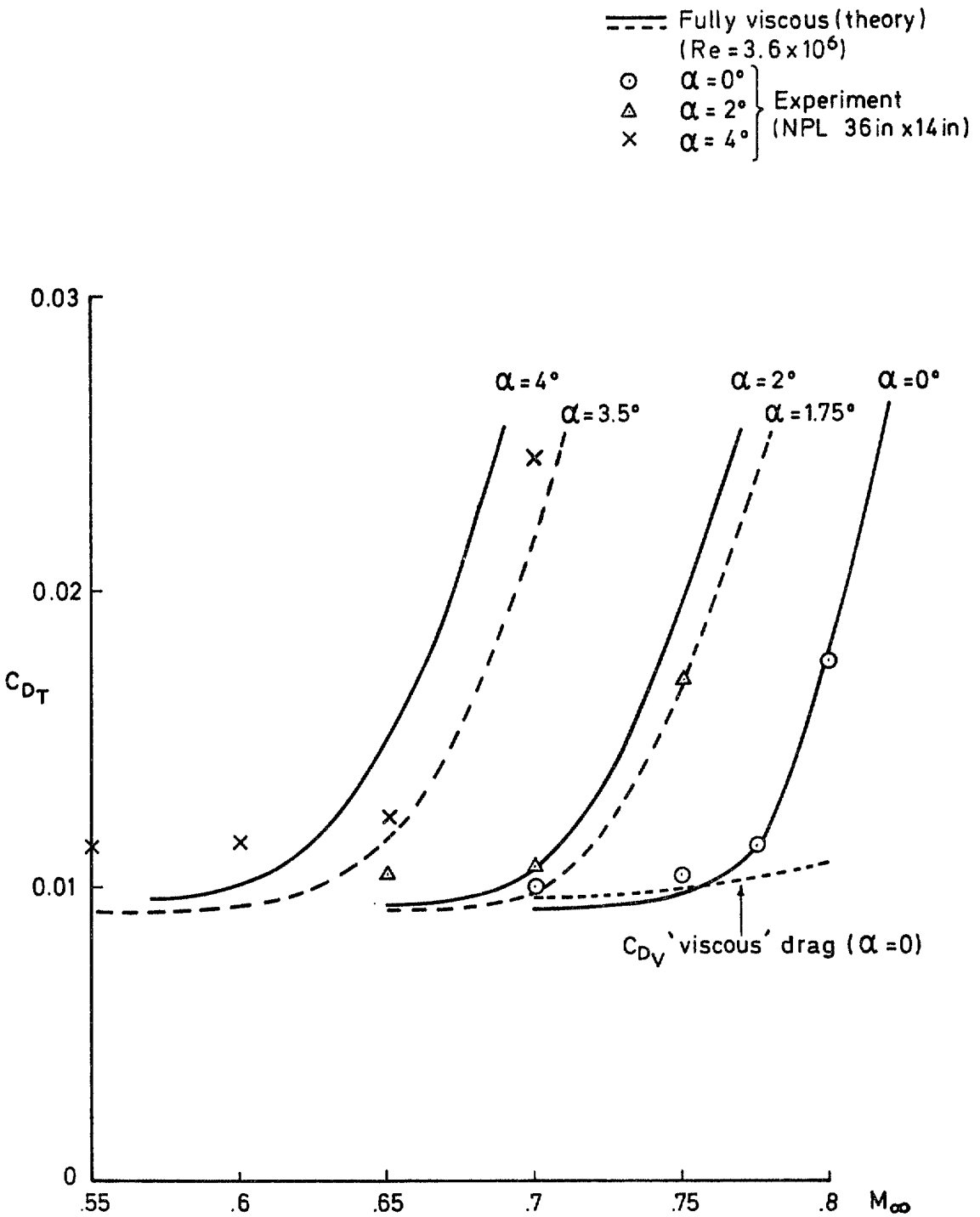

Fig 13 Variation of C_D with M_∞ for NACA 0012 aerofoil

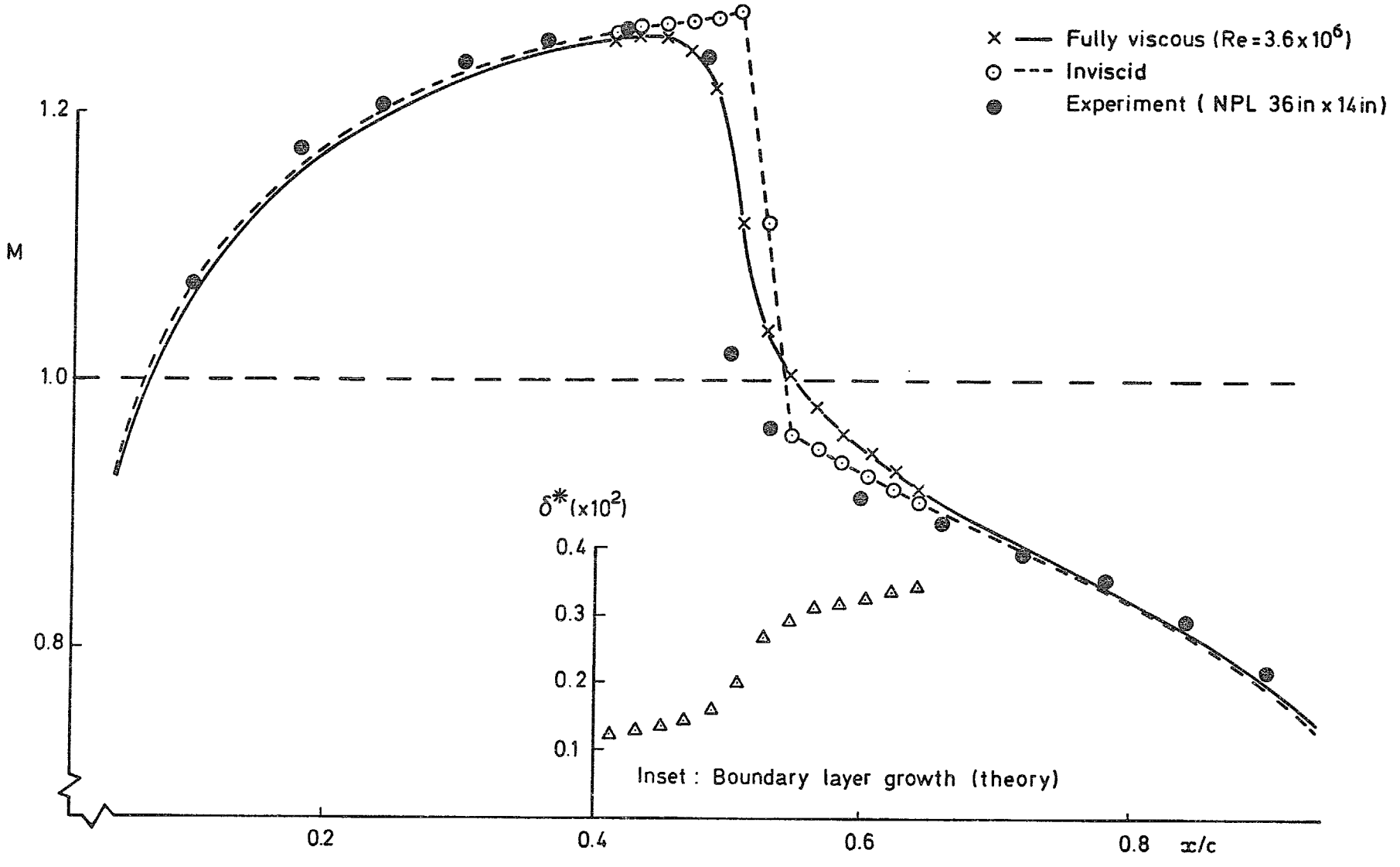

Fig 14 Comparison of inviscid and viscous solutions for NACA 0012 aerofoil at $M_\infty = 0.82$, $\alpha = 0°$

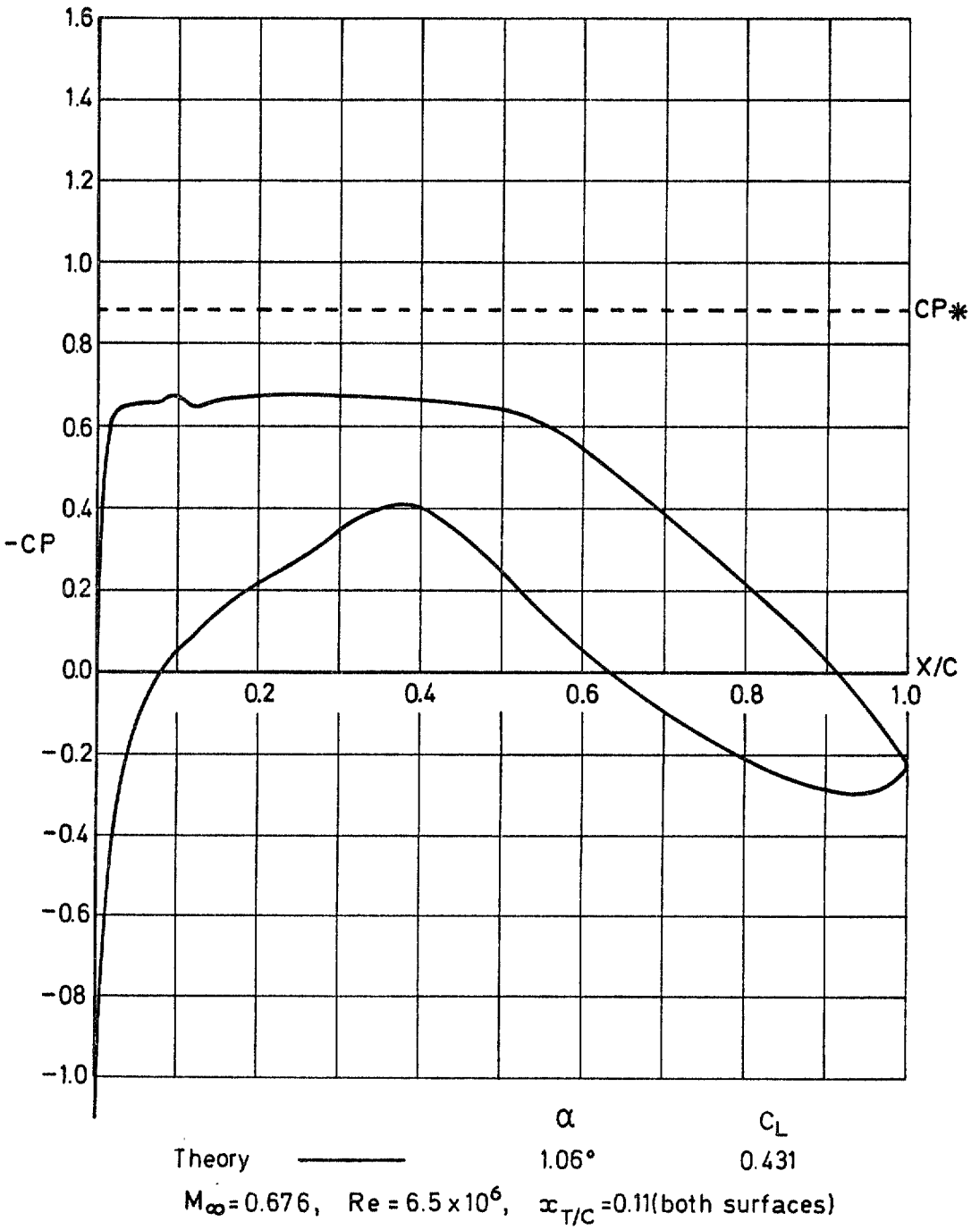

Fig 15 RAE 2822 aerofoil. A theoretical solution

Fig 16

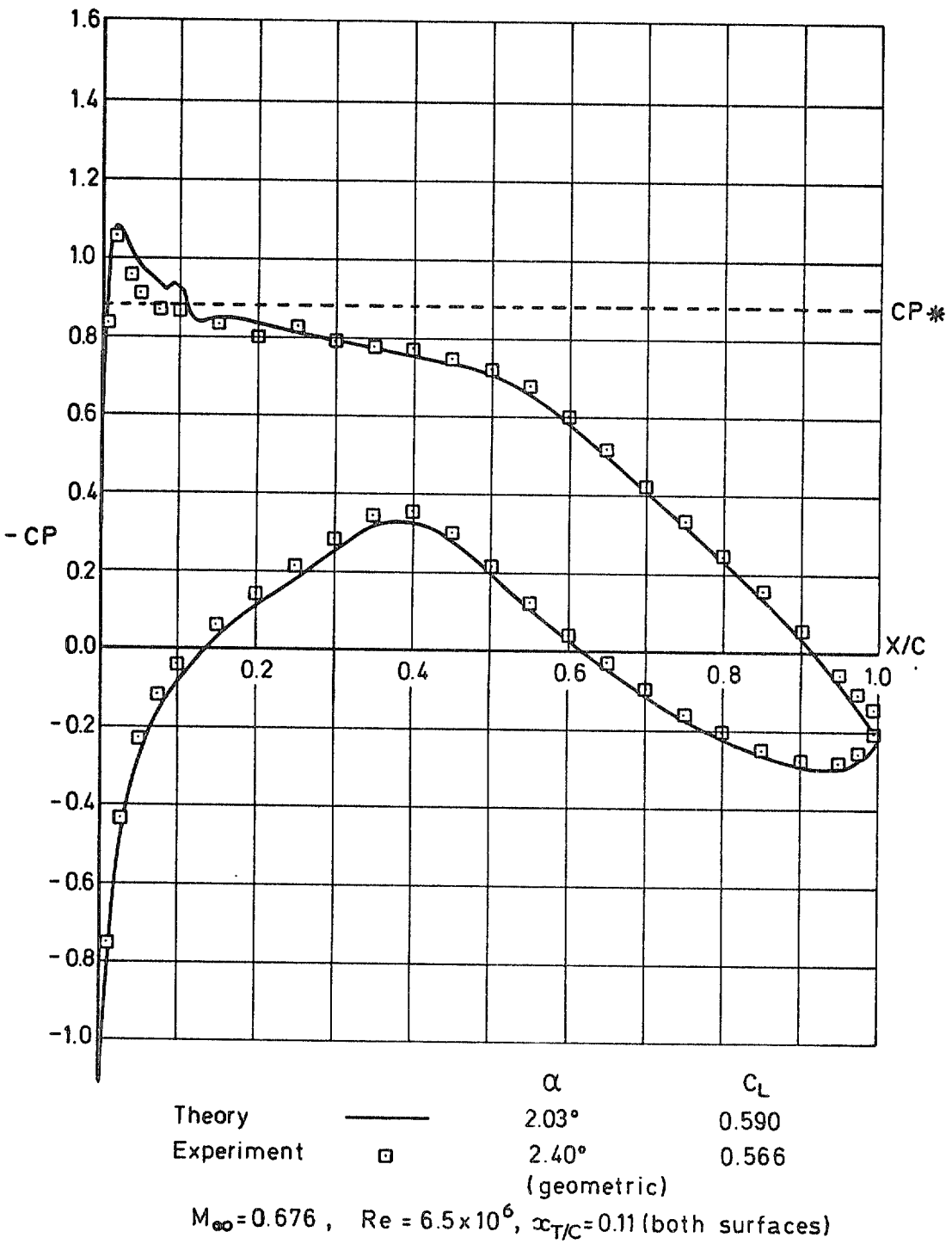

Fig 16 RAE 2822 aerofoil. A comparison between theory and experiment

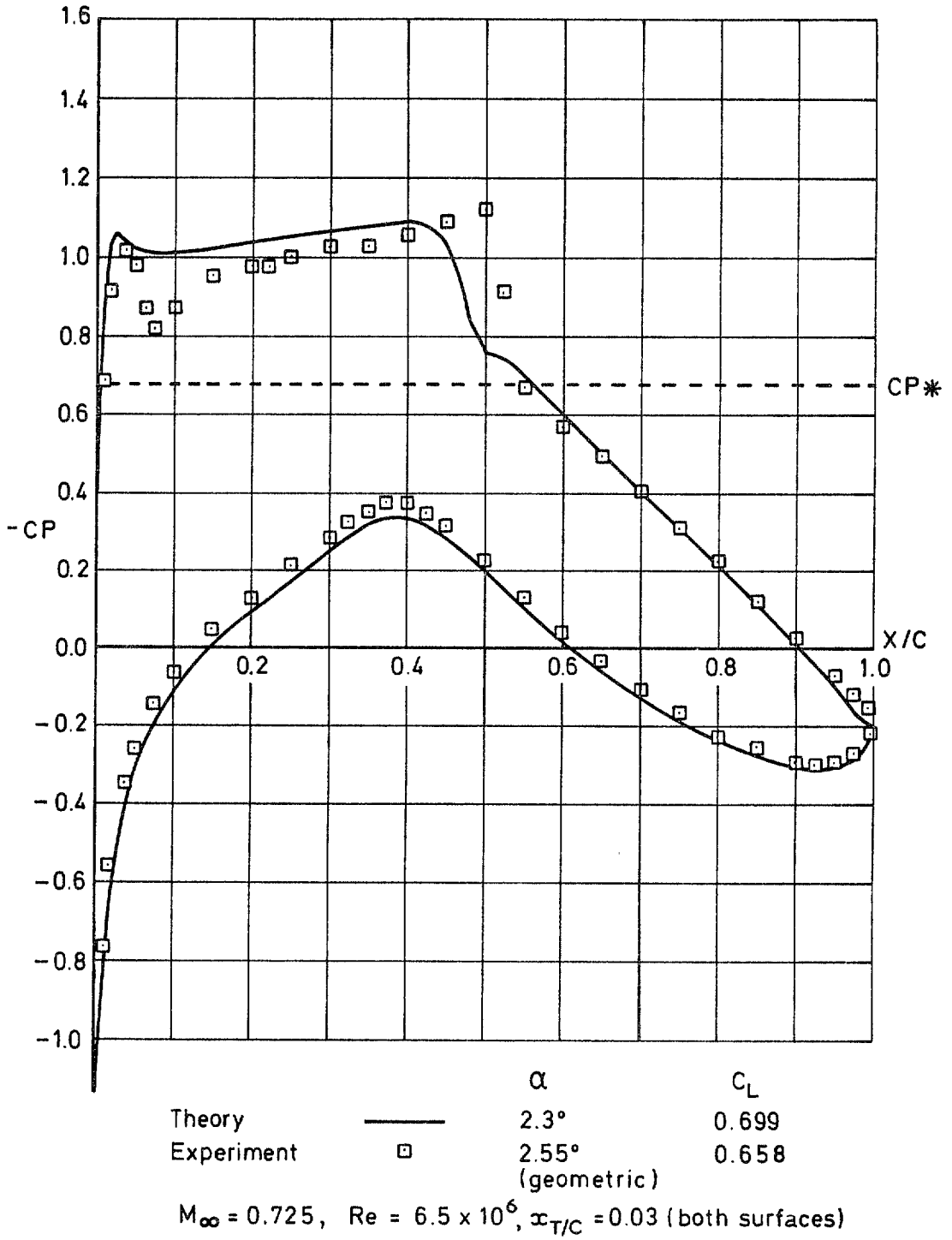

Fig 17a RAE 2822 aerofoil. A comparison between theory and experiment

Fig 17 b

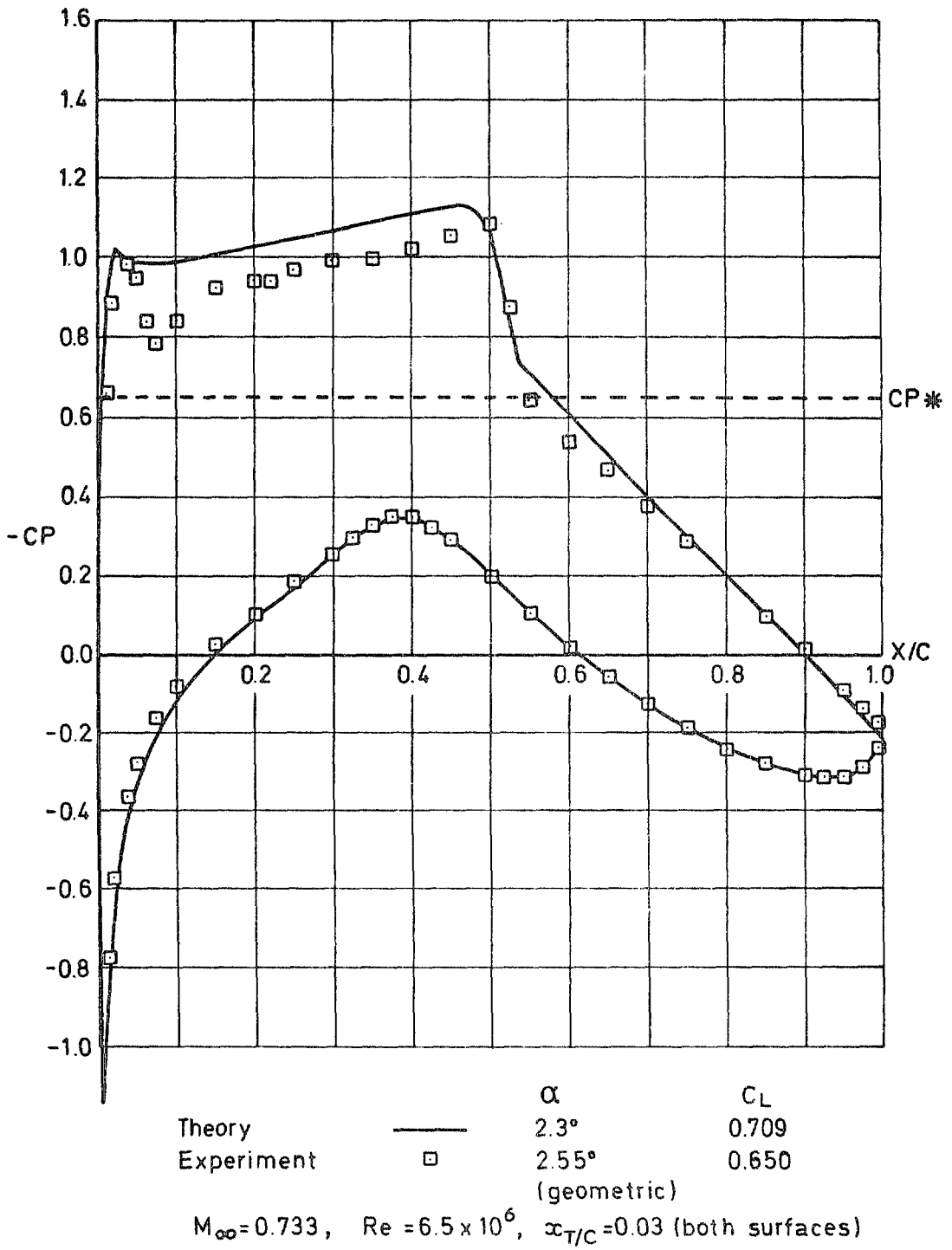

Fig 17b RAE 2822 aerofoil. A comparison between theory and experiment with M_∞ adjusted by 0.008

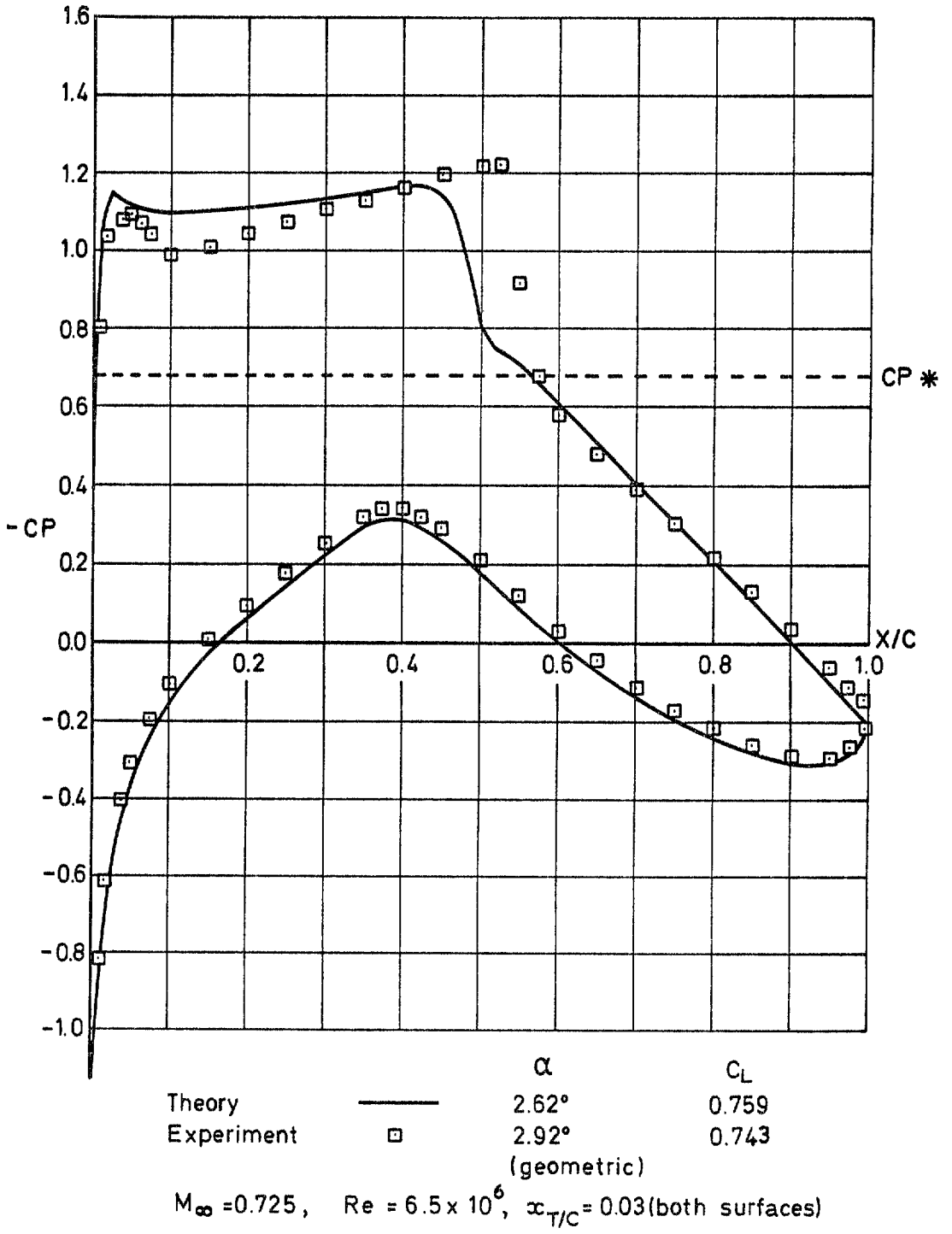

Fig 18 RAE 2822 aerofoil. A comparison between theory and experiment

Fig 19

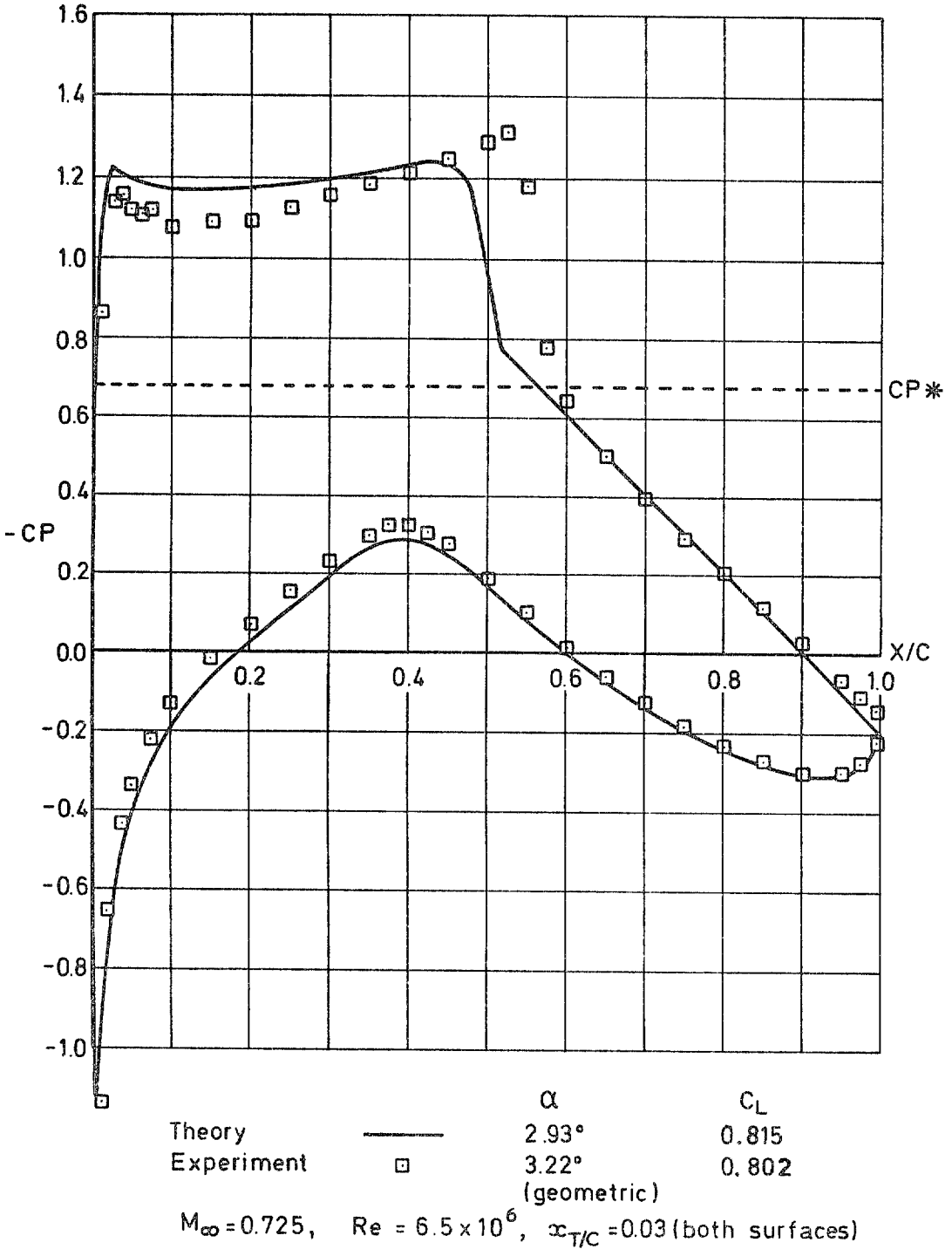

Fig 19 RAE 2822 aerofoil. A comparison between theory and experiment

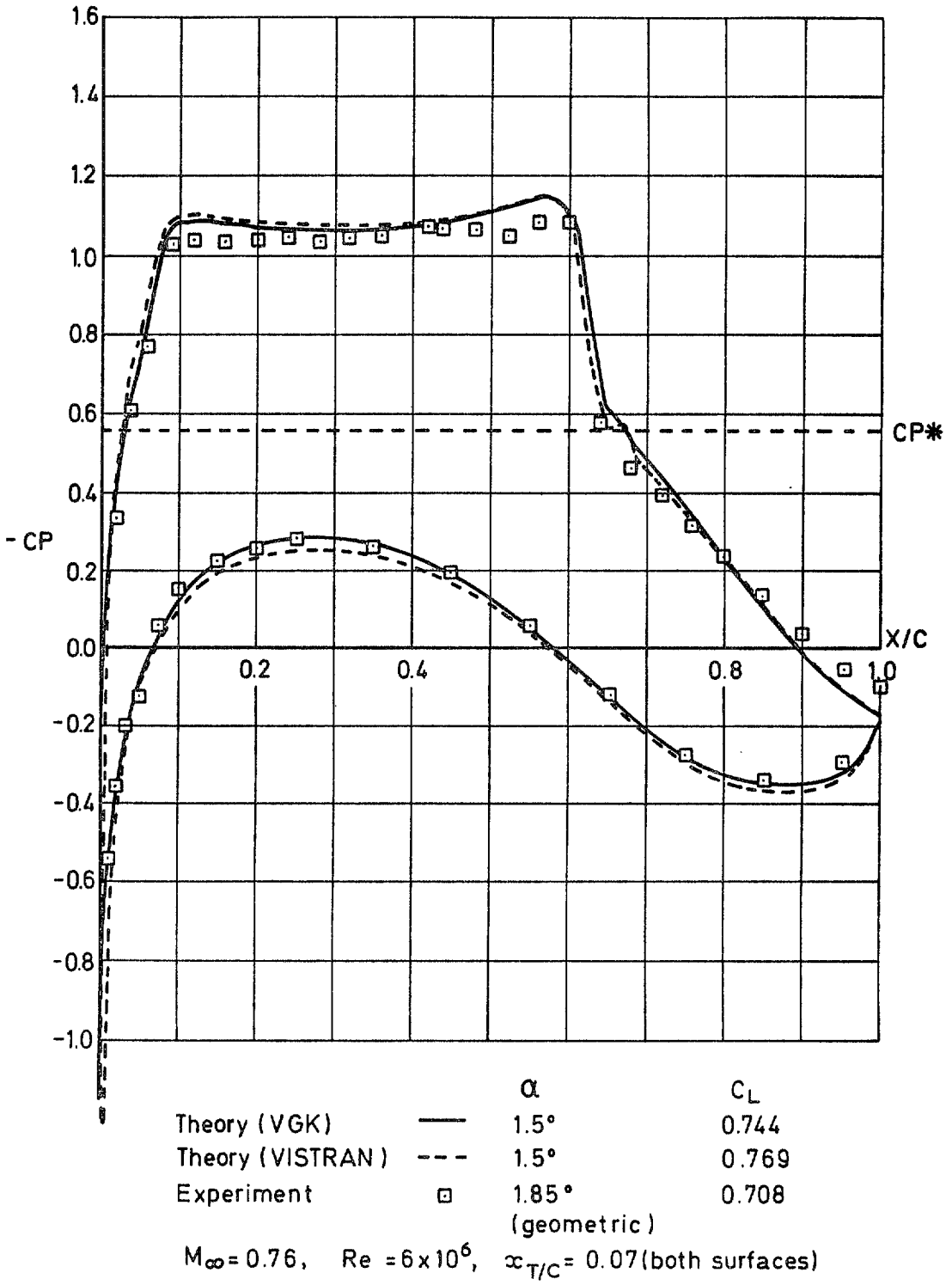

Fig 20 Korn No.1. A comparison between various theories and experiment

Fig 21

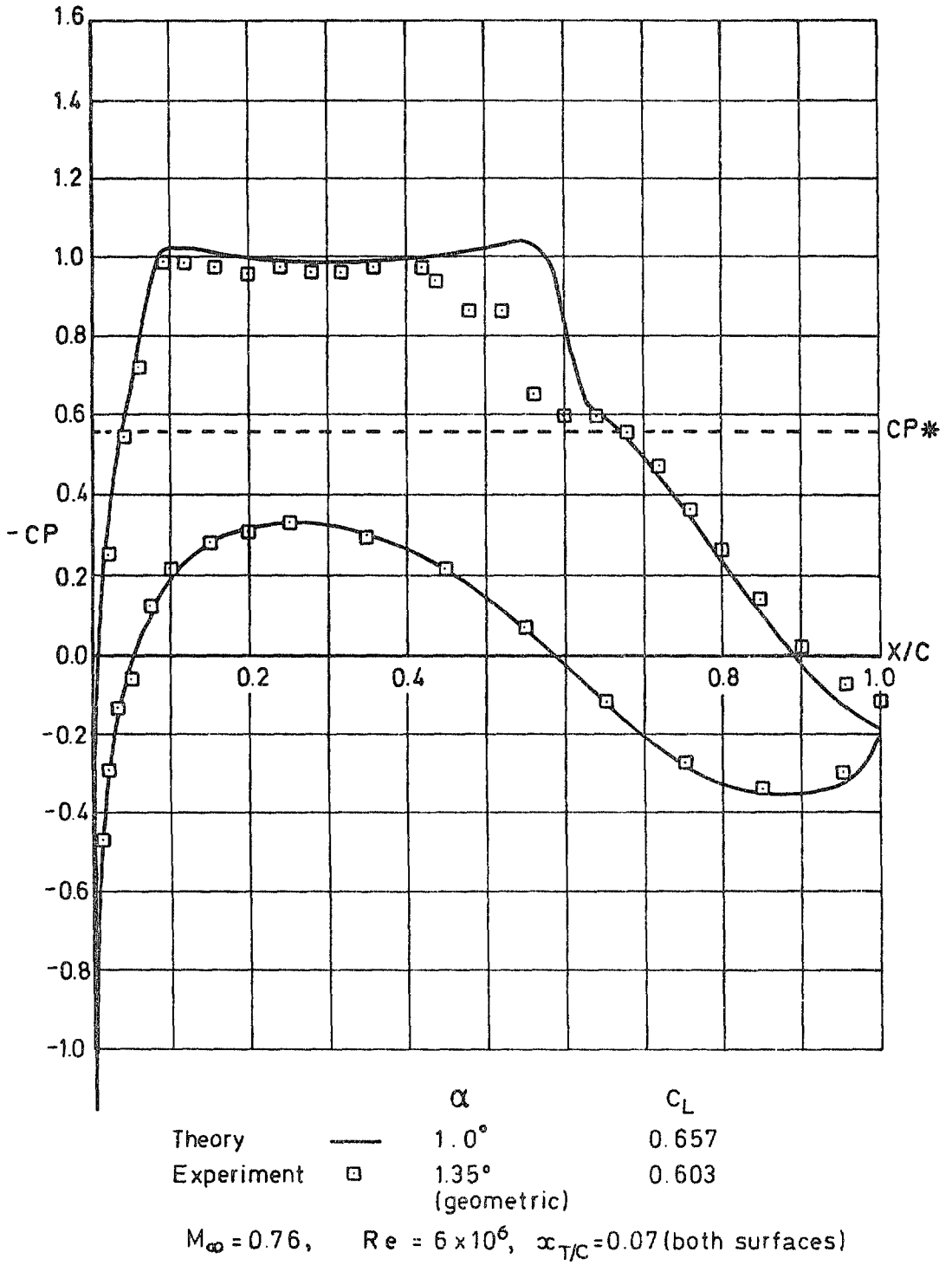

Fig 21 Korn No.1. A comparison between theory and experiment

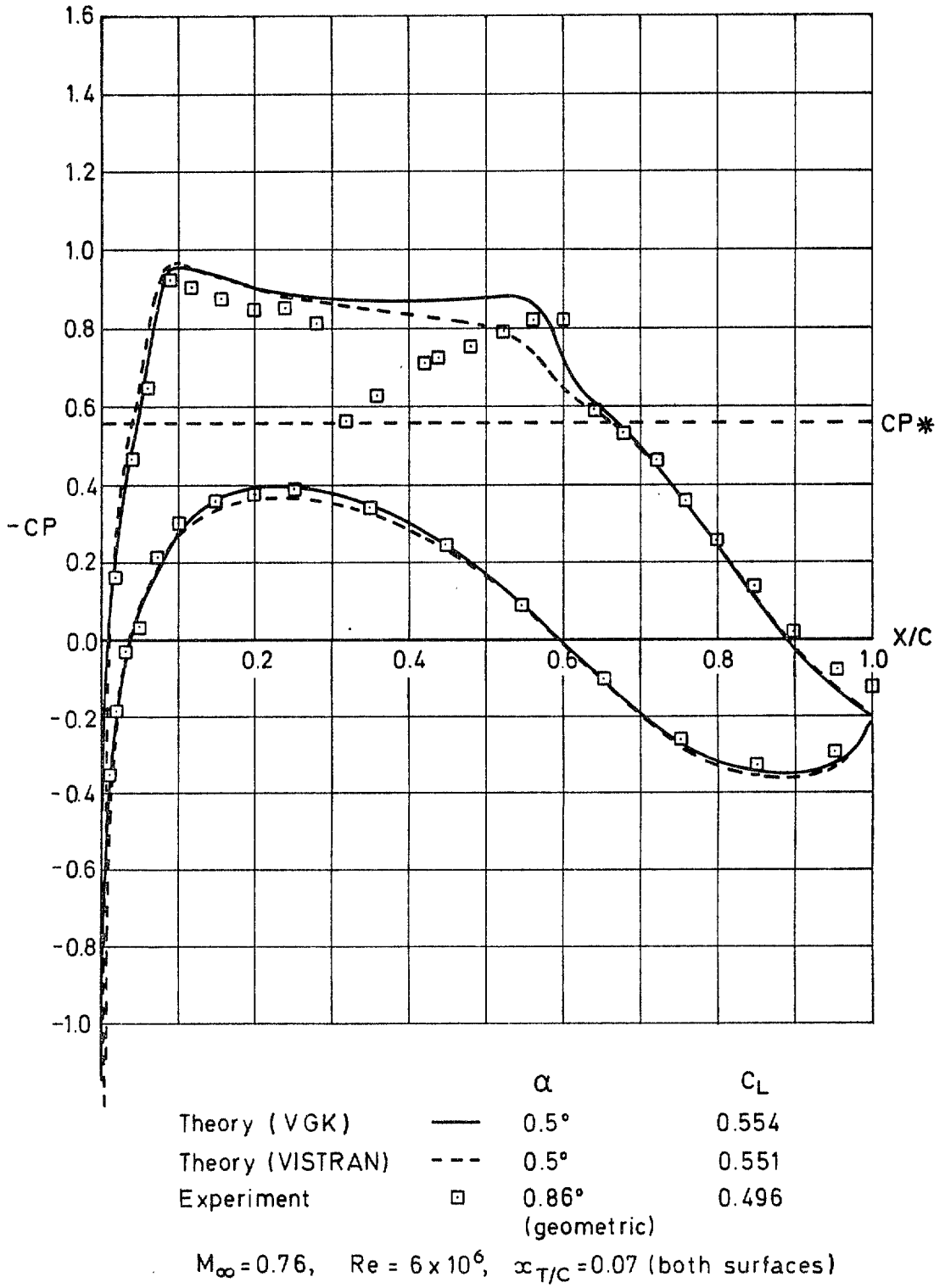

Fig 22 Korn No.1. A comparison between various theories and experiment

Fig 23

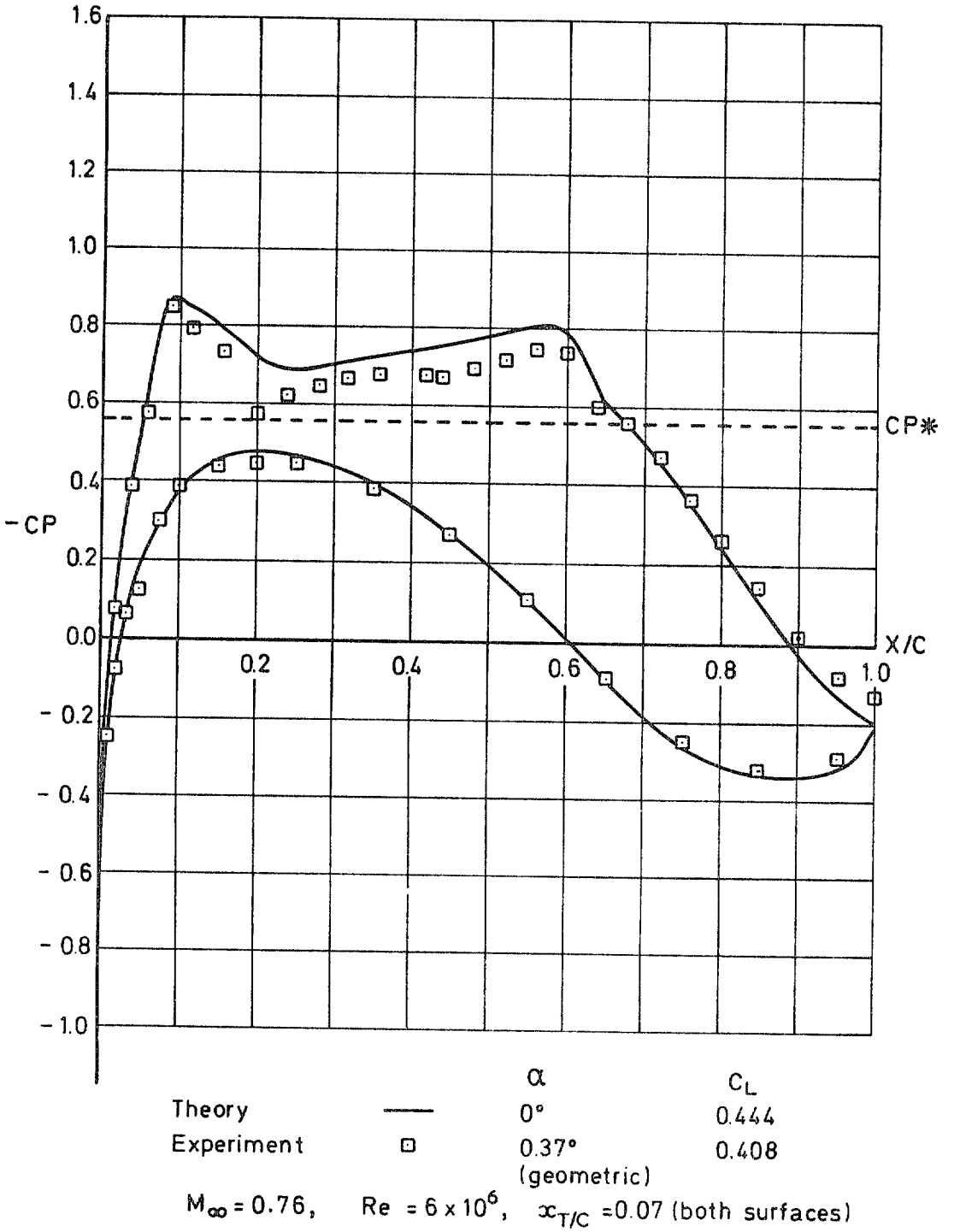

Fig 23 Korn No.1. A comparison between theory and experiment

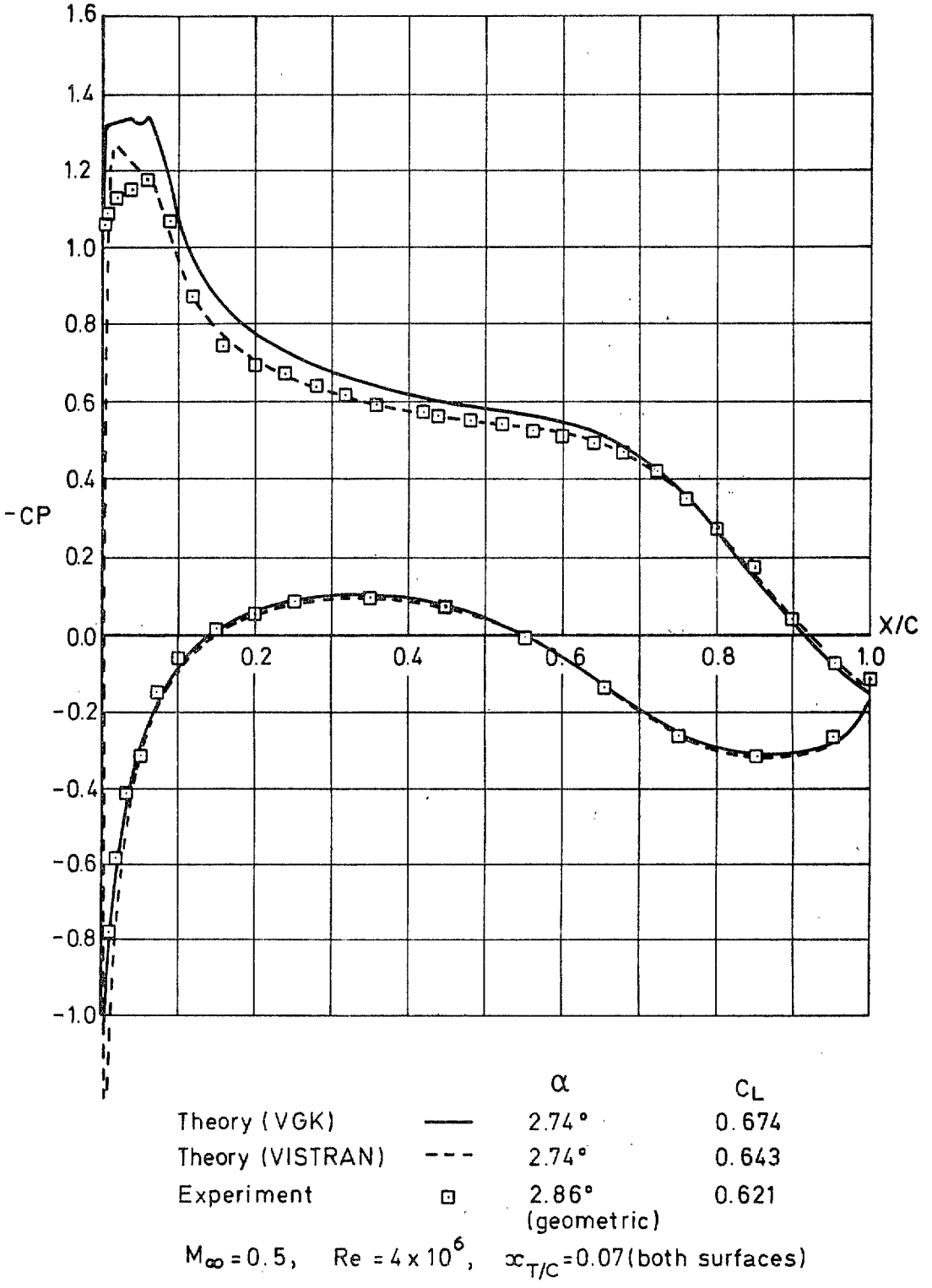

Fig 24 Korn No.1. A comparison between various theories and experiment

Fig 25

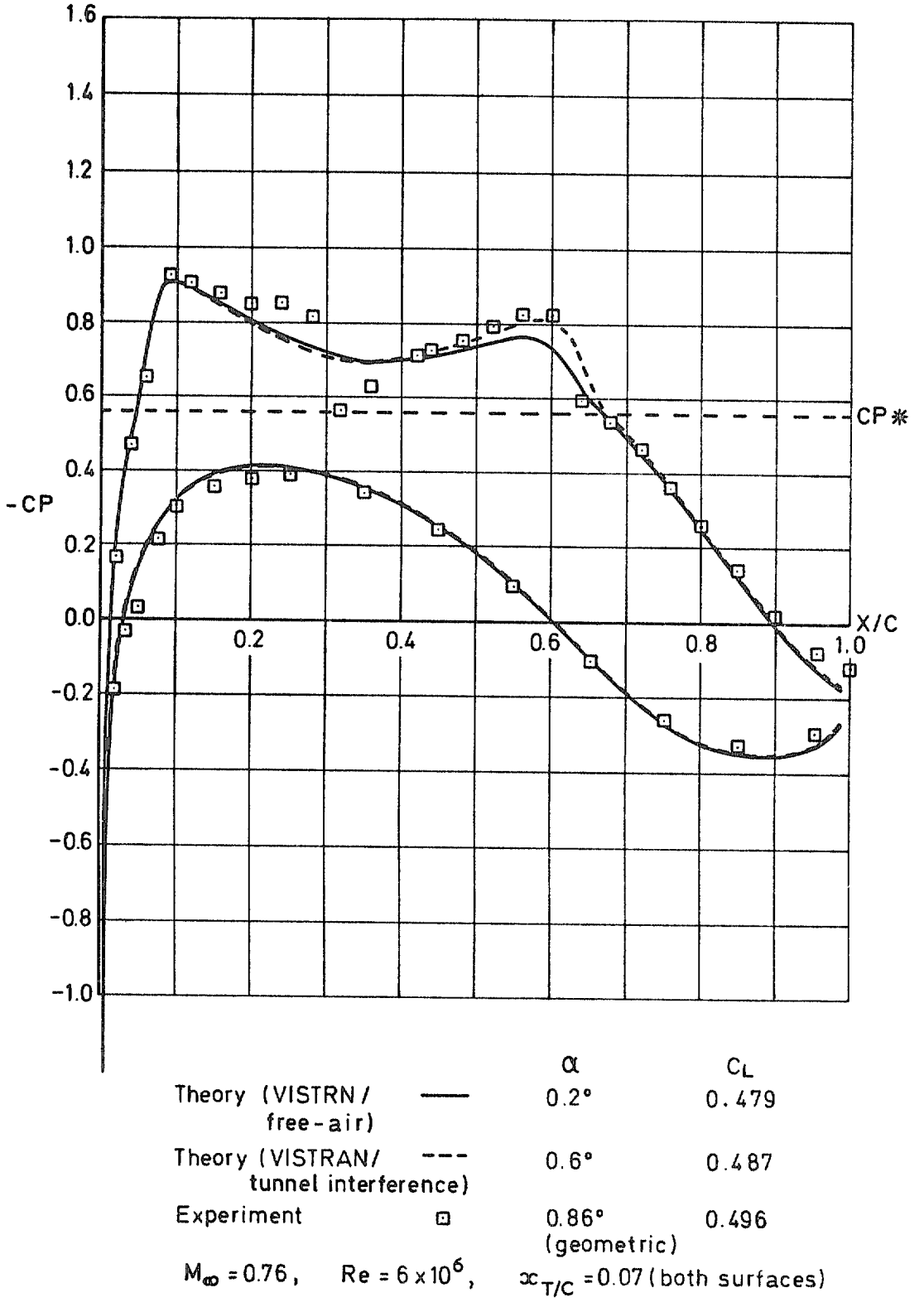

Fig 25 Korn No.1. A comparison between various theories and experiment

Printed in England for Her Majesty's Stationery Office by the Royal Aircraft Establishment, Farnborough. Dd 586386 K4 11/78.

1978

Published by
HER MAJESTY'S STATIONERY OFFICE

Government Bookshops
49 High Holborn, London WC1V 6HB
13a Castle Street, Edinburgh EH2 3AR
41 The Hayes, Cardiff CF1 1JW
Brazennose Street, Manchester M60 8AS
Southey House, Wine Street, Bristol BS1 2BQ
258 Broad Street, Birmingham B1 2HE
80 Chichester Street, Belfast BT1 4JY

Government Publications are also available through booksellers

R &M No.3828
ISBN 0 11 471161 5